Preparation and biological properties of biodegradable organic-inorganic hybrid spheres

	DA CRUZ NEVES Susana
	-
	29
	17104 312
URL	http://hdl.handle.net/10228/00006894

Preparation and biological properties of biodegradable organic-inorganic hybrid spheres

SUSANA DA CRUZ NEVES

**GRADUATE SCHOOL OF LIFE SCIENCE
AND SYSTEMS ENGINEERING
KYUSHU INSTITUTE OF TECHNOLOGY**

JAPAN

MARCH, 2018

ABSTRACT

Antibiotic resistance in bacteria is a serious problem that requires researchers to engineer new strategies to tackle this growing threat. The limited intracellular bioavailability of antibiotics decreases the efficacy of the treatments and, as a consequence promotes bacterial resistance towards antibiotics. Therefore, the development and improvement of drug controlled release systems is vital to create new approaches to deliver in the most effective manner the drugs or other bioactive compounds to the desired location. Especially if the targeted site is the gastrointestinal track, where the environmental conditions are harsh for biomolecules to maintain its stability and function. Polymeric microspheres are attractive due to their biodegradability and ability to encapsulate drugs or bioactive agents, therefore increasing their bioavailability. To address these poor bioavailability or unsustained drug release challenges, chitosan microspheres are adequate as drug delivery carriers for the gastrointestinal track due to mucoadhesive properties, which allows the drug dosage to be retained in the gastrointestinal track for extended periods of time, in addition to the presence of reactive sites in chitosan which allow the interaction with biomolecules to be carried to the targeted site.

Spherical particles were produced using chitosan and γ-glycidoxypropyltrimethoxysilane (GPTMS) as an organic-inorganic hybrid compound resorting to two different methods. The first method consisted in a microfluidic approach using chitosan–GPTMS–β-glycerophosphate (chitosan–GPTMS–β-GP) to produce microspheres with uniform size and spherical shape around 650 μm and 285 μm. Whereas, in the second method beads with diameter around 2 mm with micropores were synthetized by dropping the hybrid precursor sol into liquid nitrogen followed by a freeze drying process.

The physicochemical characterization of the microspheres from the microfluidic system was performed in which the formation of siloxane (Si-O-Si) networks was confirmed in the chitosan polymeric matrix, as well as the spheres stability in solutions. The degradation of

microspheres with different GPTMS molar ratios was evaluated under simulated gastric fluids (SGF) and neutral conditions. The microspheres incubated at pH 7.4 had the lowest weight loss (27%–32%), whereas those incubated at pH 1.7 and pH 5.4 showed greater weight losses of 43–59% and 69–77%, respectively. The inhibition of the degradation at low pH was dependent on the siloxane network formed in the chitosan matrix. Additionally, GPTMS was released with the chitosan chains via hydrolysis of the chitosan molecules.

Pelargonidin is a natural antioxidant which was incorporated in the microspheres and the releasing behavior was observed under SGF conditions and simulated time of digestion cycle in humans. The release profile observed leads to believe that these microspheres are promising for gastrointestinal drug delivery applications due to its resistance to low pH conditions present in the upper gastrointestinal track, in addition to the controlled and sustained release rate of pelargonidin and its ability to retain it in the matrix even after 57 h.

Cerium compounds have been described to possess antibacterial activity, and new strategies of treating pathogenic bacteria are needed due to the rapid increase of bacterial resistance towards common antibiotics. The bacterial behavior of *Escherichia coli* and *Staphylococcus aureus* was observed with the chitosan–GPTMS–β-GP spheres and hydrogels containing cerium(III) chloride ($CeCl_3$), and no antibacterial effect was observed due to the immediate interaction between β-GP and cerium, via the complex formation of cerium with the amino groups of chitosan, making it inaccessible to the bacteria. Furthermore, the bacterial viability increased for both gram-negative and gram-positive strains on hydrogels with and without cerium.

To achieve antibacterial applications using the chitosan-siloxane hybrid, beads without β-GP were prepared by dropping the chitosan-GPTMS precursor sols into liquid nitrogen. The beads were synthetized with and without cerium. The bacterial activity was greatly reduced with the highest tested amounts of cerium against both gram-negative (*Escherichia coli*) and

gram-positive (*Staphylococcus aureus*) strains. This microporous beads have the potential to be applied for soft tissue defect fillers materials with antibacterial properties to reduce or eradicate *in situ* bacterial infection.

CONTENTS

LIST OF FIGURES

LIST OF TABLES

LIST OF ABBREVIATIONS AND ACRONYMS

Abbreviation	Description
β-GP	β-glycerophosphate
ATR-FTIR	Attenuated Total Reflectance Fourier Transform Infrared spectroscopy
Ce	Cerium
Ch	Chitosan
ChG	Chitosan-GPTMS
ChGCe	Chitosan-GPTMS-Cerium
DMSO	Dimethyl Sulfoxide
E. coli	*Escherichia coli*
GPTMS	γ-glycidoxypropyltrimethoxysilane
HCl	Hydrochloric acid
ICP-AES	Inductively Coupled Plasma Atomic Emission Spectrometer
LB	Luria Bertani
MIC	Minimum Inhibitory Concentration
MTT	3-(4,5-dimethylthiazol-2-yl)-2,5-diphenyl tetrazolium bromide
NaOH	Sodium Hydroxide
OD	Optical density
PBS	Phosphate Buffered Saline
S. aureus	*Staphylococcus aureus*
SEM-EDS	Scanning Electron Microscopy Energy Dispersive X-Ray Spectrometry
SGF	Simulate Gastric Fluid
UV-VIS	Ultraviolet–Visible

Chapter 1.

GENERAL INTRODUCTION

1.1. Drug delivery

The improvement of controlled release systems of drugs and other bioactive agents, is an essential research topic for therapeutic treatments. It is vital to develop new approaches to deliver in the most effective manner the drugs or other bioactive compounds to the desired location.

One of the main limitations in the pharmaceutical field is the fact that the current approaches for drug delivery (for instance pills, injections, and sprays), may lack on efficiency to deliver the bioactive agents, consequently several administrations might be obligatory to preserve the drug concentration, in the blood or plasma, with the effecient drug level within the therapeutic window for the necessary time period. Figure 1-1 is a schematic representation of the conventional drug therapy by multiple dosage versus the ideal controlled and sustained drug release overtime within the effective therapeutic range. On figure 1-1a, is represented the tablet or injection types of drug administration, in which the drug levels rise to a maximum peak and decrease to a lower value until the time for the next dosage is necessary. This approach can create problems where the drug concentration has a narrow therapeutic range for the drug to work efficiently, and if the drug levels continue to rise reaching into the toxic level, the probability of occurring adverse side effects is high, and drop again below the lowest effective concentration. Therefore, the necessity for the development of controlled release systems, to effectively deliver the drug or bioactive agent at a desired rate and period of time. This is the optimal drug release scenario represented on figure 1-1b. In which, in respect to the rate and duration, the release pattern happens where the concentration of the drug in the body is

maintained within the effective therapeutic window for an extended period of time. The great

benefit from a controlled drug release approach is the fact that the drug could be administered

in a single dosage, with improved effectiveness using the same amount of drug and reduce the

possibility of side effects from sudden drug concentration spikes.
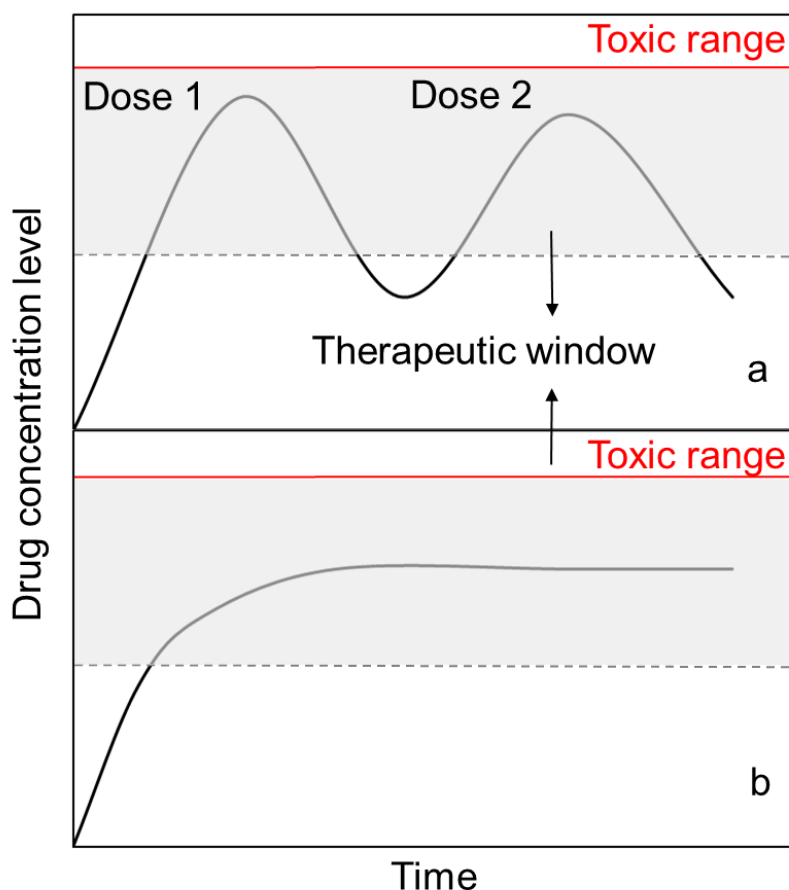
Figure 1-1 Drug concentration levels vs dosage when a) using conventional dosage or b) using a system that has a controlled and sustained release inside the therapeutic window (represented by the grey rectangle).

Most of the drug controlled release systems consist on dispersing the drug or bioactive

agent within a polymeric matrix. Polymer based hydrogels are water swelling, structures

constituted mostly of hydrophilic homopolymers or copolymers [1, 2]. In general, hydrogels

are insoluble because of the physical or chemical crosslinks. The physical crosslinks can be

crystallites, entanglements or weak interactions, like hydrogen bonds or van der Waals forces. Physical reinforcement and network structure are provided via crosslinking [2, 3].

The different type of controlled release system can be classified according to the mechanism regulating the drug release from the system. For instance, using hydrogels as an example, the drug delivery systems (DDS) are categorized as (1) swelling controlled systems, (2) diffusion controlled systems, (3) environmentally responsive systems and (4) chemically controlled systems [3, 4].

Briefly, in the (1) swelling controlled systems (figure 1-2), the bioactive agent is dispersed within a polymer. When it enters in contact with biological fluids the polymer starts to physically swell. At first, no drug diffusion occurs. As the fluid enters the polymer, the relaxation of the polymer macromolecular chains occurs. Consequently, the drug is capable of diffusing out of the swollen polymer.
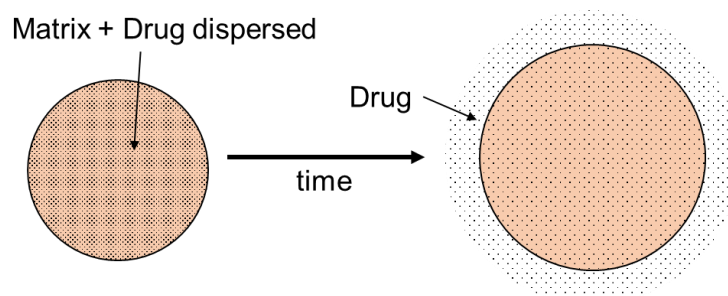
Figure 1-2 Illustration representing the swelling controlled system.

The (2) diffusion controlled release system is the most general mechanism in a DDS (figure 1-3). In this category, there are two main subtypes of diffusion systems: reservoir and matrix devices. Reservoir systems involve of a polymeric membrane surrounding a core containing the drug (e.g. capsules). The drug release rate by diffusion is limited by the outer membrane of the device. However, the drawback of this system is the potential rupture of the outer membrane and its contents will be suddenly release. Concerning the matrix systems, the

drug is distributed all over the biomaterial structure and the drug release occurs via the water

filled pores or through the macromolecular network.
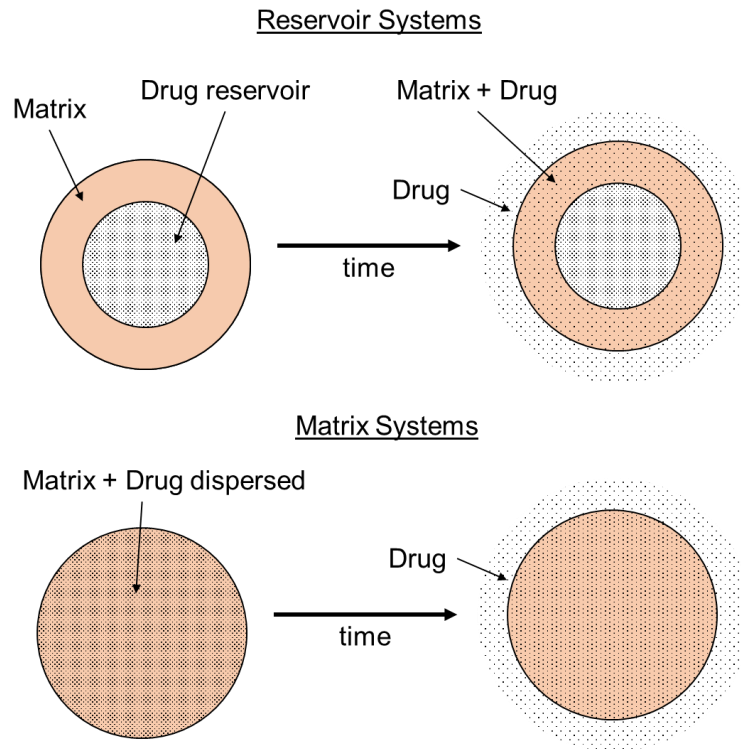
Reservoir Systems

Figure 1-3 Illustration representing the diffusion controlled release systems. Subdivided into the reservoir and matrix systems.

Regarding the (3) environmentally responsive systems (figure 1-4), the biomaterials

might exhibit swelling behavior dependent on the external environmental factors, such as

temperature, pH, ionic strength, composition, presence of enzymes, among others [4].
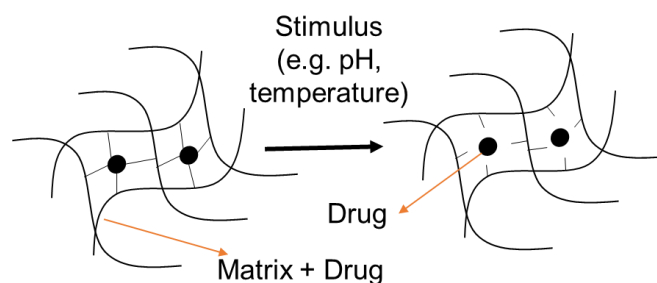
Figure 1-4 Illustration representing the environmentally responsive systems by external stimulus.

At last, in the (4) chemically controlled release mechanisms (figure 1-5), there are two main subtypes: erodible DDS and pendant chain systems [5]. As the name suggests, in the erodible systems, the regulated drug release happens because of the gradual dissolution or degradation of the hydrogel. Whereas, in pendant chain systems the bioactive agent is bonded to the side groups of the polymer skeleton via degradable linkages, and as those links degrade by the influence of enzymes or solvents, the drug is therefore released.
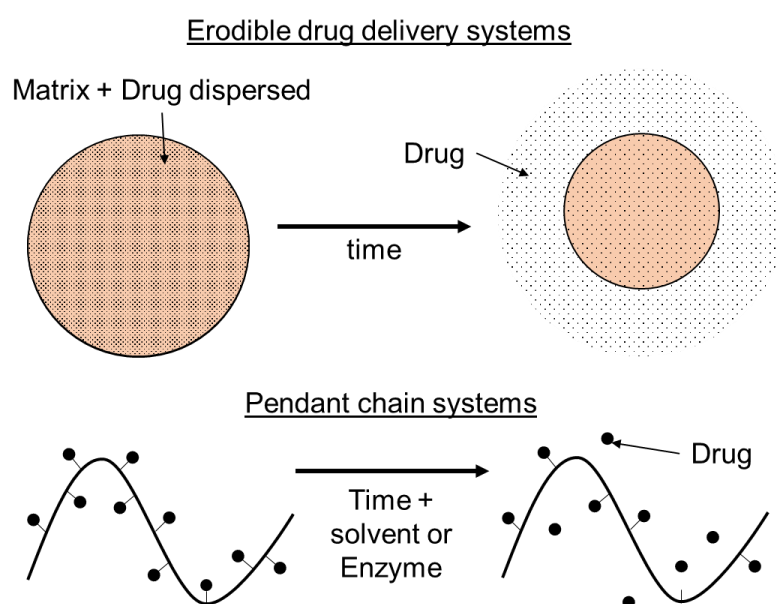
Figure 1-5 Illustration representing the chemically controlled release systems. Subdivided into erodible drug delivery or pendant chain systems.

1.1.1. Drug delivery for gastrointestinal track applications and for antibacterial strategies

The intestinal epithelium of humans has a great absorptive capacity with a surface area in the gastrointestinal (GI) tract of 300–400 m^2 [6]. Nonetheless, oral intake of drugs present some complications, especially for bioactive molecules such as proteins and peptides, due to: (1) low solubility and/or bioavailability, (2) low stability in the harsh gastric environment (low pH, breakdown by enzymes, etc.) and (3) the mucus barrier can hinder the drug penetration and

consequent drug absorption. To reduce these complications, biomaterial formulations that encapsulate and protect the drugs to release them in a time controlled manner are being developed. Another possible strategy, is the modification of the biomaterials surface to increase or reduce bioadhesion to target specific tissues [7].

If the drug delivery is targeted to the gastrointestinal track, proteins, peptides or other small molecules, need to be protected from the harsh environments, usually by encapsulation utilizing polymeric particles with mucoadhesive properties in order to improve the retention time and drug bioavailability. Or, the surface can also be engineered in order to optimize the particle mucoadhesion, cell targeting, and cellular uptake.

Besides the prolonged retention time, increasing the drug bioavailability can be credited to the shielding effect towards proteolytic enzymes. The stability of bioactive molecules is generally improved when encapsulated in polymeric particles [8, 9]. A study demonstrated that a coating of around 160 nm in polylactic acid (PLA) nanoparticles with poly(ethylene glycol) (PEG) offered additional protection against enzyme induced degradation and aggregation in *in vitro* simulated gastrointestinal fluids [10].

The increasing prevalence of multi drug resistant bacteria is a serious challenge [11-13] that requires the researchers to engineer new strategies to overcome this concern. The use of biomaterials as DDS with antibacterial agents is one of the strategies adopted by researchers. Many of the currently used antibiotics present disadvantages, such as short half-life, systemic toxicity, besides the serious concern of higher susceptibility to bacterial resistance. The administration of antibiotics is commonly systemic, via intravenous or oral routes, to treat bacterial infections. Nonetheless, sometimes the efficiency of the drug is reduced, for instance in cases of infections where the bacteria are not responsive to the drug, or in situations in which biofilm formation in the implant can cause implant failure. Therefore, the need to come up with

more efficient DDS. Taking into consideration this growing threat it is essential the development new antimicrobial delivery systems with high bactericidal rates.

The effective release of antibacterial agents at concentrations above the bacteria's minimum inhibitory concentration (MIC) it's essential to avoid infection. Localized and controlled release of antibiotic agents lowers the need of higher dosages when compared with systemic drug intake, and extended time from the release of the drug leads to the reduction of systemic toxicity (decreasing the occurrence of side effects), as well as avoidance of systemic exposure that can consequently lead to bacterial resistance [14, 15]. The reduction of multiple doses becomes easier for the patient to comply. Therefore, DDS that provide a controlled and sustained release are highly beneficial and polymeric delivery systems can be utilized to achieve that purpose. The chemical conjugation of bioactive molecules to polymeric chains proposes several benefits, such as, the tunable release rate based on the bonds that link the drug to the polymer (e.g., amide, ester, carboxyl, etc.) [16, 17], and chemical composition of the polymer (e.g., use of linker molecule) [18, 19]. Therefore, via chemical modifications, the bioactive release rate can be fine-tuned in terms of releasing rate.

1.1.2. Polymers used for controlled delivery

In the last decades, several techniques have been utilized in the pharmaceutical industry in order to improve polymers function for a controlled delivery of bioactive agents. In the case of synthetic polymers, poly(lactic-co-glycolic acid) (PLGA), polyanhydrides, poly(ethylene glycol) (PEG), poly(N-vinyl pyrrolidone), among others, have been applied. But also, natural polymers like complex sugars such as chitosan, collagen, alginate and hyaluronan can be utilized.

For the conjugation of polymer-drug to be effective, several parameters must be taken into account: (1) nonimmunogenic and not toxic carrier; (2) enough molecular weight to ensure

long circulation periods, but still under 40 kDa for nonbiodegradable polymers to guarantee renal elimination after drug release (e.g. N-(2-hydroxypropyl)methacrylamide (HPMA) has a good molecular weight of ~30 kDa [20]); (3) suitable loading/carrying capability of the drug; (4) crosslinker must be stable for the transport but cleaved fairly easy for the release upon arrival at target; and (5) the aptitude to target the desired tissue by active and/or passive methods [21].

Polymers like PLA, PLGA, poly(sebacic acid) (PSA), and poly(acrylic acid) (PAA) can be useful for gastrointestinal applications due to the mucoadhesive features via polymeric entanglements with mucins, hydrophobic interactions, hydrogen bonding or a combination of the mentioned [22]. For instance, microspheres of 680–850 μm containing fumaric acid and sebacic acid displayed prolonged retention in the rat gut, when compared to an alginate particle with weaker adhesive features [23].

Alginate is a natural polymer that has favorable properties, including ease of gelation and biocompatibility, and alginate hydrogels have been interesting for drug delivery purposes. Nonetheless, besides the mechanical weakness, another critic downside is the limited long-term stability in physiological environments due to the ionic cross-linked nature of alginate gels, since these gels can be dissolved via the release of divalent ions into the media due to exchange with monovalent cations [24].

Other more suitable candidates can be considered, such as chitosan, due to its properties and versatility in applications.

1.1.3. Chitosan as drug carrier for controlled delivery

Chitosan is a natural polymer with great potential and versatility in biomedical and pharmaceutical applications due to its biodegradability, biocompatibility, antimicrobial activity, mucoadhesive, non-toxic and non-antigenic properties [25-27], among others.

Chitosan is derived from the partial deacetylation of chitin (figure 1-6), a structural polymer that is abundant in the exoskeletons of crustaceans and insects [28]. The degree of deacetylation is determined by the proportion of D-glucosamine and N-acetyl-D-glucosamine. In terms of structure, chitosan is a straight chain copolymer. Due to its excellent biocompatibility and biodegradability, chitosan has been used in many biomedical applications, including: wound dressings, kidney dialysis membrane, reabsorbable sutures, contact lenses, drug delivery systems and space-filling implants [29]. In Japan (1983) and South Korea (1995) chitosan has been approved as a food additive [30]. Equally, the U.S. Food and Drug Administration (FDA) has approved chitosan (2012) with Generally Recognized As Safe (GRAS) status [31].
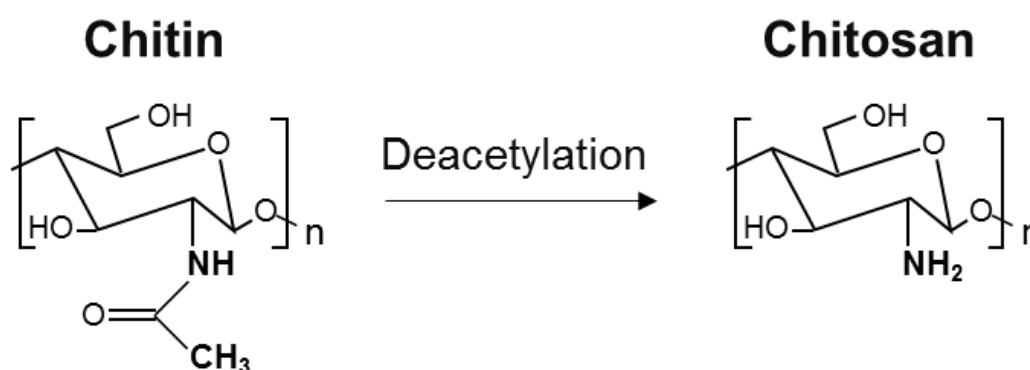
Figure 1-6 Chemical structure of chitin and chitosan.

Its solubility, reactivity, and biodegradability depend on the amount of protonated amino groups in the polymeric chain, thus depends on the proportion of acetylated and non-acetylated D-glucosamine units. The amino groups (pKa from 6.2 to 7.0) are fully protonated in acids with pKa smaller than 6.2 making chitosan soluble [28]. The positive charge from the polymer is obtained due to the free amino groups, allowing it to precede many electrostatic interactions with negatively charged molecules or ions. The amino groups along with the hydroxyl group

provide chitosan its performance by converting it into an extremely reactive polysaccharide. The cationic nature of chitosan can be strategically used for antibacterial purposes, since it inhibits the growth of bacteria [32]. Chitosan has several advantages over other types of antibacterial agents due to a broader range of activity against bacteria, and a lower toxicity towards mammalian cells [33]. It is known that antimicrobial activity of this polymer is influenced by many factors. The chitosan's polycationic structure is indispensable for antibacterial activity. When environmental pH is below the chitosan's pKa, electrostatic interaction occurs between the polycationic polymer and the predominantly anionic constituents of the microorganisms' surface (like lipopolysaccharide and cell surface proteins present in Gram-negative bacteria) play a major role for antibacterial characteristics. When the density of positive charges of chitosan increases, the antibacterial effect will also intensify, as observed with quaternized chitosan [34, 35] and with chitosan metal complex [36]. In contrast, if the polycationic property is reversed or nullified, the antibacterial ability will be weakened or lost.

Chitosan microspheres are widely studied drug delivery system for the controlled release of drugs such as antibiotics, anti-cancer agents, proteins and vaccines. Drug loading in micro/or nanoparticles is achieved via the following methods: (I) incorporation of the drug occurs during the preparation of the particles and/or (II) after the formation of the particles the drug is incubated together with the particles. In both cases, the drug is physically embedded into the matrix as well as adsorbed onto the surface of the particles. Water-soluble and water-insoluble drugs can be loaded by employing these methods [28].

By physically and chemically engineering the properties of the drug carrier to specifically regulate their environmental response, permeability, biodegradability, surface functionality, and biological recognition sites to produce "intelligent" DDS. Chitosan has been used has intelligent DDS. Some examples include the use of chitosan in the preparation of mucoadhesive

formulations improving the dissolution rate of the poorly soluble drugs [28] and drug targeting [37]. One interesting application of chitosan-based delivery systems is for gastric drug targeting because this it protects the therapeutic agents from the hostile conditions of the upper gastrointestinal tract and release the entrapped agents through degradation of the glycosidic linkages of chitosan by colonic microflora [38, 39]. It was reported that chitosan microspheres were successfully optimized for higher acidic resistance via crosslinking with pentasodium tripolyphosphate using two different microencapsulation methods. The microspheres were more stable in SGF, and also achieved a slower release of ampicillin [40].

Degradation is also an important parameter to take into account in all polymers used as DDS, since the degradation of the matrix can be closely associated to the drug release performance. The rate of chitosan degradation is highly related to its deacetylation degree and the molecular weight of the polymer. Chemical degradation is referred to acid-catalyzed degradation as occurs in the stomach, and ideally, both chemical and enzymatic degradation originates byproducts suitable for renal clearance.

In summary, chitosan was chosen as the polymeric matrix for drug delivery systems due to the following advantages:

- Biological properties: bioresorbable, biocompatible (minimal foreign body reaction), and bioactive biopolymer,
- Degradation rate can be regulated,
- The byproducts of degradation are safe,
- Consequently, is already used as food additive,
- Availability of reactive sites for attachment to other bioactive agents.

1.2. Chitosan-siloxane Hybrids

Hybrid materials with organic–inorganic character can be defined as interpenetrating networks of organic and inorganic moieties. Organic–inorganic hybrids can be generally divided into two classes. This division is dependent on the bonding strength amongst the components [41]. In class I, the organic and inorganic constituents are weakly bonded with dynamic interactions, for instance hydrogen bonding, electrostatic forces, ionic and van der Waals', while in class II, strong ionic–covalent or covalent bonds occur between the organic and inorganic constituents. With the increase of interfacial bonding strength, the distribution of the components in the organic–inorganic hybrids is more homogeneous, leading to enhanced mechanical properties [42]. The present work uses class II approach to synthetize hybrids towards the design of biomaterials for biomedical applications. Briefly, class II hybrids can be attained from polymers that contain alkoxysilane precursors in their structure. Upon the addition of these functional precursors, during the sol–gel process their alkoxysilane moieties hydrolyze and condense, forming a covalent bond inorganic network. The resulting structures can be classified into two classes: (1) as silanised polyethers and polyesters presenting sol–gel functionalities as terminal end-groups; and (2) as silanised polysaccharides, polyacrylates or polypeptides manifesting sol–gel functionalities as pendant groups along the backbone of the polymers [43].

In terms of possible applications for organic-inorganic hybrids, these materials show promising features that can be applied in diverse fields, including biomedical applications for human healthcare purposes. The literature shows a perceptible increase in the development of hybrids materials for this intent, for instance, hydrogels for drug delivery systems responsive to stimuli and for antimicrobial responses [44], nanocarriers for controlled therapeutic delivery of biomolecules [45], among many others.

In biomedical sciences, organic-inorganic hybrids that involve natural biodegradable polymers such as chitosan, are studied by researchers in the form of scaffolds, films, hydrogels and spherical particles. Nonetheless, one of the downsides of chitosan is the lack of mechanical endurance, better water-swelling and controlled degradation rate [46]. To solve this disadvantage, crosslinking agents are required. Shirosaki *et al.* prepared organic-inorganic hybrids using chitosan as the polymeric skeleton and γ-glycidoxypropyltrimethoxysilane (GPTMS) monomer as a covalent crosslinker. GPTMS is a member of the silane-coupling agents containing methoxysilane groups and an epoxy ring. Briefly, the methoxysilane groups are active and hydrolyze to yield a silanol group −Si−OH, which later undergoes condensation forming a siloxane Si–O–Si bridging network [47], whereas the epoxy ring opens and interacts with the protonated amino reactive groups of chitosan chains [48, 49]. The grafting of −Si−OH groups into the polymer induces bioactive properties [50]. Shirosaki *et al.* reported that chitosan-GPTMS porous bulk hybrids have very good cytocompatibility with various cell types [48, 49, 51], in addition to assessing the cytotoxicity of GPTMS together with other crosslinking agents for chitosan, in which GPTMS monomer proved to be less cytotoxic than glutaraldehyde for human osteosarcoma cells MG63 [52]. Nonetheless, this precursor compels pH neutralization if the purpose is to be applied in the human body. β-glycerophosphate (β-GP) is a weak base, as well as, one of the osteogenic supplements used when culturing bone marrow mesenchymal stem cells of human origin. Injectable hydrogels using chitosan–β-GP reported good cartilage tissue regeneration [53], but the long time required for their gelation limits the clinical application of these hydrogels. To overcome this, Shirosaki *et al.* synthetized a chitosan-GPTMS hybrid including β-GP, revealing that the time for the gelation of the hydrogels could be controlled by the amount added of GPTMS in the precursor sols, as well as good *in vitro* cytocompatibility with MG63 cells [54]. Figure 1-7 summarizes the reactions and structure bonding between chitosan, GPTMS and β-GP.
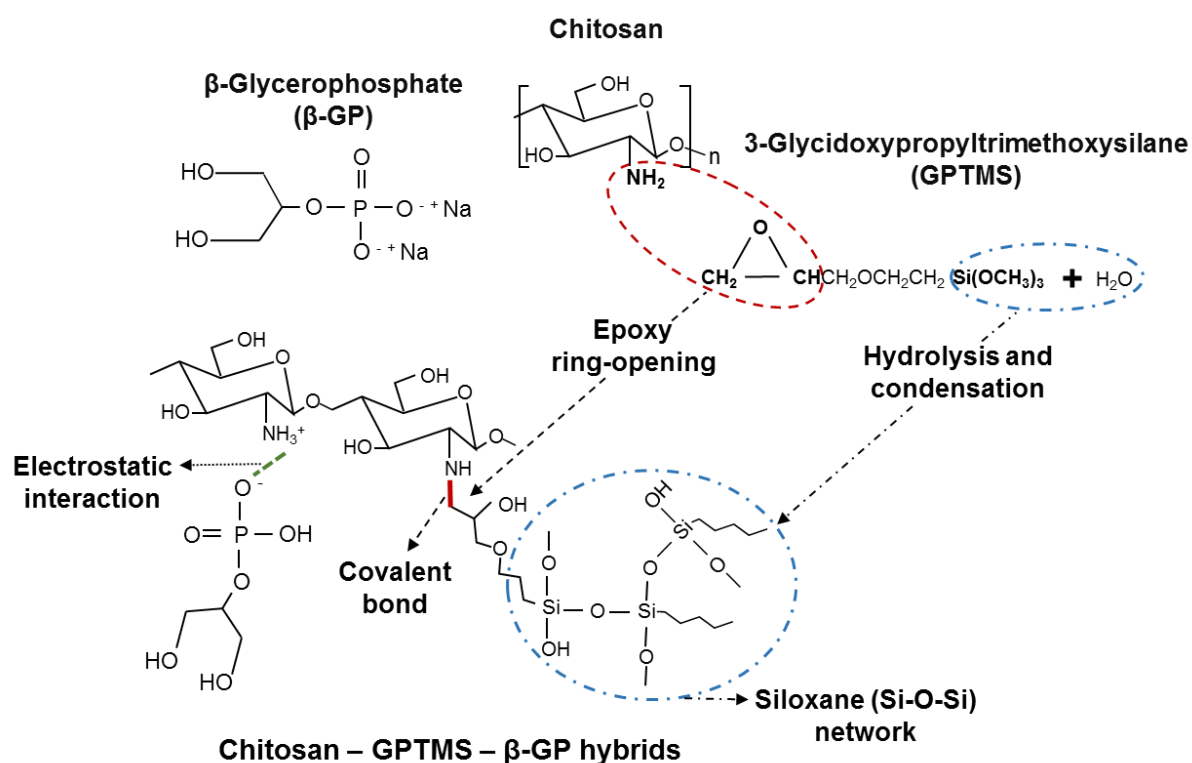
Figure 1-7 Representation of the structure of the hybrid chitosan–GPTMS–β-GP. Structural analysis, such as ninhydrin assay, ^{29}Si and ^{13}C CP-MAS NMR and FT-IR analysis provided information about the structure of chitosan-GPTMS [48, 49] and with β-GP [54].

1.3.   Aims and structure of the thesis

This thesis explores the preparation and characterization of chitosan-based organic-inorganic hybrid, focusing mainly in the spherical shape. Additionally, the release profile of pelargonidin as a drug model was evaluated, as well as, the biological properties of bacteria towards these biodegradable hybrid spheres. Therefore, this thesis is structured in the following arrangement:

Chapter 1 presents a brief background introduction highlighting points about (1) how drug delivery systems overcome the limitation of conventional drug intake, and the type of releasing methods that commonly occur when using polymeric DDS; (2) address the challenges of the drug delivery specifically targeting the gastrointestinal track, as well, as the possible

strategies to overcome these challenges by utilizing DDS, similar topics where discussed for the creation of novel and more effective antibacterial strategies using DDS, to face the growing resistance towards antibiotics. In addition, (3) a brief introduction to the advantages of the use of chitosan as a biocompatible and biodegradable controlled DDS. At last, (4) the chitosan-siloxane hybrid formulation is introduced by crosslinking the chitosan backbone with GPTMS, which leads to improve the physicochemical resistance of chitosan and bioactivity.

Polymeric microspheres are attractive due to their biodegradability and ability to encapsulate drugs or bioactive agents, increasing their bioavailability protecting them from severe environmental conditions in the human body, such as in the gastrointestinal track. Therefore, chapter 2 explores the synthesis of monodisperse and uniform spherical chitosan–GPTMS–β-GP hybrid microspheres using a microfluidic approach. The structural composition of these micro sized spheres was analyzed, as well as the degradation behavior when in contact with different pH solutions simulating gastric fluids and neutral conditions. Along with the elements release from the microspheres matrix during the degradation test. In addition, it was also evaluated the potential of the synthetized chitosan–GPTMS–β-GP hybrid microspheres as a drug delivery system, using pelargonidin as a drug model, under gastro intestinal simulated fluids and digestion cycle time.

The growing antibiotic resistance towards in bacteria is a serious health threat that requires the researchers to engineer new strategies to overcome it. The use of biomaterials as DDS carrying with antibacterial agents is one of the strategies adopted. Taking this into account, chapter 3 explores methods of including cerium, an antibacterial agent, in the chitosan–GPTMS–β-GP microspheres using incorporation and immersion methods. The bacterial growth of *E. coli* (gram-negative) and *S. aureus* (gram-positive) was evaluated, as well as in chitosan–GPTMS–β-glycerophosphate hydrogels with cerium incorporated, using a direct and indirect culture method.

Finally, the chitosan–GPTMS–β-GP microspheres system presented some limitation in the incorporation of cerium, therefore the methodology was adapted. Chapter 4 introduces an alternative microporous spheres prepared by dropping chitosan-GPTMS precursor sols, without β-GP, into liquid nitrogen followed by freeze drying, to overcome the challenges observed when including cerium chloride in the system. The morphology and composition of these hybrids was assessed, along with the antibacterial properties of the spheres containing cerium chloride against both *E. coli* and *S. aureus* bacteria.

And at last, a summary of the main conclusions from each chapter.

References

1.   Lowman, A. M. and Peppas, N. A., *Molecular analysis of interpolymer complexation in graft copolymer networks.* Polymer, 2000, **41**(1): 73-80.

2.   Peppas, N. A., *Hydrogels in medicine and pharmacy: fundamentals.* Vol. 1. 1986: CRC Press. 1-180.

3.   Langer, R. and Peppas, N. A., *Chemical and physical structure of polymers as carriers for controlled release of bioactive agents: a review.* Journal of Macromolecular Science, Part C, 1983, **23**(1): 61-126.

4.   Lowman, A. M., *Biomaterials in drug delivery*, in *Biomedical devices and their applications*, Shi, D., Editor. 2004, Springer Berlin Heidelberg. 1-31.

5.   Heller, J. and Baker, R. W., *Theory and practice of controlled drug delivery from bioerodible polymers*, in *Controlled release of bioactive materials*, Baker , R., Editor. 1980, Academic Press. 1-17.

6.   Schenk, M. and Mueller, C., *The mucosal immune system at the gastrointestinal barrier.* Best Practice & Research Clinical Gastroenterology, 2008, **22**(3): 391-409.

7.   Ensign, L. M., Cone, R., and Hanes, J., *Oral drug delivery with polymeric nanoparticles: The gastrointestinal mucus barriers.* Advanced Drug Delivery Reviews, 2012, **64**(6): 557-570.

8.   Lowe, P. J. and Temple, C. S., *Calcitonin and insulin in isobutylcyanoacrylate nanocapsules: protection against proteases and effect on intestinal absorption in rats.* Journal of Pharmacy and Pharmacology, 1994, **46**(7): 547-552.

9.   Damgé, C., Vranckx, H., Balschmidt, P., and Couvreur, P., *Poly(alkyl cyanoacrylate) nanospheres for oral administration of insulin.* Journal of Pharmaceutical Sciences, 1997, **86**(12): 1403-1409.

10.   Tobío, M., Sánchez, A., Vila, A., Soriano, I., Evora, C., Vila-Jato, J. L., and Alonso, M. J., *The role of PEG on the stability in digestive fluids and in vivo fate of PEG-PLA nanoparticles following oral administration.* Colloids and Surfaces B: Biointerfaces, 2000, **18**(3): 315-323.

11.   Chambers, H. F. and Deleo, F. R., *Waves of resistance: Staphylococcus aureus in the antibiotic era.* Nature reviews. Microbiology, 2009, **7**(9): 629-641.

12.   Levy, S. B. and Marshall, B., *Antibacterial resistance worldwide: causes, challenges and responses.* Nature Medicine, 2004, **10**(12 Suppl): S122-129.

13.   French, G. L., *Clinical impact and relevance of antibiotic resistance.* Advanced Drug Delivery Reviews, 2005, **57**(10): 1514-1527.

14.   Wu, P. and Grainger, D. W., *Drug/device combinations for local drug therapies and infection prophylaxis.* Biomaterials, 2006, **27**(11): 2450-2467.

15.   Hetrick, E. M. and Schoenfisch, M. H., *Reducing implant-related infections: active release strategies.* Chemical Society Reviews, 2006, **35**(9): 780-789.

16.   Qiu, L. Y. and Bae, Y. H., *Polymer architecture and drug delivery.* Pharmaceutical Research, 2006, **23**(1): 1-30.

17.   Uhrich, K. E., Cannizzaro, S. M., Langer, R. S., and Shakesheff, K. M., *Polymeric systems for controlled drug release.* Chemical Reviews, 1999, **99**(11): 3181-3198.

18.   Prudencio, A., Schmeltzer, R. C., and Uhrich, K. E., *Effect of linker structure on salicylic acid-derived poly(anhydride–esters).* Macromolecules, 2005, **38**(16): 6895-6901.

19.   Göpferich, A. and Tessmar, J., *Polyanhydride degradation and erosion.* Advanced Drug Delivery Reviews, 2002, **54**(7): 911-931.

20.   Duncan, R., *The dawning era of polymer therapeutics.* Nature Reviews Drug Discovery, 2003, **2**: 347-360.

21.   Duncan, R., *Polymer conjugates as anticancer nanomedicines*. Nature Reviews Cancer, 2006, **6**: 688-701.

22.   Lai, S. K., Wang, Y.-Y., and Hanes, J., *Mucus-penetrating nanoparticles for drug and gene delivery to mucosal tissues*. Advanced Drug Delivery Reviews, 2009, **61**(2): 158-171.

23.   Chickering, D. E., Jacob, J. S., Desai, T. A., Harrison, M., Harris, W. P., Morrell, C. N., Chaturvedi, P., and Mathiowitz, E., *Bioadhesive microspheres: III. An in vivo transit and bioavailability study of drug-loaded alginate and poly(fumaric-co-sebacic anhydride) microspheres*. Journal of Controlled Release, 1997, **48**(1): 35-46.

24.   Lee, K. Y. and Mooney, D. J., *Alginate: properties and biomedical applications*. Progress in polymer science, 2012, **37**(1): 106-126.

25.   Coue, G. and Engbersen, J. F. J., *Cationic polymers for intracellular delivery of proteins*, in *Cationic polymers in regenerative medicine*, Samal, S. and Dubruel, P., Editors. 2014, The Royal Society of Chemistry. 365-367.

26.   Chandy, T. and Sharma, C. P., *Chitosan-as a biomaterial*. Biomaterials, Artificial Cells and Artificial Organs, 1990, **18**(1): 1-24.

27.   Khor, E. and Lim, L. Y., *Implantable applications of chitin and chitosan*. Biomaterials, 2003, **24**(13): 2339-2349.

28.   Elsabee, M. Z. and Morsi, R. E., *Chitosan: amazing controlled delivery system*, in *Chitin and chitosan derivatives: advances in drug discovery and developments*, Kim, S.K., Editor. 2013, CRC Press. 262-274.

29.   Dutta, P. K., Ravikumar, M. N. V., and Dutta, J., *Chitin and chitosan for versatile applications*. Journal of Macromolecular Science, Part C, 2002, **42**(3): 307-354.

30.   Weiner, M. L., *An overview of the regulatory status and of the safety of chitin and chitosan as food and pharmaceutical ingredients*, in *Advances in chitin and chitosan,*

Brine, C.J., Standford, P.A., and Zikakis, J.P., Editors. 1992, Elsevier Applied Science. 663-672.

31. Fda. *Gras notices: Shrimp-derived chitosan.* [cited 2016 16 March]; Available from: https://www.fda.gov/downloads/Food/IngredientsPackagingLabeling/GRAS/NoticeInventory/ucm337459.pdf.

32. Wu, S., Liu, X., Yeung, A., Yeung, K. W. K., Kao, R. Y. T., Wu, G., Hu, T., Xu, Z., and Chu, P. K., *Plasma-modified biomaterials for self-antimicrobial applications.* ACS Applied Materials & Interfaces, 2011, **3**(8): 2851-2860.

33. Kong, M., Guang Chen, X., Xing, K., and Jin Park, H., *Antimicrobial properties of chitosan and mode of action: a state of the art review.* International Journal of Food Microbiology, 2010, **144**(1): 51-63.

34. Xie, Y., Liu, X., and Chen, Q., *Synthesis and characterization of water-soluble chitosan derivate and its antibacterial activity.* Carbohydrate Polymers, 2007, **69**: 142-147.

35. Ignatova, M., Starbova, K., Markova, N., Manolova, N., and Rashkov, I., *Electrospun nano-fibre mats with antibacterial properties from quaternised chitosan and poly(vinyl alcohol).* Carbohydrate research, 2006, **341**(12): 2098-2107.

36. Wang, X., Du, Y., and Liu, H., *Preparation, characterization and antimicrobial activity of chitosan-Zn complex.* Carbohydrate Polymers, 2004, **56**: 21-26.

37. Gallo, J. M. and Hassan, E. E., *Receptor-mediated magnetic carriers: basis for targeting.* Pharmaceutical Research, 1988, **5**(5): 300-304.

38. Hejazi, R. and Amiji, M., *Chitosan-based gastrointestinal delivery systems.* Journal of Controlled Release, 2003, **89**(2): 151-165.

39. Hyung Park, J., Saravanakumar, G., Kim, K., and Kwon, I., *Targeted delivery of low molecular drugs using chitosan and its derivatives.* Advanced Drug Delivery Reviews, 2009, **62**(1): 28-41.

40. Anal, A. K., Stevens, W. F., and Remuñán-López, C., *Ionotropic cross-linked chitosan microspheres for controlled release of ampicillin.* International Journal of Pharmaceutics, 2006, **312**(1): 166-173.

41. Novak, B. M., *Hybrid nanocomposite materials—between inorganic glasses and organic polymers.* Advanced Materials, 1993, **5**(6): 422-433.

42. Mammeri, F., Bourhis, E. L., Rozes, L., and Sanchez, C., *Mechanical properties of hybrid organic-inorganic materials.* Journal of Materials Chemistry, 2005, **15**(35-36): 3787-3811.

43. Poologasundarampillai, G. and Maçon, A. L. B., *Organic–inorganic hybrid biomaterials*, in *Bioactive glasses: fundamentals, technology and applications*, Boccaccini, A.R., Brauer, D.S., and Hupa, L., Editors. 2016, Royal Society of Chemistry. 286-299.

44. Ye, E. and Loh, X. J., *Polymeric hydrogels and nanoparticles: a merging and emerging field.* Australian Journal of Chemistry, 2013, **66**(9): 997-1007.

45. Loh, X. J., Lee, T. C., Dou, Q., and Deen, G. R., *Utilising inorganic nanocarriers for gene delivery.* Biomaterials Science, 2016, **4**(1): 70-86.

46. Remuñán-López, C. and Bodmeier, R., *Mechanical, water uptake and permeability properties of crosslinked chitosan glutamate and alginate films.* Journal of Controlled Release, 1997, **44**(2-3): 215-225.

47. Brinker, C. J. and Scherer, G. W., *Sol-gel Science: The Physics and Chemistry of Sol-gel Processing.* 1990: Academic Press.

48. Shirosaki, Y., Tsuru, K., Hayakawa, S., Osaka, A., Lopes, M. A., Santos, J. D., Costa, M. A., and Fernandes, M. H., *Physical, chemical and in vitro biological profile of chitosan hybrid membrane as a function of organosiloxane concentration.* Acta Biomaterialia, 2009, **5**(1): 346-355.

49.   Shirosaki, Y., Tsuru, K., Hayakawa, S., Osaka, A., Lopes, M. A., Santos, J. D., and Fernandes, M. H., *In vitro cytocompatibility of MG63 cells on chitosan-organosiloxane hybrid membranes.* Biomaterials, 2005, **26**(5): 485-493.

50.   Negahi Shirazi, A., Fathi, A., Suarez, F. G., Wang, Y., Maitz, P. K., and Dehghani, F., *A Novel Strategy for Softening Gelatin–Bioactive-Glass Hybrids.* ACS Applied Materials & Interfaces, 2016, **8**(3): 1676-1686.

51.   Shirosaki, Y., *Preparation of organic-inorganic hybrids with silicate network for the medical applications.* Journal of the Ceramic Society of Japan, 2012, **120**(1408): 555-559.

52.   Shirosaki, Y., Okayama, T., Tsuru, K., Hayakawa, S., and Osaka, A., *In vitro bioactivity and MG63 cytocompatibility of chitosan-silicate hybrids.* International Journal of Materials and Chemistry, 2013, **3**(3A): 1-7.

53.   Chenite, A., Chaput, C., Wang, D., Combes, C., Buschmann, M. D., Hoemann, C. D., Leroux, J. C., Atkinson, B. L., Binette, F., and Selmani, A., *Novel injectable neutral solutions of chitosan form biodegradable gels in situ.* Biomaterials, 2000, **21**(21): 2155-2161.

54.   Shirosaki, Y., Hirai, M., Hayakawa, S., Fujii, E., Lopes, M. A., Santos, J. D., and Osaka, A., *Preparation and in vitro cytocompatibility of chitosan–siloxane hybrid hydrogels.* Journal of Biomedical Materials Research Part A, 2015, **103**(1): 289-299.

Chapter 2.

SYNTHESIS OF CHITOSAN-SILOXANE HYBRID MICROSPHERES USING A MICROFLUIDIC APPROACH AND RELEASE OF PELARGONIDIN IN GASTROINTESTINAL SIMULATED CONDITIONS

2.1. Introduction

Biodegradable microspheres present a number of advantages compared to conventional drug delivery systems. For example, they permit the release of insoluble allow, and the release is done in a more sustained and controlled way over time, as a result reducing the necessity for multiple doses [1, 2]. Moreover the polymeric based system, either from natural or synthetic source, are normally cleaved into biocompatible byproducts bringing no harm to the human body [3]. Even if microspheres are small in size, they possess large surface area to volume ratios [1, 2]. Chitosan-mediated systems can significantly improve the bioavailability of drugs across the epithelial layer of the oral cavity [4] and gastrointestinal track [5], most likely due to its mucoadhesiveness. In Japan (1983) and South Korea (1995) chitosan has been approved as a food additive [6]. Equally, the U.S. Food and Drug Administration (FDA) has approved chitosan (2012) with Generally Recognized As Safe (GRAS) status [7]. Chitosan is a natural polymer that comprises polysaccharide linear chains. The bioresorbable, biocompatible, non-toxic, mucoadhesive and non-antigenic [8-10] properties of chitosan make it a promising and versatile candidate for medical applications. However, chitosan lacks controlled degradation rate and mechanical endurance [1]. To overcome these drawbacks, crosslinking agents without toxic effects are required. Shirosaki *et al.* [11] described that MG63 cells from human osteosarcoma, exhibited good cytocompatibility on chitosan–GPTMS–β-GP hybrid hydrogels

rather than chitosan–β-GP system. Due to its *in vitro* cytocompatibility, this chitosan–GPTMS–β-GP hybrid could potentially be applied in other shapes or for alternative purposes besides the sole of as an injectable biomaterial.

Good size uniformity has been reported when using a microfluidic approach for the synthesis of microspheres [12]. For drug delivery systems, the uniformity of microparticle size is a particular important parameter to take into account. Cruz-Neves *et al.* [13] reported the production of chitosan-siloxane hybrid microspheres using a microfluidic approach that are able to withstand harsh pH gastric simulated environments, in addition to fulfilling the size uniformity requirement, and the obtained size is adequate for gastrointestinal drug delivery because it avoids internalization by gastric cells. In fact, some researchers [14, 15] reported the use of microparticles for gastrointestinal drug delivery with size ranging from 400-1000 μm presenting good drug entrapment efficiency. Additionally, this microfluidic method is simple and generally uses small volumes of solutions.

The evaluation of the degradation rate of a biomaterial is an essential parameter. The human body possesses a different range of pH levels. The neutral pH reference for the arterial blood ranges from 7.35 to 7.45 [16-18]. In opposition, the pH of the stomach fluids of healthy individuals in the second and third postprandial period ranged from 1.7 to 4.3 [19]. Whereas, the pH in the duodenum when a meal is ingested decreased from 6.1 to 5.4 [20]. Then, the pH gradually increases again, reaching around pH 6.7 in the rectum [21]. Schwarz *et al.* reported the gastric emptying and gastrointestinal transit times in humans after the ingestion of ^{19}F-filled capsule, the capsule remained in the stomach for 2 h. The tracking capsule was eventually excreted after 57 h [22]. Pelargonidin ($C_{15}H_{11}ClO_5$) is one of the anthocyanins which possesses antioxidant properties and, consequently, plays a role on the protection against a myriad of human diseases, such as prevention of cardiovascular and neuronal diseases, diabetes, among others [23-25]. Figure 2-1 illustrates the gastrointestinal track in terms of pH and time of

digestion cycle, as well as the chitosan–GPTMS–β-GP spheres including pelargonidin with the purpose of increasing the delivery of pelargonidin throughout the intestinal villi to protect its bioavailability and increase the absorption rate of this antioxidant agent.
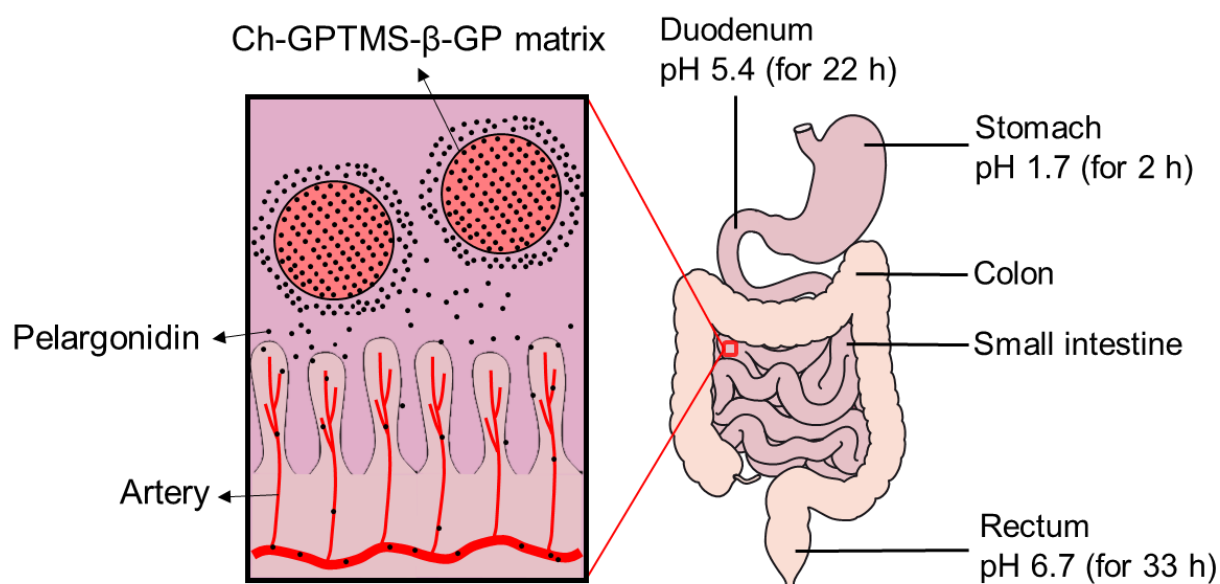
Figure 2-1 Schematic representation of the simulated gastrointestinal conditions in terms of pH and a whole digestion cycle in humans (total time of 57 h) and delivery of pelargonidin for an increased absorption by the intestinal villi.

In the present chapter, a microfluidic system was used to synthesize chitosan-GPTMS-β-GP hybrid microspheres. The structural composition of the microspheres was analyzed and the degradation rates were observed under several pH conditions. In addition, their stability and elemental release from the microspheres matrix were evaluated. The microspheres also incorporated pelargonidin as a drug model and the *in vitro* releasing behavior was tested in a simulated stomach environment pH and human digestion cycle period.

2.2.   Materials and methods

2.2.1 Synthesis of chitosan-siloxane hybrid microspheres

To attain a concentration of 2% (w/v), chitosan (high molecular weight, DA > 75%, Sigma-Aldrich®, Saint Louis, USA) was dissolved in 0.1 M hydrochloric acid (HCl). The polymeric solution was homogenized in a planetary centrifugal mixer (ARE-310, Thinky, Tokyo, Japan) at room temperature, followed by autoclaving for 20 min at 121°C. While still hot, the solution was filtered (polyethersulfone, 0.22 μm pore) using a vacuum system to obtain a more homogeneous solution. A determined amount of GPTMS (97%, Alfa Aesar, Heysham, UK) was inserted drop by drop in the chitosan solution, and the mixture stirred for 2 h at room temperature. To neutralize the precursor sol pH to 7, for 10 mL of chitosan-GPTMS, 3.25 mL of 2.5 M β-GP (pH 9.6, Sigma-Aldrich®, Saint Louis, USA) was added drop by drop and stirred at 0°C for 10 min. The microfluidic method consisted of two syringe pumps (KeyChem, YMC CO. LTD, Kyoto, Japan), one containing the oil solution and the other holding the hybrid solution. Both syringes were attached to a Y-shaped microchannel displayed in figure 2-2. The precursor sol was the dispersed phase, while the oily solution of 4% (w/v) span/squalene (Fluka, Tokyo, Japan / Sigma-Aldrich®, Saint Louis, USA) was the continuous phase. When both solutions merged inside the Y microchannel, the microspheres were formed as depicted in figure 2-2. Some of the tested, as well as, the optimized conditions used in the microfluidic system are listed in table 2-1. Then, the micro sized drops were gelated for 1 h at 60°C in the 4% (w/v) span/squalene oil solution. The microspheres were washed in a series of graded ethanol dilutions of 100, 90, 80, 70, 60, 50 and 25%, and finally kept in distilled water, to remove the oil. The microspheres were sterilized by autoclaving at 121°C for 20 min in distilled water.

Table 2-1 Some of the tested conditions and the optimized parameters used in the microfluidic system and its starting compositions.

Sample	Molar ratio		Flow rate (mL/min)		Channel (mm)		Outlet (mm)	Shape
	Chitosan	GPTMS	Oil	Sol	Depth	Width		
ChG10	1.0	1.0	0.100	0.005	1.0	0.8	1.0	Sphere
ChG15	1.0	1.5	0.100	0.005	1.0	0.8	1.0	Sphere
SChG10	1.0	1.0	0.012	0.001	0.5	0.5	0.5	Sphere
SChG15	1.0	1.5	0.012	0.001	0.5	0.5	0.5	Sphere
TChG10	1.0	1.0	0.080	0.010	1.0	0.8	1.0	Tube like
STChG15	1.0	1.5	0.020	0.003	0.5	0.5	0.5	Tube like
-	1.0	1.0	0.050	0.010	0.5	0.8	0.3	x
-	1.0	1.0	0.008	0.001	0.3	0.5	0.3	x
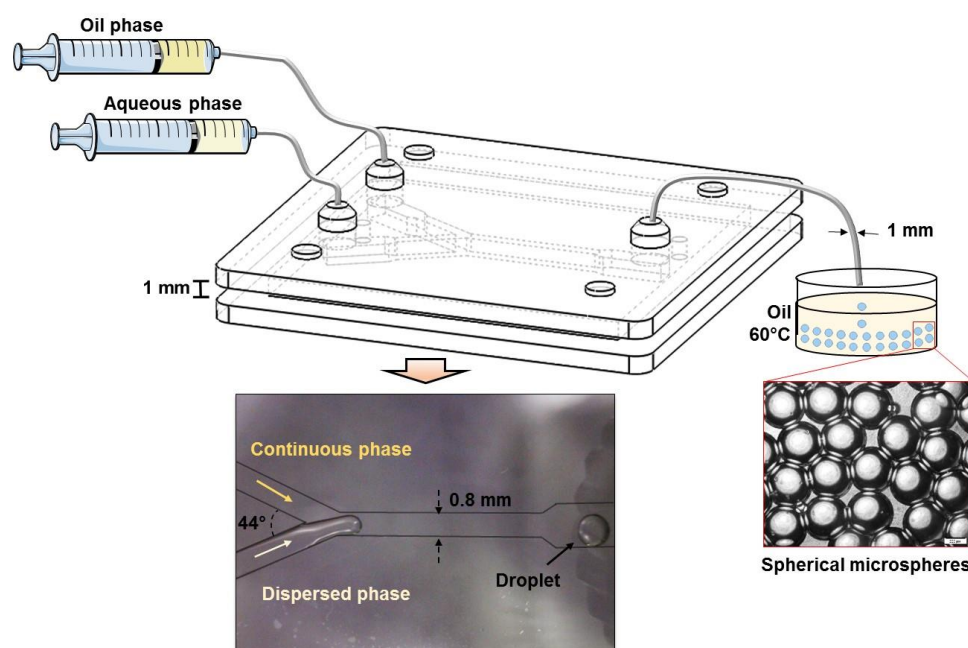
Figure 2-2 Schematic representation of the microfluidic system constituents and microspheres before the gelation. The shape and dimensions of the microchannel used in the production of ChG10 and ChG15 are also represented.

2.2.2 Structural characterization of the microspheres

The produced samples were examined under a bright-field microscope (IX73, Olympus, Tokyo, Japan) to determine the size and shapes. To measure the diameter of > 100 microspheres ImageJ v1.48 software (National Institutes of Health, USA) was utilized. The surface morphology of the ChG10 and ChG15 microspheres was examined using scanning electron microscopy (SEM, JMS-6010 PLUS/LA, JEOL, Tokyo, Japan) equipped with an energy dispersive X-ray spectrometry (EDS) to detect the elements existing in the samples at a working distance of 10 mm and 15 kV of operating voltage. The microspheres were coated for 30 s corresponding to a 15 nm thick layer of Pt/Pd using a magnetron-sputter coater (MSP-1S Magnetron Sputter, Vacuum Device Inc., Mito, Japan).

To determine the internal water content of the samples, weight measurements were executed before and after drying at 100°C until the samples were completely dried. The subsequent equation was used to determine the water content:

$$\text{Water content (\%)} = (Ww - Wd)/\ Ww \times 100 \qquad (1)$$

where, Ww and Wd symbolizes the wet and dry weight, respectively.

The microspheres surface charge and potential stability in phosphate buffered saline (PBS, pH 7.4, Gibco, New York, USA) and in distilled water were measured via Zeta Potential (ELS-Z, Photal Otsuka Electronics Co. LTD, Osaka, Japan) using the rectangular cell. Attenuated Total Reflectance Fourier Transform Infrared spectroscopy (ATR-FTIR, FT/IR-6100, JASCO Co., Tokyo, Japan) was carried out to assess the structure of the samples, using an attenuated total reflectance method (ATR PRO0450-S JASCO Co., Tokyo, Japan) with a diamond prism. The characterization was done at a spectral resolution of 4 cm^{-1} on a frequency region of 400 to 4000 cm^{-1} and 200 scans were accumulated per sample. Solid-State ^{13}C, ^{29}Si, ^{31}P, and ^{1}H NMR measurements were performed to acquire a structural insight of the samples

structures, using an Agilent DDS 500 MHz NMR spectrometer (Agilent Technologies, Inc., Santa Clara, USA) operating at 11.7 Tesla. A zirconia rotor with 3.2 mm of diameter was used with an Agilent HXY T3-MAS probe. For magic angle spinning (MAS) the rotor spinning frequency was set at 15 kHz. ^{1}H → ^{13}C cross-polarization (CP)-MAS NMR experiments were carried out with contact time of 500 μs and recycle delay of 10 s, in which the signals of 3700 and 5400 pulses were collected for ChG15 and ChG10 samples, respectively, with adamantane ($C_{10}H_{16}$) as the external reference (38.52 ppm vs. 0 ppm TMS). Additionally, ^{1}H MAS NMR spectra was recorded at 499.8 MHz with a 1.15 μs pulse length (pulse angle, π/4) and 5 s recycle delays, where the obtained signals of 8 pulses were accumulated with adamantane ($C_{10}H_{16}$) as the external reference (1.91 ppm vs. 0 ppm TMS). Moreover, ^{1}H → ^{29}Si CP-MAS NMR measurements were carried out with contact time of 5 ms and recycle delay of 5 s, where the acquired signals of 40,580 and 79,460 pulses were accumulated for ChG15 and ChG10 miscrospheres, respectively, with polydimethylsilane (PDMS) as the external reference (−34.44 ppm vs. 0 ppm TMS). Direct polarization ^{31}P MAS NMR spectra were measured at 202.3 MHz at a 1.4 μs pulse length (π/4-pulse angle) and 120 s recycle delays with $NH_4H_2PO_4$ as the external reference (1.0 ppm vs. 0 ppm 85% H_3PO_4). The obtained signals of 508 and 718 pulses were accumulated for ChG15 and ChG10 samples, respectively. ^{1}H high-power decoupling was used during the ^{31}P acquisition. ^{1}H → ^{31}P CPMAS NMR measurements were also carried out with a contact time of 1 ms and recycle delay of 5 s, where the measured signals of 1000 and 2720 pulses were accumulated for ChG15 and ChG10 microspheres, respectively.

The amount of free amino groups ChG10 and ChG15 microspheres was evaluated using the ninhydrin (2,2-dihydroxyindane-1,3-dione) assay [26]. Ninhydrin solution (Ninhydrin coloring solution Kit for HITACHI, Wako, Osaka, Japan) was added in a ratio (v/v) of buffer:ninhydrin=3:1 into the tubes containing the dried microspheres and control. Glucosamine hydrochloride (U. S. Pharmacopeia, Rockville, USA) was used as a reference

control. The samples and control (2 mg) were kept at 80°C for 20 min in static conditions. The samples cooled down for 1 h. The supernatant was collected and the optical absorbance of the solutions was recorded at 570 nm with an ultraviolet–Visible (UV-VIS) spectrophotometer (DeNovix DS-11+/W, SCRUM Inc., Wilmington, USA). The free amino groups on the spheres were calculated using the following formula:

Sample (moles/mg) = (Abs$_{570\,nm}$ sample / Abs$_{570\,nm}$ control) × control (moles/mg) (2)

where, Abs stands for absorbance.

2.2.3 Compression test and thermogravimetric analysis

Compression assays (Rheoner II Creep meter RE2-3305C, Yamaden, Tokyo, Japan) were carried out to evaluate the stress-deformation behavior of the micro sized spheres under a uniaxial compressive load. A load of 20 N was applied via a cylindrical probe with a diameter of 3 mm, and a descending speed of 0.05 mm/s. Individual microspheres were subjected to these compression conditions, and replicates were performed for ChG10 and ChG15 samples.

The samples were subjected to high heat conditions to analyze its thermal decomposition with simultaneous recordings of the samples weight loss during the analysis using thermogravimetric (TG) and differential thermal analysis (DTA) (TG-DTA 2000S, Mac Science, Co., Yokohama, Japan) using a heating rate of 10°C/min, from room temperature to 800°C in regular atmospheric conditions.

2.2.4 Degradation assay under several pH conditions

For the degradation measurements 200 microspheres were soaked in solutions of three different pH environments. The gastric juices secreted by parietal cells present in the stomach consist of 0.1 M HCl [27, 28]. For that reason, to mimic the acidic gastric environments, the micro sized spheres were incubated in 0.1 M HCl solutions of pH 1.7 and 5.4 (adjusted with

0.2 M NaOH, Nacalai Tesque, Kyoto, Japan). The flasks (Simport, Québec, Canada) containing the samples were submitted to a water bath set at 36.5°C and agitated at 100 rpm for 14 days. For the neutral pH condition experiment, n=200 samples were incubated in PBS (pH 7.4) under the same experimental parameters. At the designated time points, the microspheres were collected and the surrounding excess of soaking solution was thoughtfully pipetted and the weight was recorded. The mass percentage in the samples was calculated by comparing the remaining weight with the initial weight, by means of the following equation:

$$\text{Weight loss (\%)} = (Wb - Wa)/ Wb \times 100 \qquad (3)$$

where, Wb and Wa stands for the weight before and after soaking, respectively.

The supernatant from the degradation experiments was reserved to track pH changes (pH meter LAQUAtwin B-712, Horiba, Kyoto, Japan) and also to evaluate the elements released from the matrix of the microspheres to the supernatant. The detection of the phosphate and silicon released into the supernatant during the degradation test was carried out using inductively coupled plasma atomic emission spectrometer (ICP-AES; ICPE-9820, Shimadzu, Kyoto, Japan).

After the degradation tests, the surface morphology as well as the elements present at the surface of the samples were observed via SEM. To identify changes in the microspheres crystallinity after the degradation tests, the samples were scanned using powder X-Ray Diffraction (XRD, MXP3V, Mac Science, Co., Yokohama, Japan) with CuKα radiation. The analysis were carried out using the following parameters: for the 2θ angle ranging from 5.020° to 40.000° with a step size of 0.020°, an operating voltage of 40 kV and current of 30 mA, and a counting time of 1 s.

2.2.5 Incorporation of pelargonidin in chitosan-siloxane hybrid microspheres

The incorporation of pelargonidin followed similarly the conditions used as in the synthesis of the ChG10 and ChG15 microspheres. Briefly, a fresh 2% (w/v) chitosan solution was prepared, autoclaved and filtered. GPTMS was added to chitosan solution in the molar ratios to produce ChG10 and ChG15 microspheres, and the mixture was stirred at RT for 2 h. Pelargonidin chloride ($C_{15}H_{11}ClO_5$, Sigma-Aldrich®, Saint Louis, USA) was dissolved in a 50% (v/v) solution of 100% ethanol / 0.1 M HCl to achieve a 1 mg/mL. Afterwards, 0.5 mL of pelargonidin were added to 2 mL of ChG10 or ChG15 precursor sols. The solutions were mixed for 20 min at RT. A volume of 0.67 mL of 2.5 M β-GP were then added on each composition. The solution was applied in a microfluidic system to produce microspheres with pelargonidin chloride, using the same production parameters as described in section 2.2.1. The microspheres with pelargonidin chloride were denoted as ChG10P and ChG15P, respectively. The gelation of the microspheres occurred at 60°C for 1 h. The obtained microspheres were rinsed with ethanol dilutions of 100 (3x), 90 (1x), 70 (1x), 50 (1x), 25% (1x), and finally kept in distilled water.

2.2.6 *In vitro* release of pelargonidin in simulated gastrointestinal conditions

To simulate gastric fluids conditions microspheres, n=400/replicate of ChG10P and ChG15P were incubated in 1.5 mL of 0.1 M HCl [27, 28] solutions of pH 1.7 for 2 h, followed by 1.5 mL of solution at a pH 5.4 from 2 h to 24 h, and finally at 1.5 mL of pH 6.7 from 24 h to 57 h (pHs previously adjusted with 0.2 M NaOH). The microspheres containing pelargonidin were incubated at 37°C and agitated at 700 rpm (Block Bath Shaker MyBL-100S, AsOne, Osaka, Japan) during a total time of 57 h. In terms of controls, ChG10 and ChG15 were also incubated in SGF. The UV-VIS readings were performed at several time points (1, 2, 4, 6, 8, 12, 24, 36, 48 and 57 h). The supernatant was collected and the optical absorbance of the

solutions was recorded with an UV-VIS spectrophotometer. After each reading, fresh SGF solution was inserted and the incubation proceeded.

The standard curve for pelargonidin was performed in identical situations as in the incorporation of pelargonidin in the microspheres. Pelargonidin chloride was completely dissolved in a 50% (v/v) solution of 100% ethanol / 0.1 M HCl making a 1 mg/mL (ChG10P1 and ChG15P1) and 3 mg/mL (ChG10P3 and ChG15P3) stock solution. Afterwards, 1 mL of the pelargonidin stock solution was dissolved in 19 mL 0.1 M HCl. Afterwards. 6.5 mL of β-GP were slowly added to reach a pH 7. The solution was submitted to 60°C for 1 h. Subsequently, for each 3 mL of the previously prepared solution, the pH was adjusted to 1.7 slowly adding 0.74 mL of 1 M HCL. Like the samples, the solution was incubated at 37°C and the UV-VIS was measured in the chosen time points. Next, the pH of the solution was slowly increased to 5.4 using 1.38 mL of 0.2 M NaOH, and submitted to 37°C and measured the absorbance in the respective time points. Finally, the pH was slowly raised to 6.7 using 2.1 mL of 0.2 M NaOH and incubated for the last time points at 37°C. The baseline solutions for the UV-VIS recording of the standard curve of pelargonidin was performed using the corresponding SGF solutions prepared using exactly the same steps, but without pelargonidin. To assess the swelling behavior of the microspheres containing pelargonidin, the size of the microspheres containing pelargonidin together with the respective controls were evaluated under a bright-field microscope at 0, 2 h (pH 1.7), 24 h (pH 5.4) and 57 h (pH 6.7). The diameter of more than 50 microspheres was measured using the same software as before.

2.2.7 Statistical analysis

The statistical analysis was performed using one-way analysis of variance ANOVA followed by Tukey's test and the significance level of $p < 0.05$. GraphPad Prism (GraphPad Prism Software version 6, CA, United States) was used to run the statistical analysis.

2.3.   Results

2.3.1 Synthesis of microspheres by microfluidic system and their microstructure

The production of the chitosan and chitosan-β-GP without GPTMS as controls system was attempted on the microfluidic. However, the microspheres were not obtained due to the slow gelation time, as a result the samples crumbled when handling. Therefore, GPTMS plays a necessary role in the production of the micro sized spheres using this microfluidic approach.

Using the optimized conditions reported in table 2-1, monodispersed micro sized spheres with uniform dimensions were acquired (figure 2-3a,b), namely 638 ± 15 µm for ChG10 and 661 ± 23 µm for ChG15. Additionally, the produced samples had a spherical morphology regardless of the molar ratio composition. Moreover, by varying the microfluidic system parameters (table 2-1) such as microchannel dimensions, inlet and outlet tube diameters and speed on the syringe pumps, SChG15 smaller spheres with size around 285 ± 34 µm could be obtained (figure 2-3b). Furthermore, additional microparticles with other shapes besides spherical could also be acquired, like microfibers or tube like particles as STChG15 (figure 2-3c). Though, the effort of this work was towards producing microspheres.

Similarly to what was perceived in previous studies [11], a higher content of GPTMS caused a decrease on the gelation time of the hybrid solution into hydrogels. As a result, the maximum molar ratio applied was chitosan:GPTMS = 1:1.5. When above this ratio, early gelation of the solution rapidly occurred inside the syringe, inlet tube and microchannel. Leading to a higher viscosity of the solution, which interrupted the normal flow rate of the solutions, and as a result it hindered the ability to continue and perform a long-term synthesis of samples.
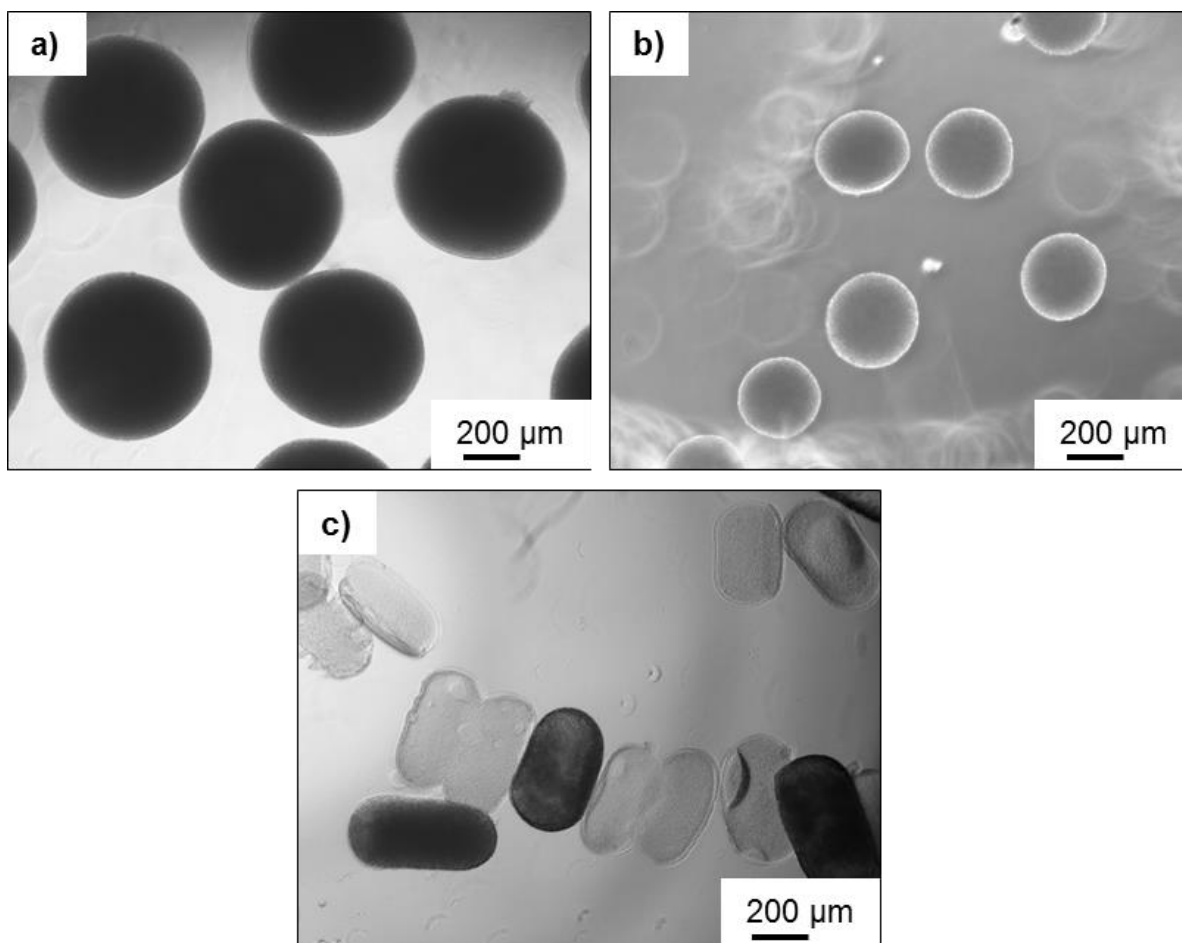
Figure 2-3 Brightfield images (obj. 4×) of a) ChG15, b) SChG15 microspheres and c) STChG15 tube like shape sample, all after gelation.

ChG10 and ChG15 micro sized spheres confined different water amounts in the matrix depending on the GPTMS molar ratio applied. Specifically, ChG10 retained 87.5% of water, while ChG15 only held 59.1% of water. Figure 2-4 displays the SEM images of the ChG10 and ChG15 surfaces. The samples were of spherical shape, even after drying. Regardless of the composition, the samples surface topography was rugged with visible nanosize pores.

The produced microspheres displayed zeta potential values closer to +30 or −30 mV and half of those amounts. When in PBS, ChG10 and ChG15 spheres showed zeta potential values of −13.80 ± 1.49 mV and −27.41 ± 0.92 mV, respectively. Whereas, in distilled water ChG10 and ChG15 samples presented values of 33.68 ± 1.84 mV and 15.59 ± 2.38 mV, respectively.
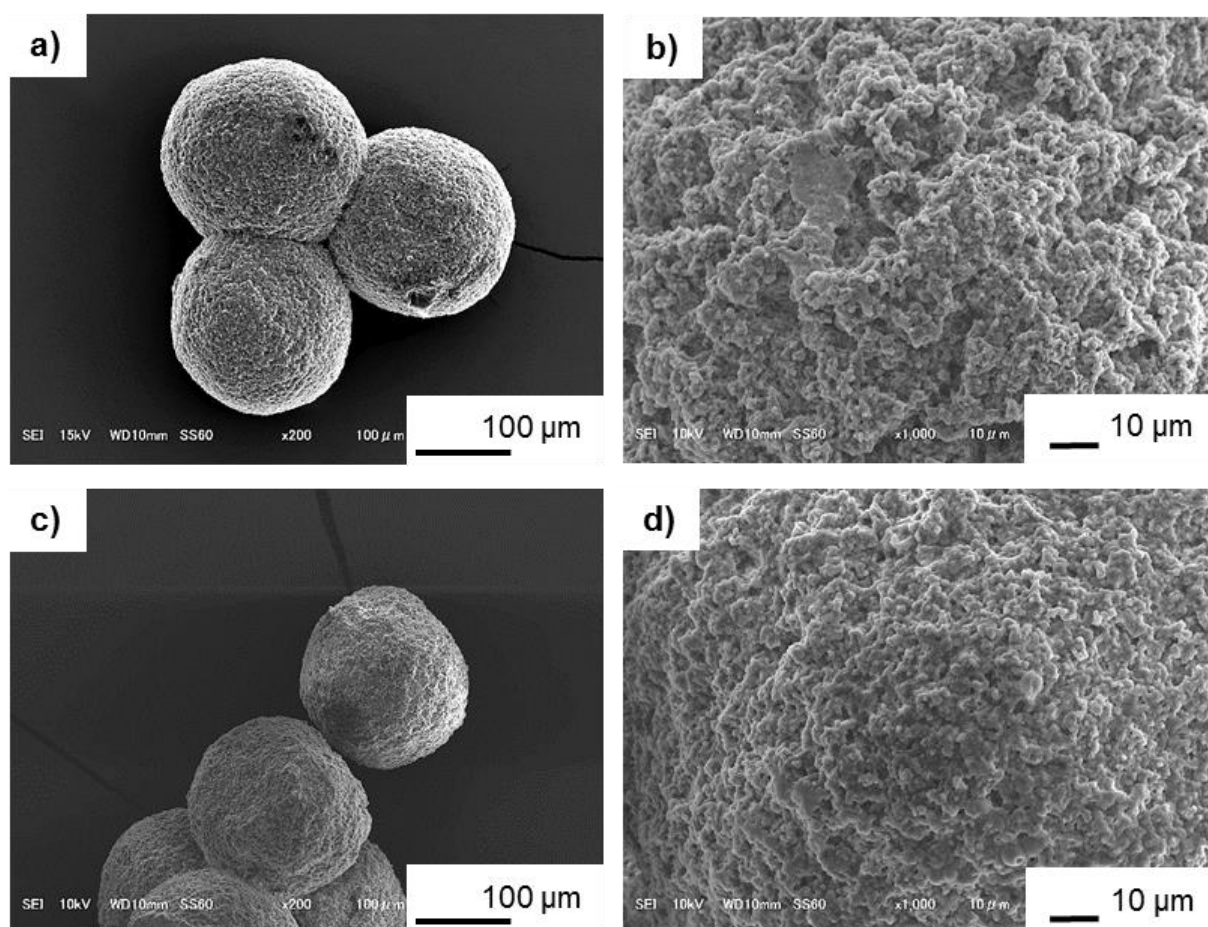
Figure 2-4 SEM images of a) ChG10 and c) ChG15 dried microspheres before degradation test. b) and d) are a magnified view of a) and c), respectively.

ATR-FTIR spectra of the samples is displayed in figure 2-5. β-GP presented a band at 912 cm^{-1} which is characteristic for PO_4^{2-} group, at 966 cm^{-1} indicated the presence of HPO_4^{-} group, whereas the band at 1050 cm^{-1} is attributed to aliphatic P–O–C stretching [29, 30]. In the monomer form GPTMS has three characteristic peaks at 2840 cm^{-1} assigned to the methoxy group, 1186 and 908 cm^{-1} corresponding to the epoxy group [31]. In addition to a strong peak attributed to C-O-C str at 1073 cm^{-1}. The bands around 1641 cm^{-1} and 1576 cm^{-1} corresponded to the characteristic peaks of amide I and amide II from chitosan, respectively [31]. Regarding ChG10 and ChG15 samples, their curve pattern is similar to chitosan.

Figure 2-6 illustrates the ^{13}C CP-MAS-NMR and ^{31}P DDMAS-NMR spectra of the ChG10 and ChG15 samples. From a previous study [11], the peaks C-1 to C-6 were assigned to N-acetyl C] O, and N-acetyl-methyl CH_3 signals attributed to chitosan, while Cb and Ca to GPTMS. In addition, two signals from β-GP overlapped with those of C-5, C-3 and C-6. The increase of the intensity on the C-6 peak is also attributed to β-GP [11]. On the hybrid microspheres the ^{31}P peaks were noticeably identified at 5.0 ppm for ChG10 and sharper for ChG15 at 4.7 ppm. The ^{29}Si CP-MAS-NMR spectra for ChG10 and ChG15 microspheres is displayed on figure 2-7. The signals obtained were deconvoluted into four near peaks around −39, −49, −57 and −66 ppm equivalent to the T^0, T^1, T^2 and T^3 species, respectively. The quantity of Si−O−Si bridging bonds per Si atom depicts the degree of polymerization of the −Si−OR or −Si−OH groups at the end of the GPTMS molecules and can be quantified using the equation described below:

Degree of polymerization $= [(\text{fraction of } T^1) \times 1] + [(\text{fraction of } T^2) \times 2] + [(\text{fraction of } T^3) \times 3]$ (4)

The number of Si−O−Si bridging bonds per Si atom results from the relative peak area of each T^n unit. As shown in table 2-2, it increased from 2.24 for ChG10 to 2.34 for ChG15.

Figure 2-8 displays the free amino groups present in the ChG10 and ChG15 hybrid microspheres. ChG10 holds higher amount of free amino groups than ChG15, precisely $5.49E^{-07} \pm 4.84E^{-08}$ and $2.58E^{-07} \pm 1.28^{-07}$ moles, respectively.
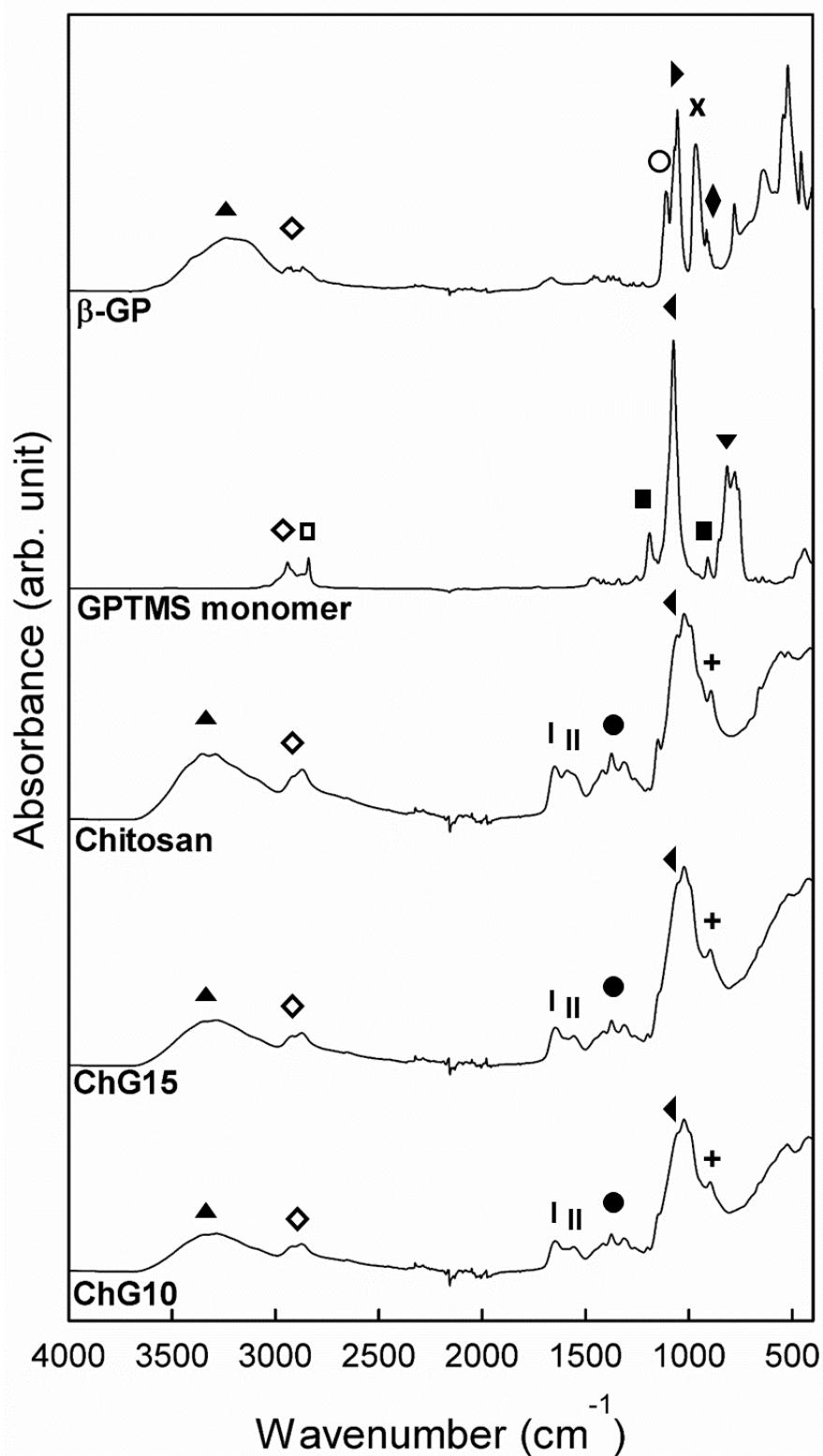
Figure 2-5 ATR-FTIR spectra of β-GP, GPTMS monomer, chitosan flakes, ChG10 and ChG15 microspheres. ▲ OH str; ◊ CH_2 str; | Amide I; || Amide II; ● CH_2 def; ◄ C-O-C str; + C-N str; □ -O-CH_3 str; ■ epoxide; ▼ CH_3; ○ P-OH; ► P-O-C str; x HPO_4^- and ♦ PO_4^{2-}. "Str" stands for stretch vibration and "def" for deformation vibration.
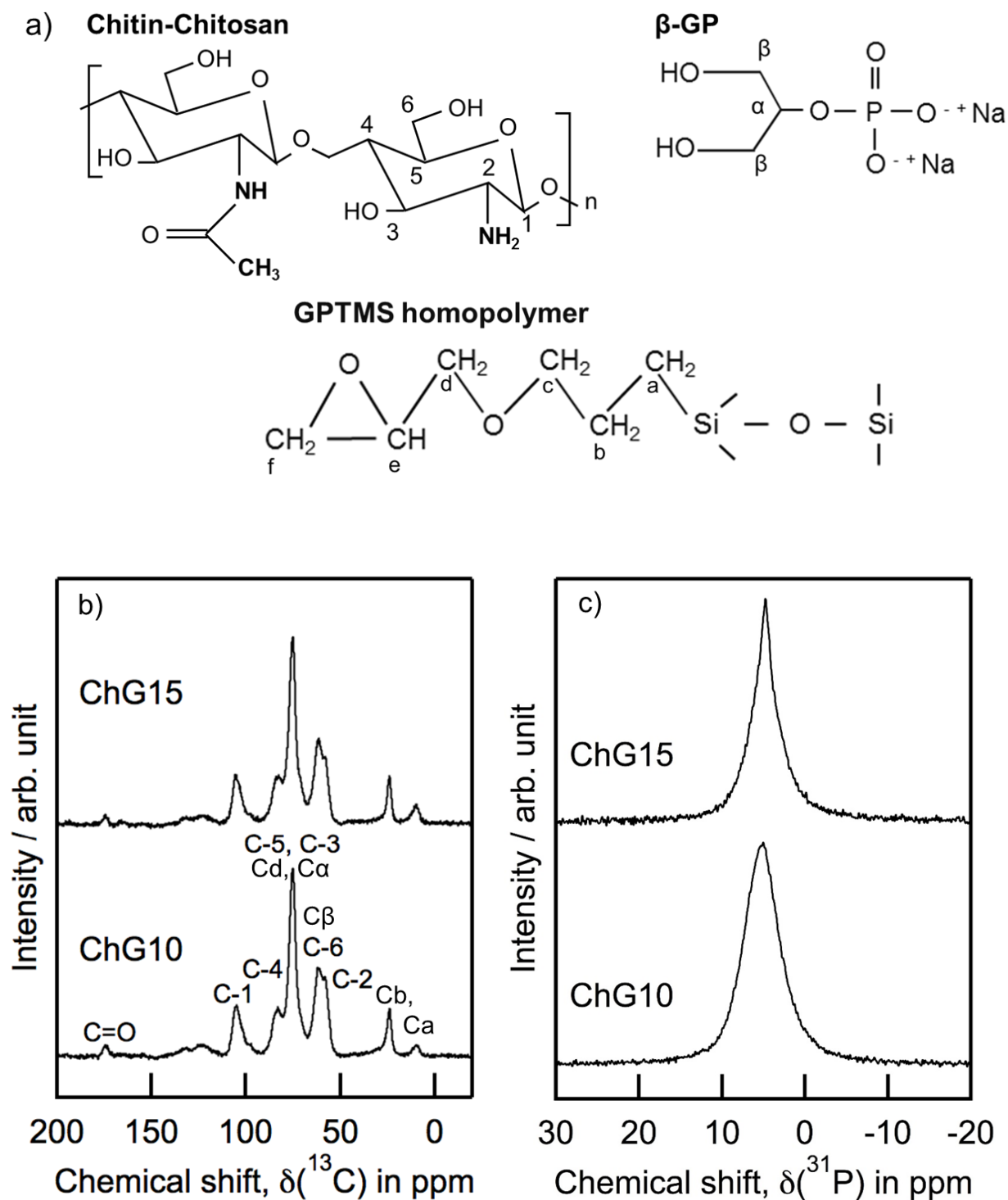
Figure 2-6 a) Molecular structure of the b) ^{13}C CP-MAS-NMR and c) ^{31}P DD-MAS-NMR spectra of ChG10 and ChG15 micro sized spheres. The equivalent signals are labelled with the chemical structures.
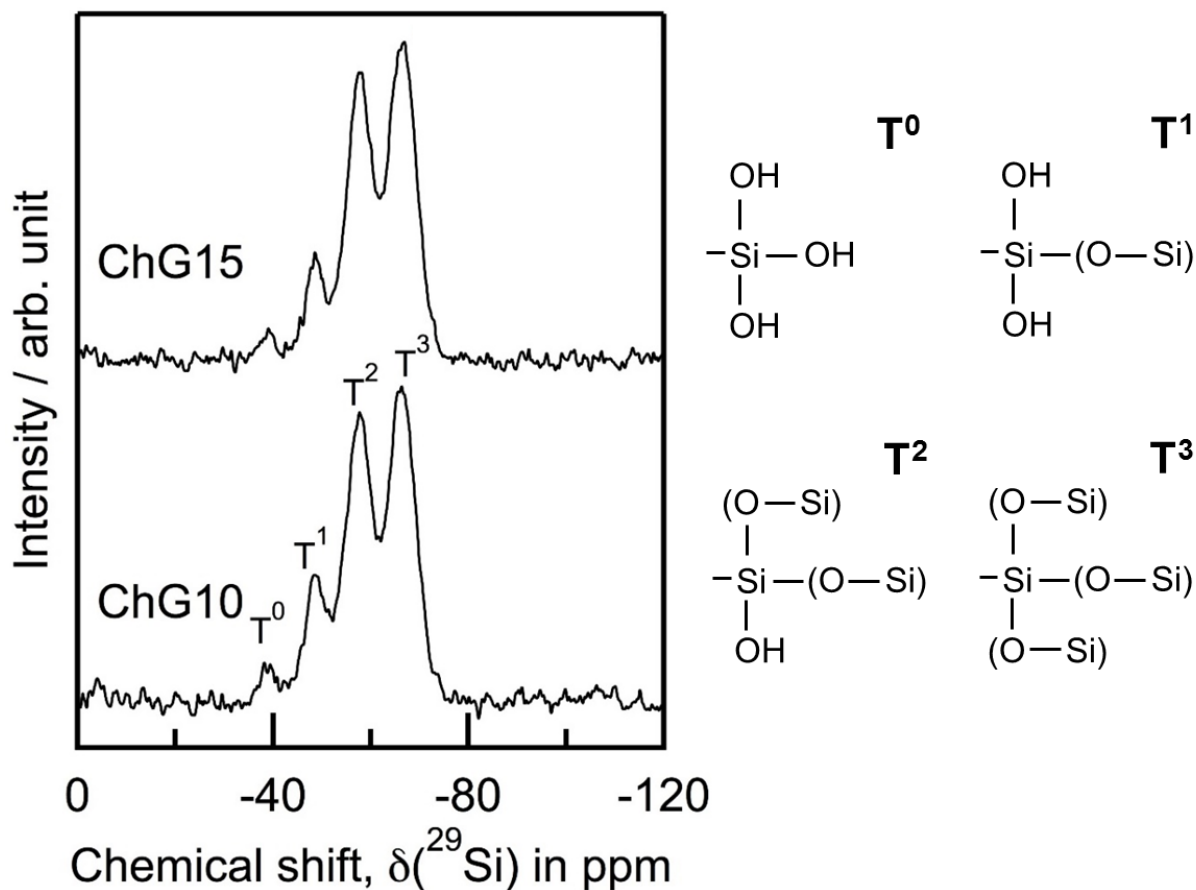
Figure 2-7 ^{29}Si CP-MAS-NMR spectra of ChG10 and ChG15 micro sized spheres. The equivalent signals are labelled with the chemical structures.
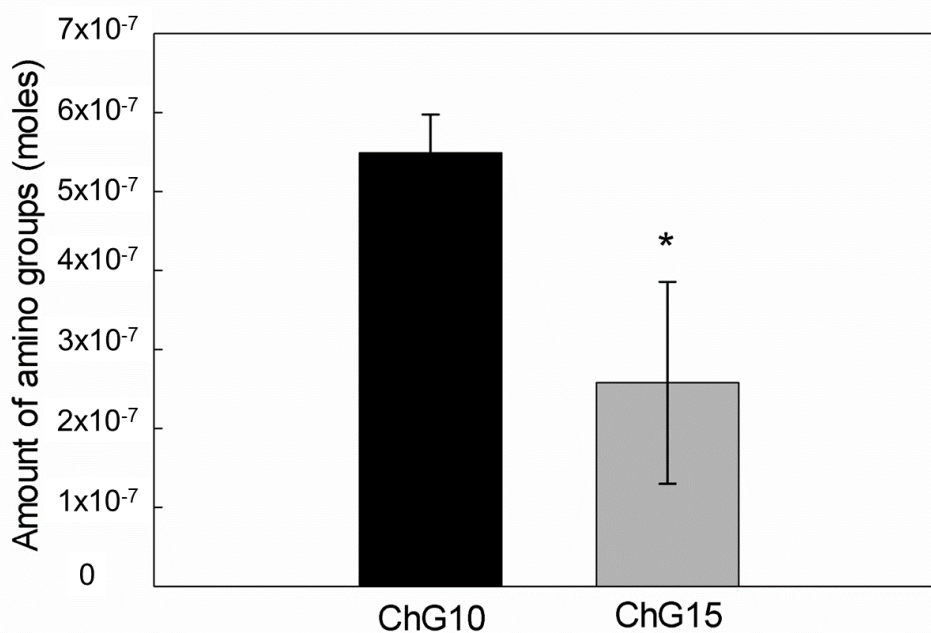
Figure 2-8 Amount of free amino groups on ChG10 and ChG15 hybrid microspheres determined by ninhydrin assay. * represents a statistically significant difference between ChG10 and ChG15 microspheres (p<0.05).

Table 2-2 ^{29}Si chemical shifts (δ (ppm)), full width at half maximum (FWHM (ppm)), and quantification using the relative peak area (I (%)) for T units derived from ^{29}Si CP-MAS NMR spectra.

T unit sample	T^0			T^1			T^2			T^3			N$_{bo}$/Si
	δ^a	FWHM^b	I^c	δ^a	FWHM^b	I^c	δ^a	FWHM^b	I^c	δ^a	FWHM^b	I^c	
ChG10	-39.1	4.3	3.1	-48.8	5.8	14.7	-57.5	6.2	37.3	-66.4	6.8	44.9	2.24
ChG15	-38.9	3.5	1.9	-48.7	5.1	10.9	-57.6	6.0	38.5	-66.5	6.8	48.7	2.34

^{a} The estimated error of the chemical shifts was less than $\pm$ 0.1 ppm.
^{b} The estimated error of the FWHM was less than $\pm$ 0.2 ppm.
^{c} The estimated error of the relative peak area was less than $\pm$ 0.3%.

2.3.2 Compressive strength and thermal decomposition

In figure 2-9 are shown the stress-deformation performances of the ChG10 and ChG15 microspheres. Several measurements were executed, and for each condition, the replicates displayed a nearly overlapping curve. At the highest elastic-plastic loading achieved, the maximum stress for both ChG10 and ChG15 samples was around 15 MPa (figure 2-9a). Nearly 20% distortion, the stress values of the ChG10 microspheres were to some extent higher than those for ChG15. For that reason, at 50% distortion point (figure 2-9b), the averages of the measured replicates were compared, and a statistical difference was perceived among the two microspheres compositions.
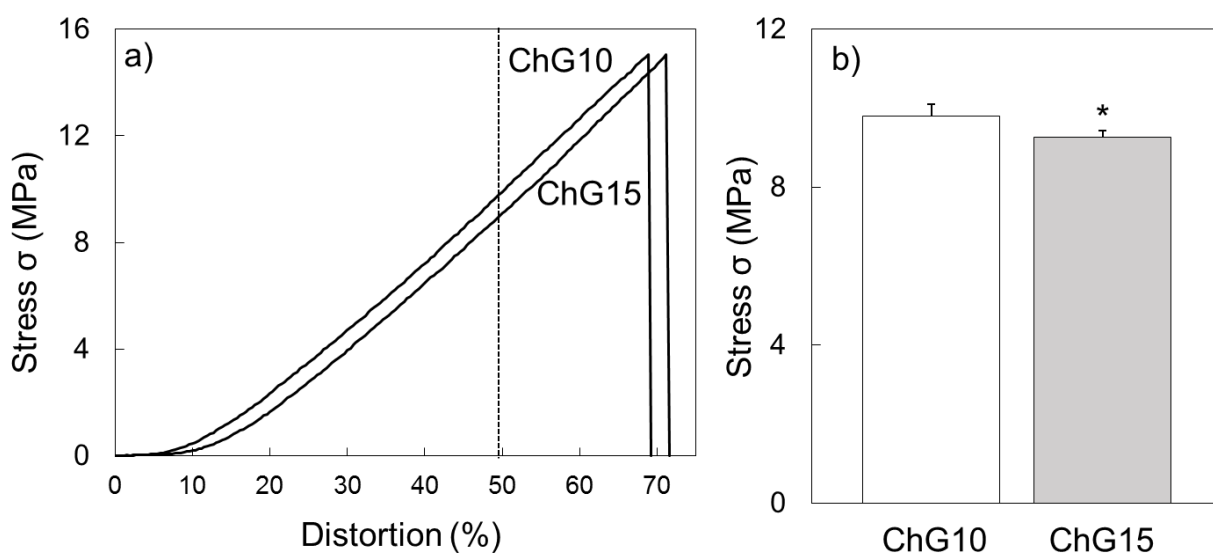
Figure 2-9 Compression assay of ChG10 and ChG15 samples. a) ChG10 and ChG15 curves under uniaxial compression force. b) Stress average of 3 replicates for both ChG10 and ChG15 microspheres at the same distortion point (50%). * represents a statistically significant difference between ChG10 and ChG15 at 50% ($p < 0.05$).

The TG-DTA curves of the raw chitosan flakes, GPTMS monomer, and ChG10 and ChG15 hybrid microspheres are displayed in figure 2-10. Commonly, the first stage on TG up to 260°C is attributed to the vaporization of moisture, and that was observed for all the samples (figure 2-10a).
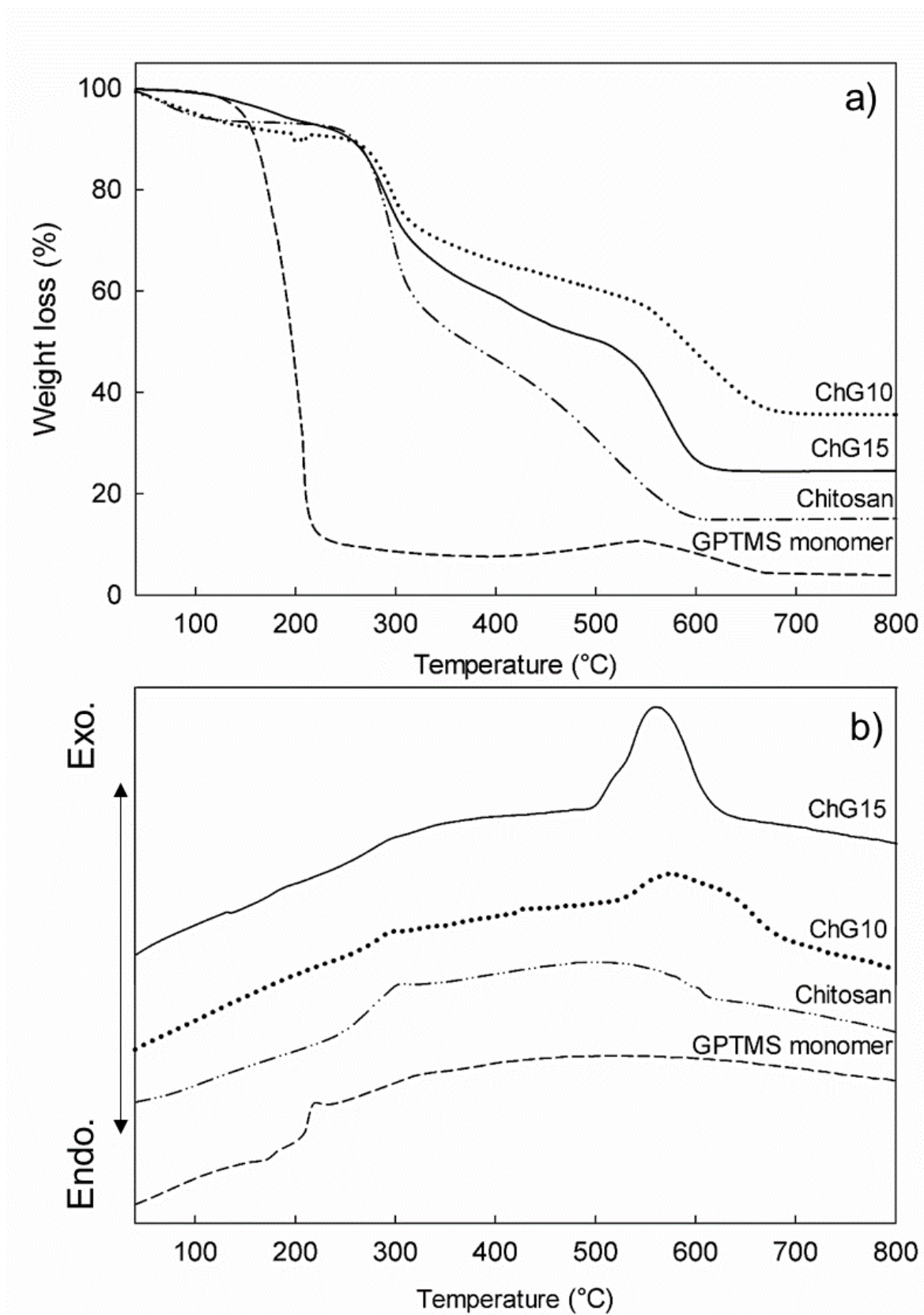
Figure 2-10 a) TG and b) DTA curves of the original chitosan flakes, GPTMS monomer, and ChG10 and ChG15 micro sized spheres.

All the DTA peaks were exothermic (figure 2-10b). Concerning the chitosan TG curve, after the vaporization step the weight loss happened from 251°C to 588°C in two phases. The weight loss at each phase was of 32% and 37%. The original chitosan flakes exhibited a round and very broad DTA curve. Regarding the GPTMS monomer, the curve had a sudden slope starting from 159°C until 215°C with 5% of remaining weight. In the case of the microspheres, one additional stage occurred for the weight loss when compared with original chitosan flakes, in addition to the existence of a perceptible DTA curvy peak at 560°C and 580°C. Concerning the weight loss, ChG10 microspheres lost roughly 13% from 274°C to 316°C, 18% to 554°C with a final stage of 19% mass loss. Likewise, the ChG15 spheres experienced mass losses of nearly 18% from 261°C to 311°C, 25% to 537°C, and 20% in the final slope.

2.3.3 Degradation profile of microspheres under several pH conditions

The weight loss (%) assessment of the hybrid microspheres under 1.7, 5.4 and 7.4 pH conditions is shown in figure 2-11a-c. The neutral pH 7.4 series displayed the lowest mass losses of $27 \pm 9\%$ for ChG10 and $32 \pm 6\%$ for ChG15. Though degradation of the micro sized spheres was faster in the pH 1.7 and pH 5.4 series, the weight losses of ChG10 of ChG15 samples were of $43 \pm 3\%$ and $59 \pm 8\%$, respectively, for pH 1.7 and $77 \pm 9\%$ and $69 \pm 7\%$, respectively, on behalf of pH 5.4. The pH changes during the 14 days are summarized in table 2-3. When subjected to pH 1.7 and 7.4 environments, both ChG10 and ChG15 microspheres were constant with almost no deviation from the initial pH. Concerning pH 5.4 series, a rise in the pH was perceived mainly at 7 days with a final pH of 6.4 after 14 days.

The released amount (mM) of phosphorus and silicon from the microspheres matrix to the solutions with different pH values are displayed in figures 2-12a-c and 2-13a-c, respectively. In case of phosphorus the released amount increased within 14 days. Afterwards, nearly all the samples had released similar amounts, namely around 0.0421 ± 0.0050 mM, regardless of the

pH. Concerning the silicon, the released amount of it also increased with the continuing soaking time. The microspheres belonging to the ChG15 sequence released more silicon than the ChG10 sequence. Additionally, higher amounts of silicon were released at pH 1.7. Figure 2-14a-c, 2-15a-c and Table 2-4 display the information obtained from the linearization of the ICP results in order to determine the releasing rate of P and Si elements from the ChG10 and ChG15 matrix at pH 1.7, 5.4 and 6.7 solutions. The table 2-4 shows the release rate of P and Si due to the pH variation. The pH 1.7 displayed the highest release rate of Si from the matrix. In case of P, a release rate trend by pH influence was not identified.

Table 2-3 pH values of the supernatant of each solution in which the microspheres were soaked for the degradation test.

Soaking time (days)	ChG10			ChG15		
	pH 1.7	pH 5.4	pH 7.4	pH 1.7	pH 5.4	pH 7.4
7	1.7 ± 0.0	6.2 ± 0.0	7.3 ± 0.1	1.8 ± 0.1	6.2 ± 0.0	7.3 ± 0.1
14	1.7 ± 0.0	6.4 ± 0.1	7.2 ± 0.1	1.7 ± 0.0	6.4 ± 0.1	7.3 ± 0.1

To perceive morphological changes on the samples, SEM observations of the dried microspheres after 14 days of degradation at pH 1.7, 5.4 and 7.4 are displayed in Figure 2-16. The samples before soaking presented a rugged surface topography with microporosity and a spherical shape. With the exemption of ChG10 at pH 1.7, there were no intense signs of harsh surface deterioration for most of the pH series after 14 days, nevertheless, the initially rugged surface became slightly smoother after 14 days. In case of the pH 5.4 series, both ChG10 and ChG15 lost its round shape after 14 days because of the degradation. The elements present on the samples at 0 days and 14 days are displayed on table 2-5. In general, it can be observed a decrease of the amounts of Si and P on all pH series after 14 days of degradation. The decrease supports the observations obtained from ICP. Figure 2-17 displays a replicate from the EDS spectra from table 2-5.
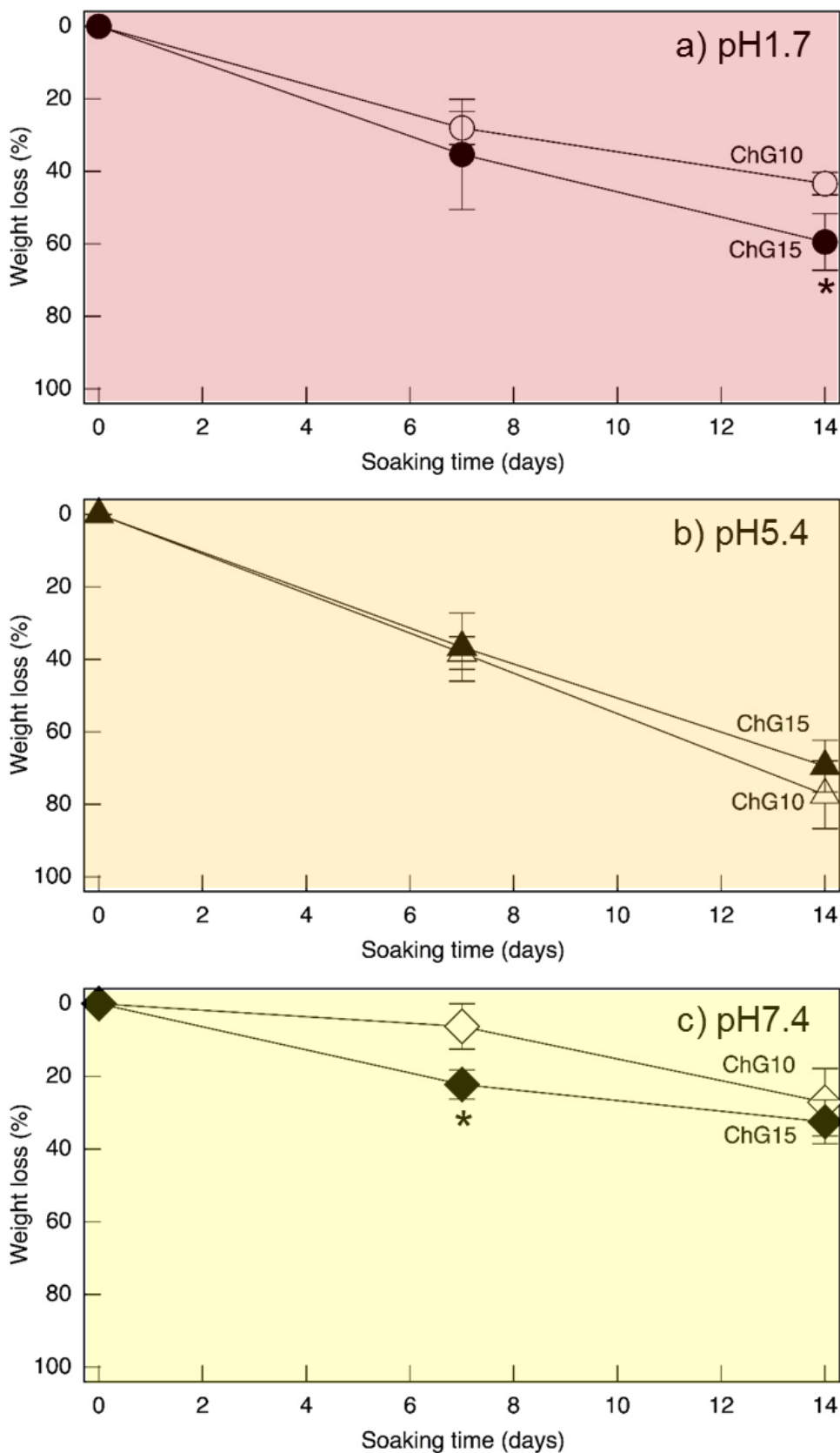
Figure 2-11 Weight loss (%) of ChG10 and ChG15 microspheres over 14 days at 37°C. pH series of: a) pH 1.7, b) pH 5.4, and c) pH 7.4. * represents a statistically significant difference between ChG10 and ChG15 microspheres at the same time point ($p<0.05$).
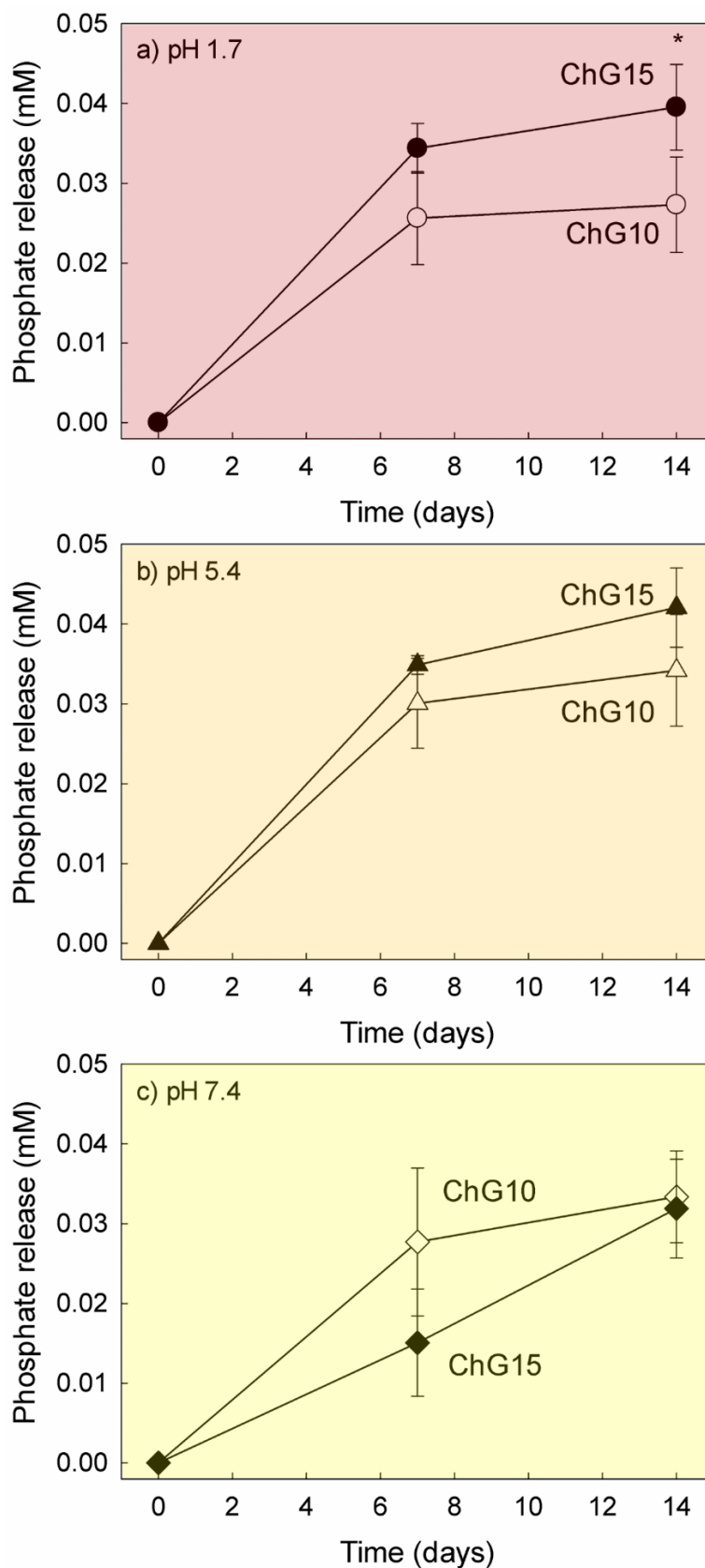
Figure 2-12 Concentration of phosphorus (mM) released from ChG10 and ChG15 spheres over 14 days at 37°C. pH series: a) pH 1.7, b) pH 5.4, and c) pH 7.4. * represents a statistically significant difference between ChG10 and ChG15 microspheres at the same time point (p<0.05).
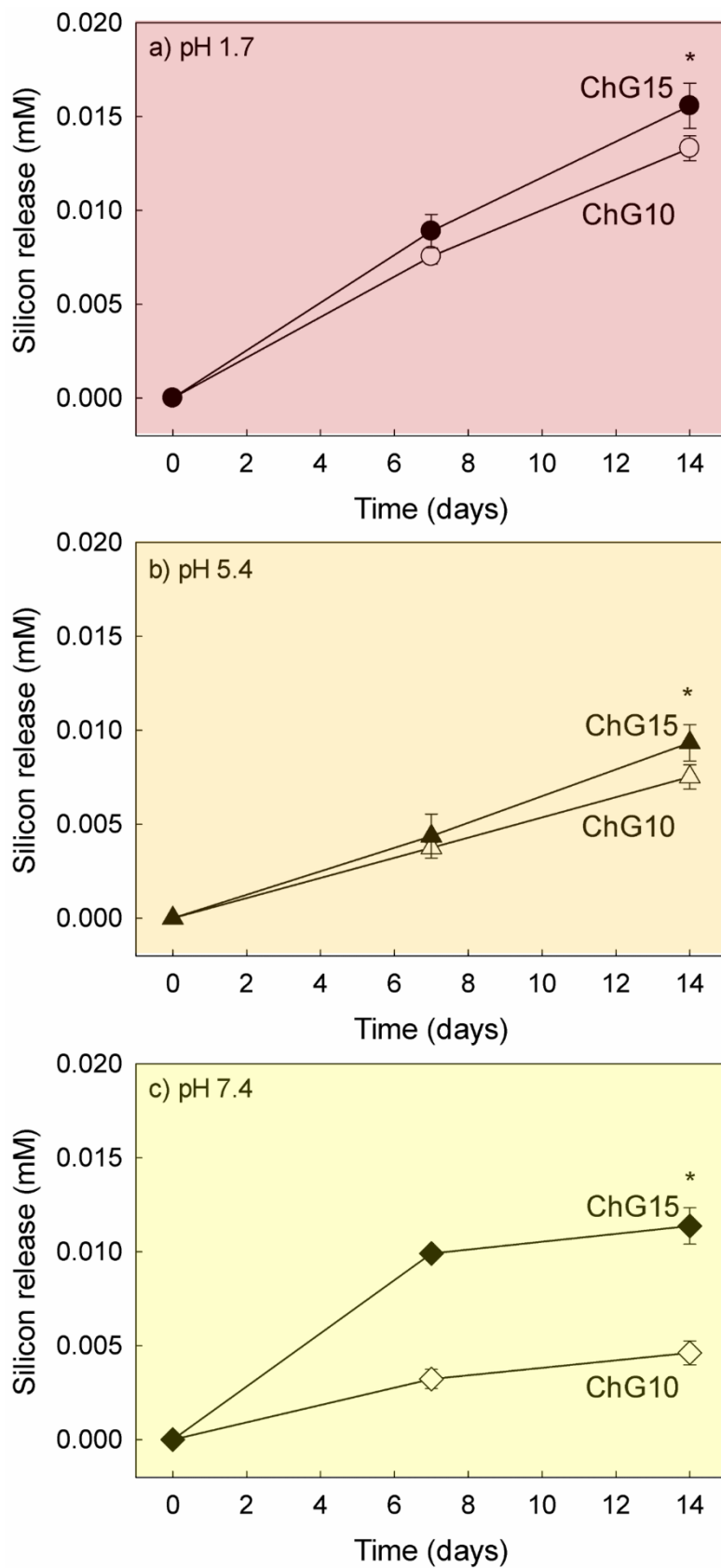
Figure 2-13 Concentration of silicon (mM) released from ChG10 and ChG15 spheres over 14 days at 37°C. pH series: a) pH 1.7, b) pH 5.4, and c) pH 7.4. * represents a statistically significant difference between ChG10 and ChG15 microspheres at the same time point ($p < 0.05$).
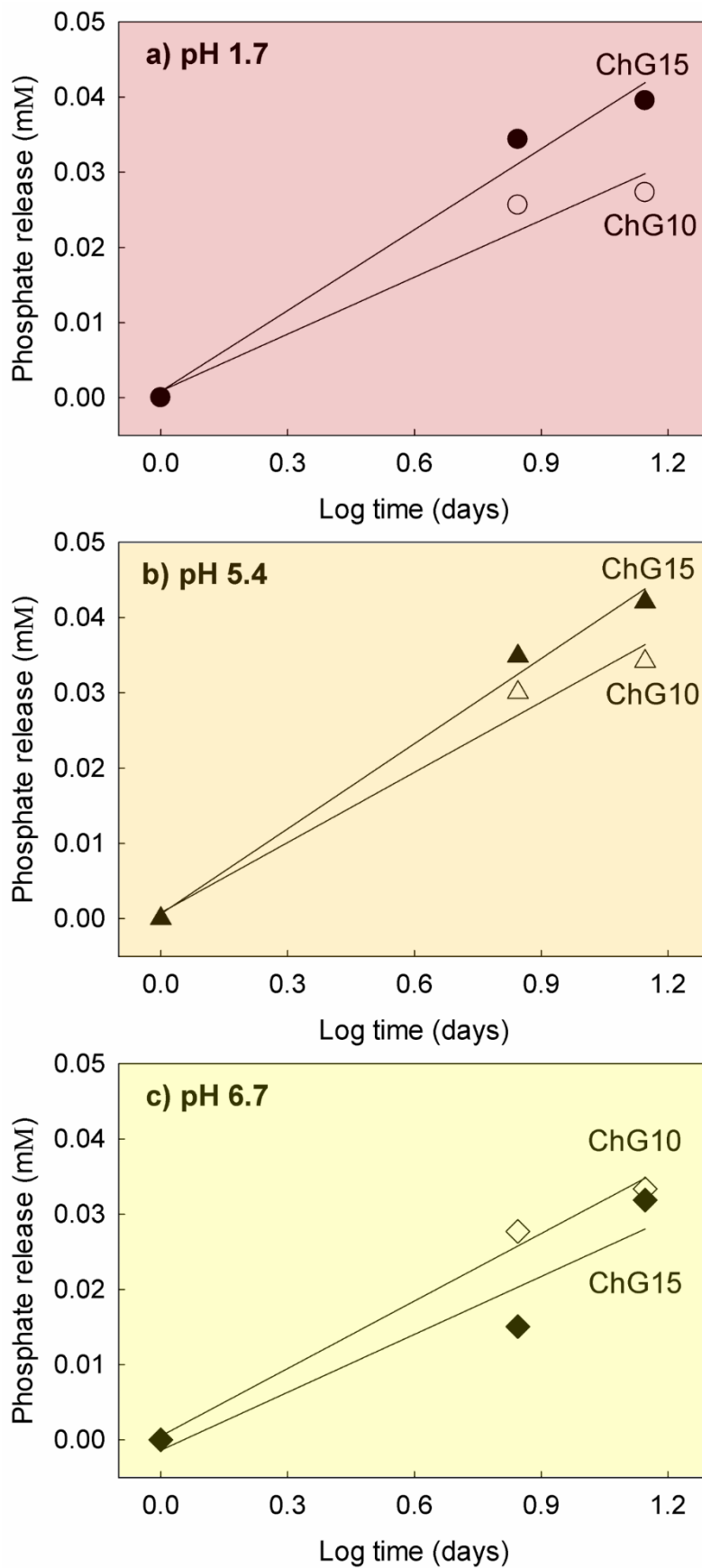
Figure 2-14 Release rate of phosphorus (mM) from ChG10 and ChG15 spheres over 14 days at 37°C. pH series: a) pH 1.7, b) pH 5.4, and c) pH 7.4. Linearization from ICP data.
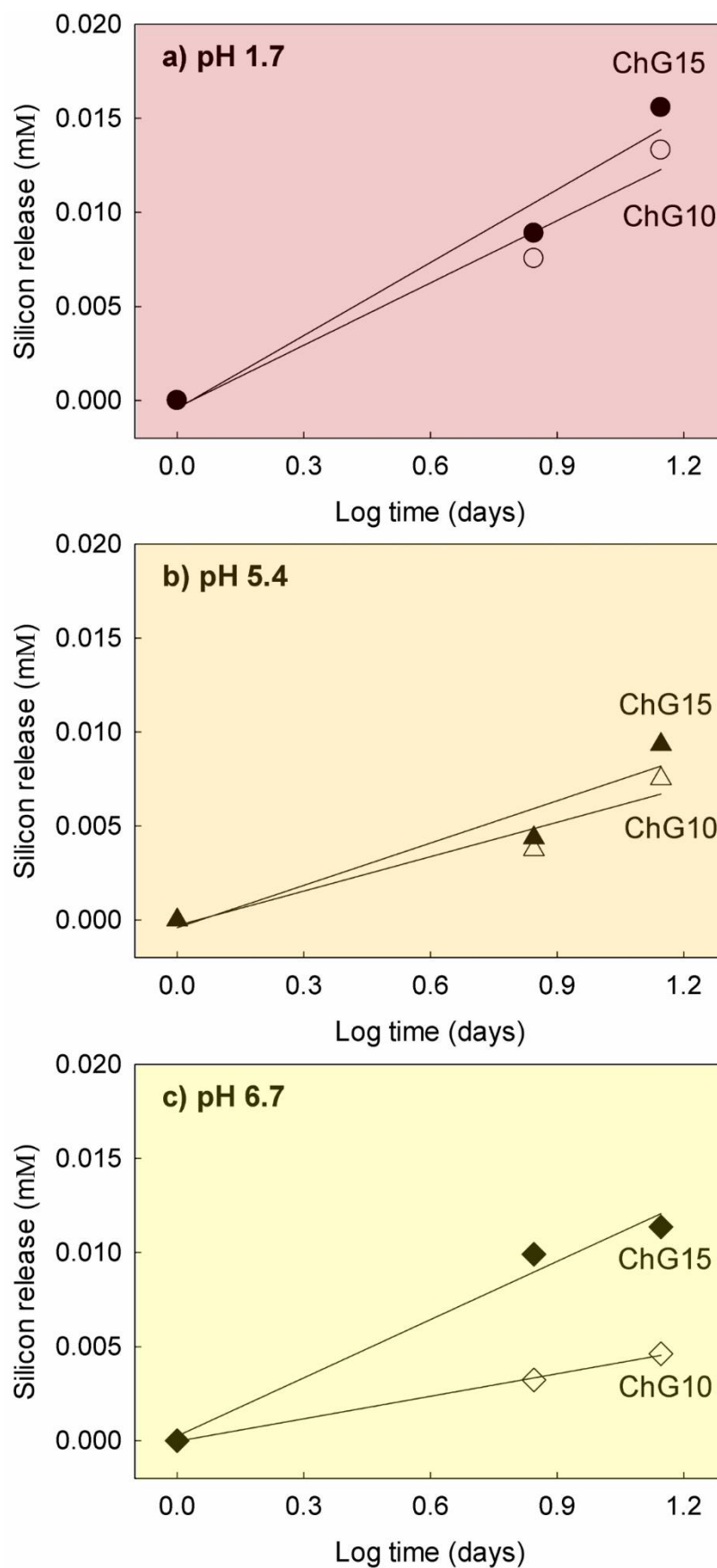
Figure 2-15 Release rate of silicon (mM) from ChG10 and ChG15 spheres over 14 days at 37°C. pH series: a) pH 1.7, b) pH 5.4, and c) pH 7.4. Linearization from ICP data.
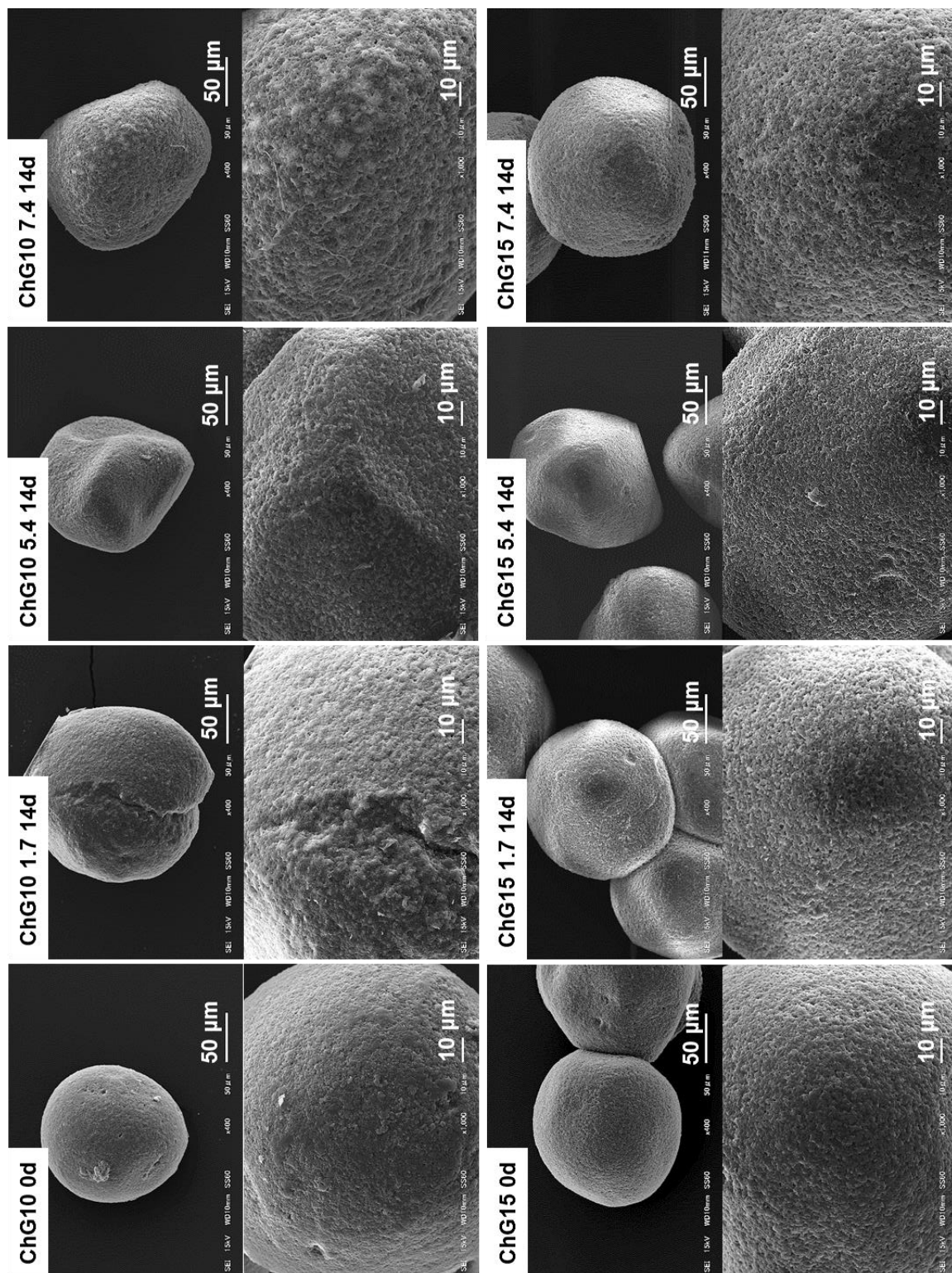
Figure 2-16 SEM images of ChG10 and ChG15 dried microspheres before and after 14 days degradation test at pH 1.7, 5.4 and 7.4 with respective magnifications.

Figure 2-18 shows the XRD spectra, in which was confirmed the chitosan degradation with the loss of the peak at $2\theta = 20°$ (corresponding to (022) and (102) planes) for both ChG10 and ChG15 microspheres after 14 days of degradation under acidic and neutral pH solutions. Although, the neutral series of pH 7.4 still exhibited a very weak peak.

Table 2-4 Release rate of P and Si of the ChG10 and ChG15 microspheres matrix obtained from the slope of the linearization of the ICP data.

Element	ChG10			ChG15		
	pH 1.7	pH 5.4	pH 7.4	pH 1.7	pH 5.4	pH 7.4
P	0.025	0.031	0.030	0.036	0.038	0.026
Si	0.011	0.006	0.004	0.013	0.008	0.010

Table 2-5 Elements ratio determination by SEM-EDS on sample surface before and after 14 days of degradation.

Samples	Elements ratio (atomic %)	
	Si/C	P/C
ChG10 0d	3.0 ± 0.4	2.3 ± 0.3
ChG15 0d	8.3 ± 2.9	10.8 ± 6.5
ChG10 1.7 14d	2.8 ± 0.2	0.7 ± 0.1
ChG15 1.7 14d	4.2 ± 0.3	0.3 ± 0.0
ChG10 5.4 14d	2.3 ± 0.7	0.5 ± 0.2
ChG15 5.4 14d	4.0 ± 0.3	0.4 ± 0.0
ChG10 7.4 14d	2.5 ± 0.9	0.6 ± 0.1
ChG15 7.4 14d	4.7 ± 1.1	0.7 ± 0.2
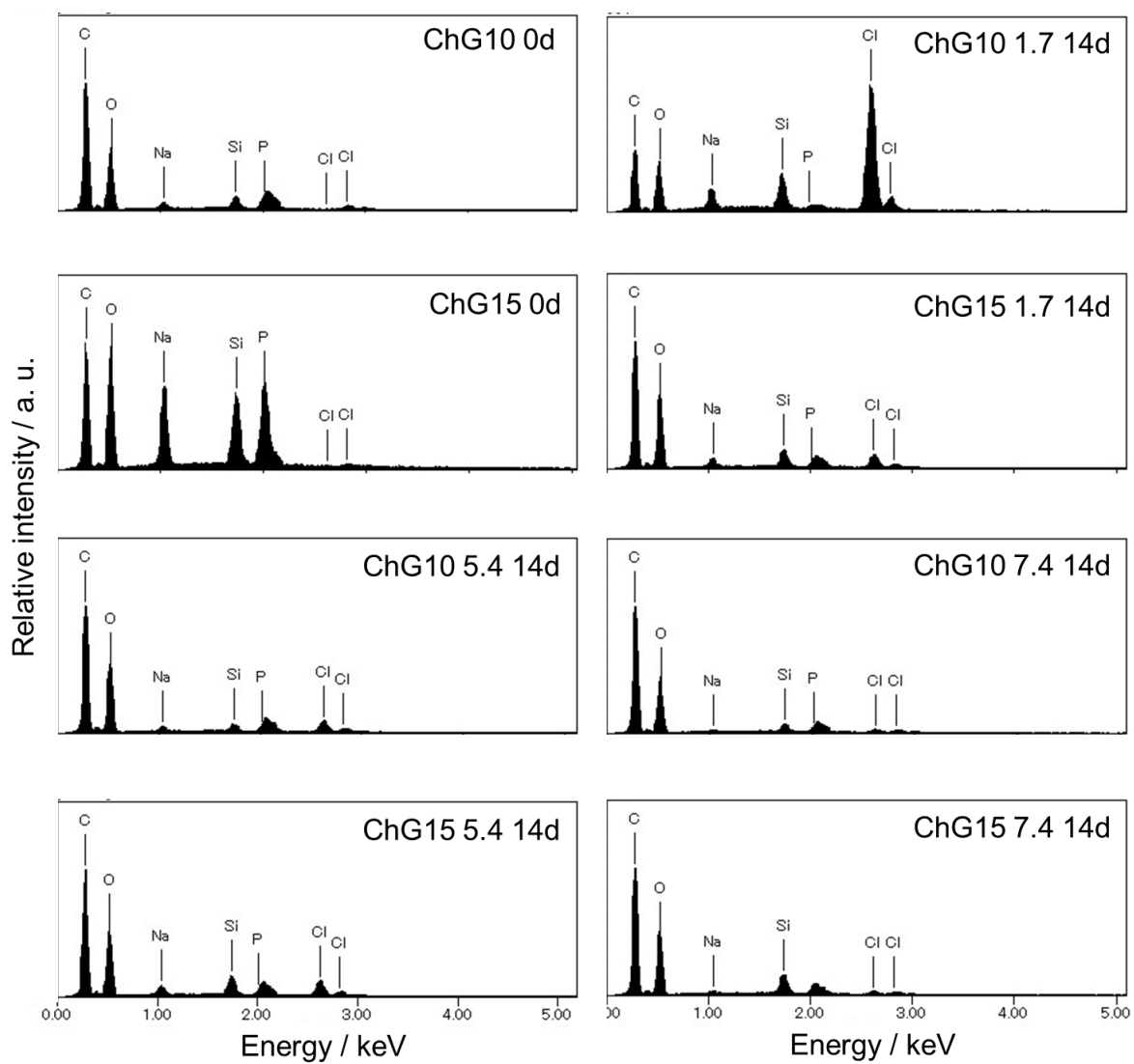
Figure 2-17 EDS spectra from the ChG10 and ChG15 dried samples before and after 14 days of degradation at different pH conditions.
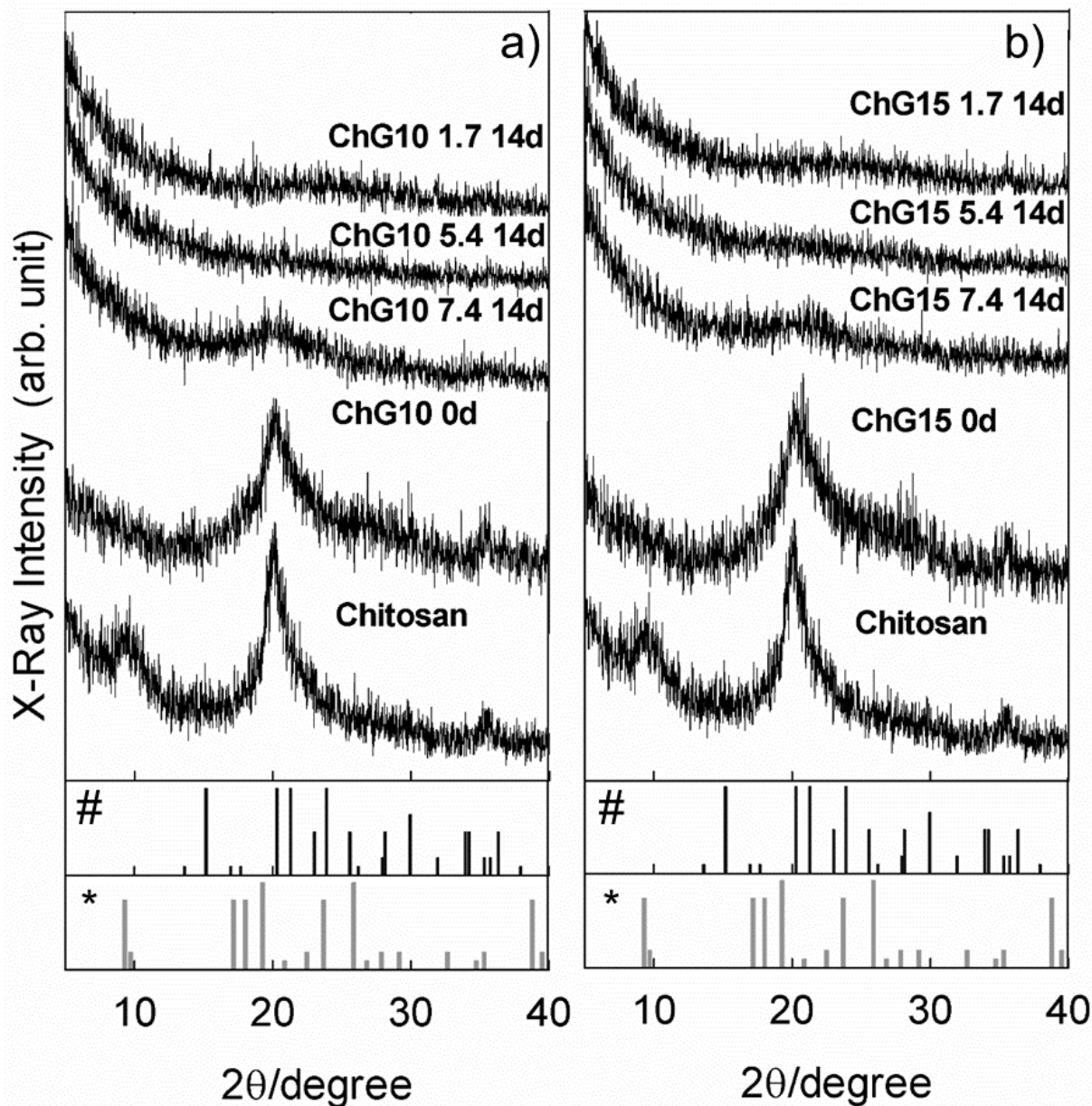
Figure 2-18 XRD patterns of original chitosan flake, a) ChG10 and b) ChG15 micro sized spheres before and after 14 days of degradation submitted to different pH conditions. #, corresponds to the reference peaks ICDD #39-1894 of chitosan. *, corresponds to the reference peaks ICDD # 35-1974 of chitin.

2.3.4 Release profile of pelargonidin from microspheres in SGF conditions and full digestion cycle

Figure 2-19 displays the *in vitro* release of pelargonidin as a drug model from the hybrid microspheres in different pHs and incubation periods mimicking the digestive system, specifically at pH 1.7 for 2 h, 5.4 for 22 h and 6.7 for 33 h, making a total of 57 h of incubation. It can be observed, that at pH 1.7 the pelargonidin released from ChG10P1, ChG15P1, ChG10P3 and ChG15P 3 occurred in a burst, releasing around 10 µg/mL within the first 2 h of incubation. Similarly to the initial 2 h, a slower burst was observed from 2 h to 8 h on both compositions soaked in SGF of pH 5.4, releasing an amount of pelargonidin around 16 µg/mL for the P1 series of microspheres containing pelargonidin, whereas in the P3 series it was released around 22 µg/mL. When the microspheres were soaked solely in SGF of pH 5.4 a slower and more sustained release occurred when compared to pH 1.7, with similar quantities of pelargonidin released from the matrix within the same concentration series, namely 23 and 21 µg/mL for ChG10P1 and ChG15P1 and 29 and 26 µg/mL for ChG10P3 and ChG15P3, respectively. In contrast to ChG10P1, ChG15P1 and P3 series of microspheres continued releasing in a slower and sustained way until 48 h (in SGF of pH 6.7). But, from 48 h to 57 h a spike in the release was observed once again. After a total of 57 h of incubation, 72 and 32 µg/mL of pelargonidin were released for ChG10P1 and ChG15P1, respectively, while for ChG10P3 and ChG15P3 was released 39 and 34 µg/mL, respectively.

Figure 2-20 and Table 2-6 display the information obtained from the linearization of the results from the cumulative release of pelargonidin in order to determine the releasing rate of the anthocyanidin from the ChG10 and ChG15 matrix at pH 1.7, 5.4 and 6.7 solutions. At pH 1.7 the release rate of pelargonidin from the matrix was high and similar within the series. When in pH 5.4 the release rate decreases considerably to around half and ChG10 series have a slightly

higher release profile. Finally, at pH 6.7 the antioxidant release rate increase again and the sample showing the highest release rate was ChG10P1 samples followed by the ChG15P1 and ChG10P3.
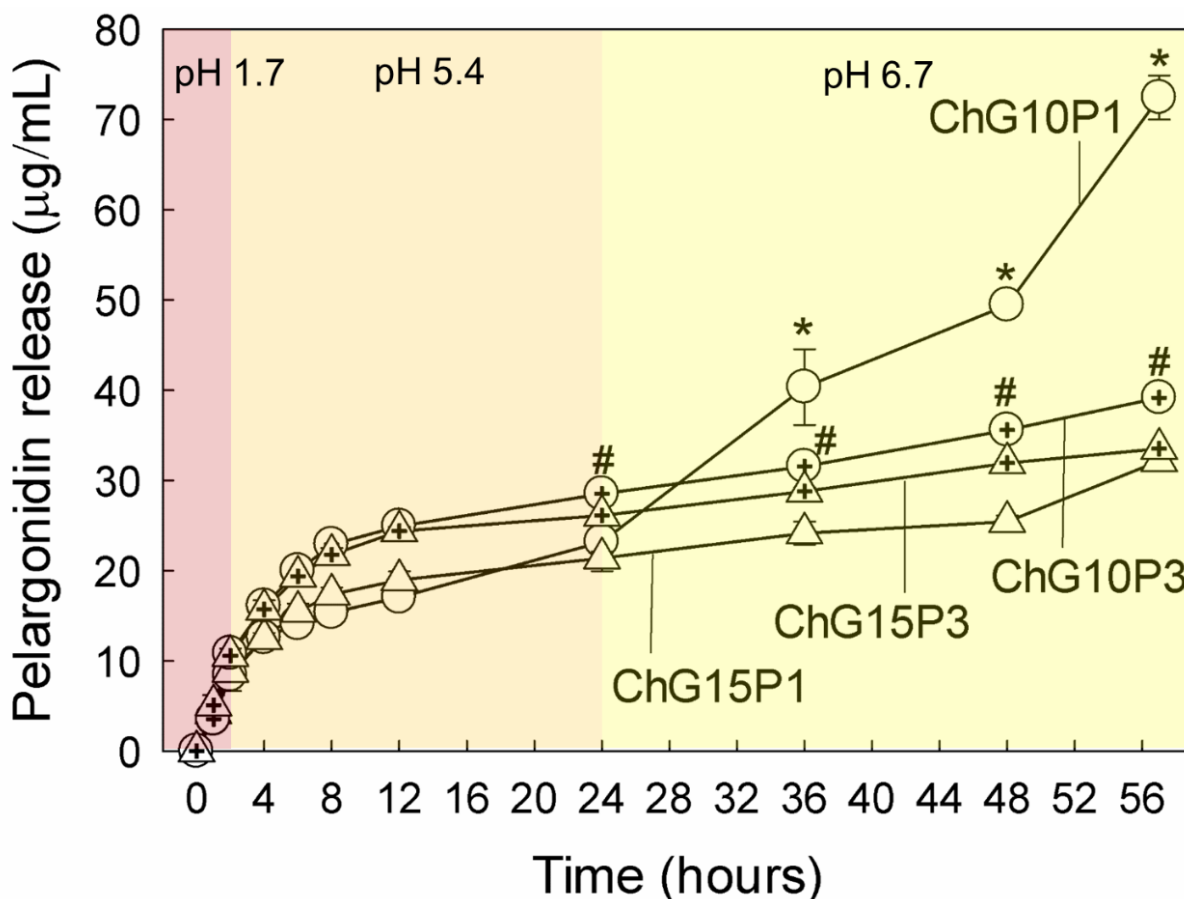
Figure 2-19 Cumulative release of pelargonidin (µg/mL) from ChG10 and ChG15 spheres with different drug loading concentrations throughout the 57 h of incubation at different SGFs, specifically at pH 1.7 for 2 h, 5.4 for 22 h and 6.7 for 33 h. *, # represent a statistically significant difference when comparing ChG15P1 and ChG15P3, respectively, at the same time point (p<0.05).

The weight variation of the microspheres containing pelargonidin was evaluated (figure 2-21), together with the measurement of the diameter (figure 2-22) during the incubation in different SGFs for a total of 57 h. Concerning the weight variation, microspheres with and without pelargonidin suffered a weight gain in the first 2 h in pH 1.7. In the pH5.4 and 6.7 domain, the weight of the samples did not fluctuate much from the observations made at 2 h.

The focus goes to ChG10P1 and ChG10P3 samples in which showed the highest weight gain with around 70% more, where a statistical difference at 2, 24 and 57 h when compared to the other group of samples. In opposition, the samples maintaining a similar initial weight are the ChG15 microspheres.

Table 2-6 Release rate of pelargonidin of the microspheres matrix obtained from the slope of the linearization of the cumulative release data.

	pH 1.7	pH 5.4	pH 6.7
ChG10P1	21.99	13.50	151.90
ChG15P1	22.27	11.20	37.02
ChG10P3	29.97	15.66	37.56
ChG15P3	26.68	13.33	23.92

Visually, the microspheres containing pelargonidin on both P1 and P3 series were swollen, semitransparent and less sturdy than the respective controls (figure 2-23). On ChG15P1 and ChG15P3 microspheres, very similar observations were made, with the difference that, nonetheless, the ChG15P were still slightly more colored even after 57 h of incubation, than ChG10P1 and ChG10P3. Due to the swelling the size of the spheres increased after 57 h of incubation, as observed in figure 2-21 together with figure 2-23. This behavior was more noticeable in the ChG10P1 and ChG10P3 microspheres, in which after 57 h the size increased from 647 ± 33 μm to 935 ± 51 μm and to 1037 ± 82 μm, respectively, while the ChG10 control was 844 ± 48 μm. Meanwhile, ChG15P1 and ChG15P3 microspheres also increased in size from 661 ± 23 to 854 ± 13 μm and to 919 ± 55 μm, respectively, similarly to its control. Besides from microspheres swelling effect, figure 2-23 also displays that at 57 h, microspheres containing pelargonidin present some loose particle fragments indicating higher fragility than the control, especially on ChG10P1 and ChG10P3 microspheres.
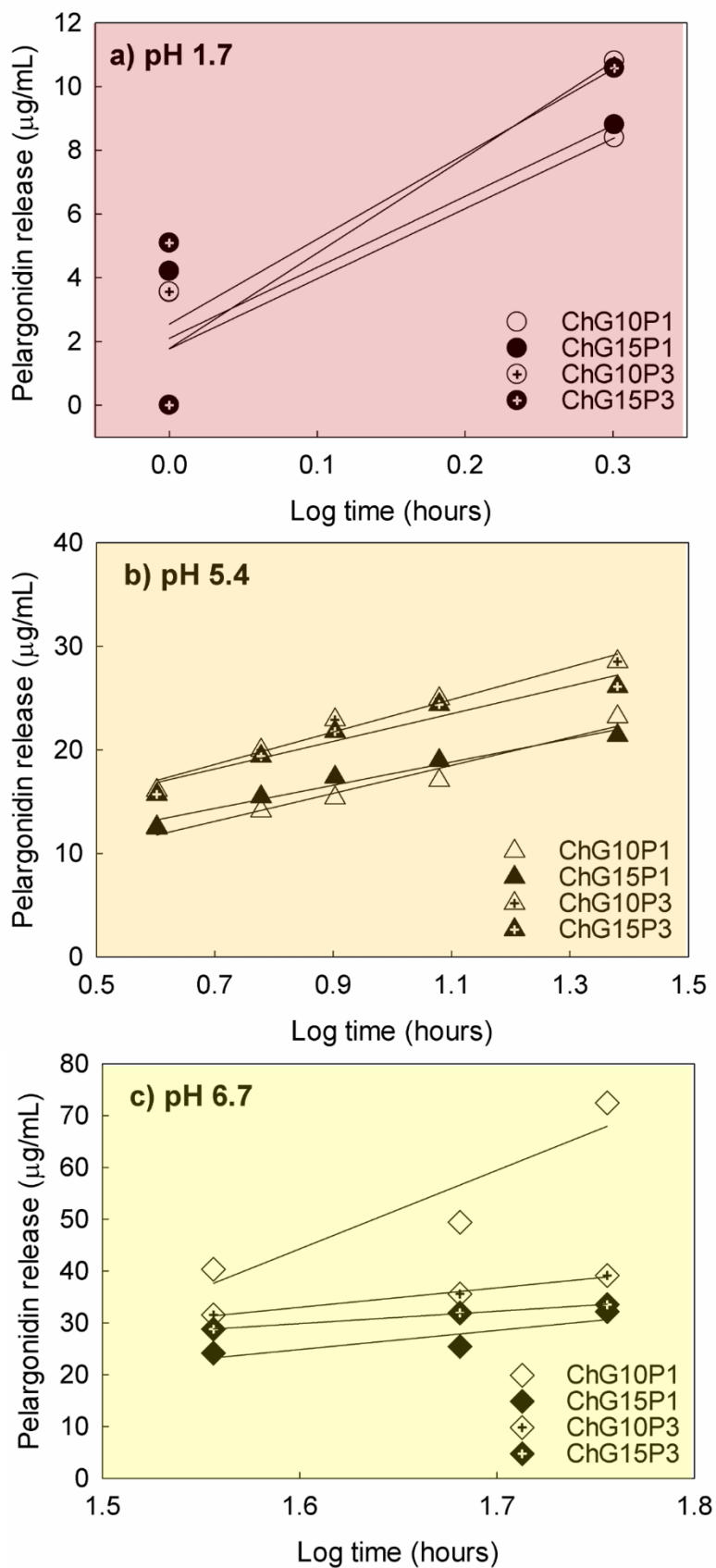
Figure 2-20 Release rate of pelargonidin from ChG10 and ChG15 spheres with different drug loading concentrations during 57 h at 37°C. pH series: a) pH 1.7, b) pH 5.4, and c) pH 6.7. Linearization from the cumulative release data.
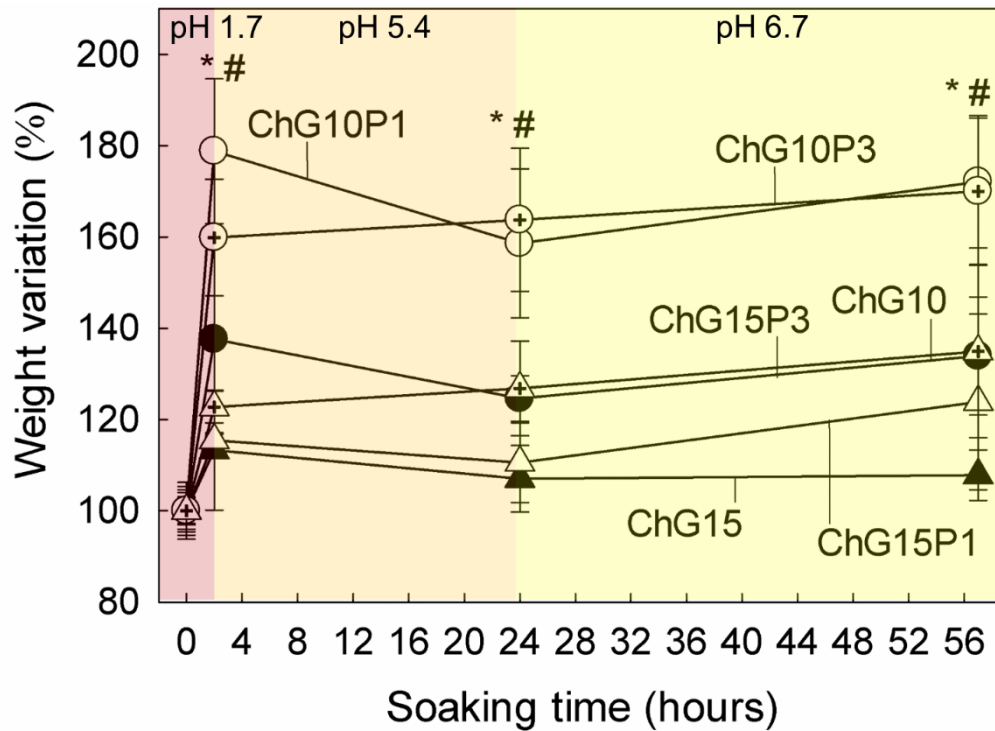
Figure 2-21 Weight variation (%) of the microspheres with and without pelargonidin in different SGFs during the simulated transit time. *, # represent a statistically significant difference when comparing ChG15P1 and ChG15P3, respectively, at the same time point (p<0.05).
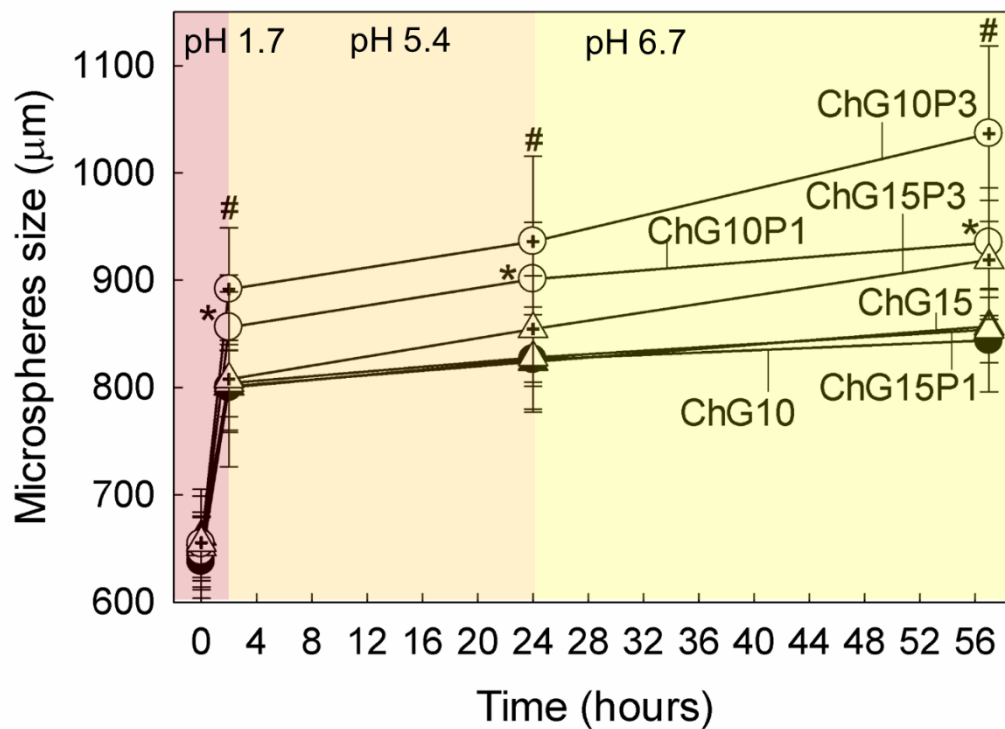
Figure 2-22 Size (μm) variation of the microspheres with and without pelargonidin when soaked in different SGFs during the simulated transit time. *, # represent a statistically significant difference when comparing ChG15P1 and ChG15P3, respectively, at the same time point (p<0.05).
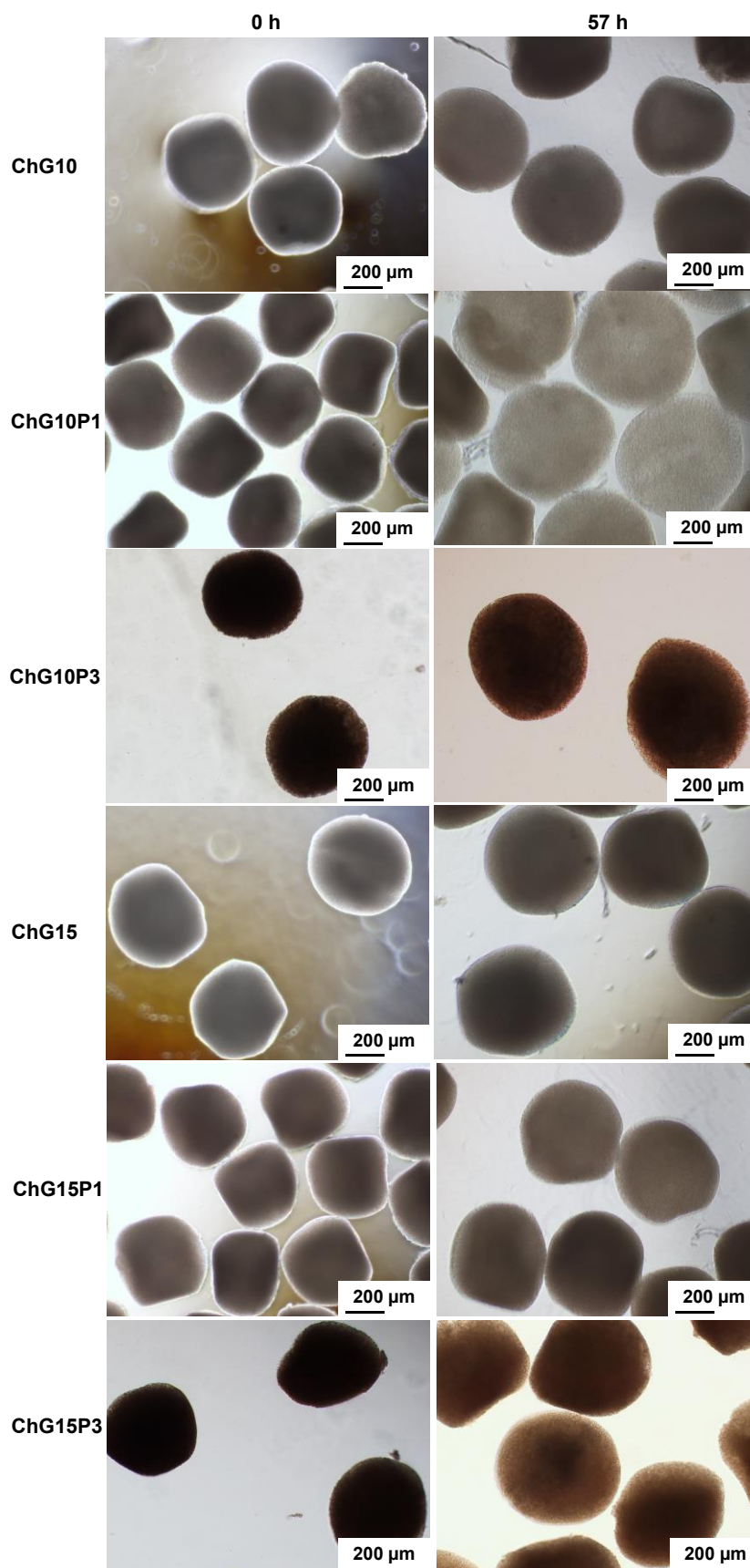
Figure 2-23 Brightfield images (obj. 4×) of ChG10 and ChG15 controls, as well as the microspheres containing pelargonidin (ChG10P1, ChG10P3, ChG15P1 and ChG15P3) at 0 and 57 h of incubation at different SGF solutions.

2.4.   Discussion

Uniformity of size of microspheres is an essential parameter, especially if applied as drug carriers. The produced hybrid micro sized spheres achieved the size uniformity requisite, and the obtained size was satisfactory for drug delivery in the gastrointestinal track because it avoids internalization by gastric cells. In fact, some researchers [14, 15] stated the use of micro sized spheres ranging from 400 to 1000 μm with good drug entrapment efficiency, for drug delivery applications targeted for the gastrointestinal track. Using the optimized conditions monodispersed micro sized spheres with uniform dimensions were acquired with approximate size of 650 μm.

Regarding the water content, the inferior water amount in the ChG15 spheres was predictable due to the increased GPTMS content in its matrix when compared to ChG10. This reduced presence of water induced a higher crosslinking with the chitosan skeleton, along with, higher condensation of the Si−O−Si network [32], and so affecting the water amount in the matrix. Commonly, when microscopic materials enter in contact with a liquid suspension, they are likely to gain an electronic charge on its surface [33]. The zeta potential analysis is useful to indicate the potential stability and charge of the colloidal system. In general, a higher zeta potential points toward a better stability of the suspension attributable to the repulsion occurring between charged particles, this way overcoming the natural predisposition to aggregate that generally take place as zeta approaches zero [34]. Preferably, the particles with zeta potential values superior to +30 mV or more negative than −30 mV are usually considered more stable. Nevertheless, these zeta potential values can be influenced by the pH and ionic strength, amongst other causes. Consequently, the zeta potential should not be exclusively considered to determine the stability of the system. The produced microspheres displayed zeta potential values closer to +30 or −30 mV and half of those amounts. As observed, the surface charge of

the synthetized microspheres varied depending on the dispersing solution on which the samples were subjected to, implying that the microspheres have a tendency to interact with ions from the dispersing solution. Hence, the negative charge could be attributed to the interaction between the micro sized spheres with the phosphate ions from PBS.

The characteristics peaks for chitosan, GPTMS monomer and β-GP were present, but on ChG10 and ChG15 samples the presence of the Si−O−Si bands on the microspheres could not be clearly observed on FTIR due to chitosan curve overlapping or to lack of sensitivity on the detection as a result of the small amount of GPTMS present in each microsphere. In these cases, nuclear magnetic resonance spectroscopy is a helpful technique to obtain more precise structural information. And so ^{13}C CP-MAS-NMR, ^{31}P DDMAS-NMR and ^{29}Si CP-MAS-NMR analysis of ChG10 and ChG15 microspheres aided to conclude that chitosan and β-GP signals were detected in the samples. Regarding the ^{29}Si CP-MAS-NMR spectra for ChG10 and ChG15, the condensation of GPTMS molecules was accelerated by the quantity of GPTMS, as similarly observed on a previous study [11]. The epoxy groups from GPTMS effectively opened, increasing the reaction quota with the amino groups of the chitosan chains. And, signals from both ChG10 and ChG15 similarly displayed T^3 species, indicating that condensation reactions occurred though not completely, corresponding to the T^0, T^1, and T^2 species.

Concerning the compression tests among the two microspheres compositions. ChG10 slightly higher stress value could be attributed to the higher water content and the Si−OH groups present in the matrix of ChG10 microspheres. When the test ended, the spheres did not regained their original shape, indicating that the samples passed the elastic behavior and entered in the plastic domain.

Regarding the thermal degradation of raw chitosan flakes, the first stage after water vaporization was linked with the thermal decomposition of the polymeric chains of chitosan with vaporization of volatile compounds [35]. The pyrolysis of the polysaccharides initiates

with the disintegration of the glycosidic links and is related with mass loss from the acetylated and non-acetylated units of the polymer [36, 37]. The second stage of chitosan degradation was associated to the residual decomposition of chitosan [35, 38]. Regarding the GPTMS monomer, the abrupt slope was linked with the organic chains degradation of the GPTMS (CH_2 and CH), since the boiling point of GPTMS is referenced to be 120°C (2 mm Hg). In the case of the ChG10 and ChG15 microspheres, one additional stage occurred for the weight loss when compared with original chitosan flakes, possibly related to the presence of hydrolyzed GPTMS and β-GP. The ChG10 and, especially ChG15, comprise the highest exothermic peak, indicating that from 500°C pyrolysis or oxidative decomposition occurred, which is higher when compared to other siloxanes (~225°C) [39]. As confirmed by NMR, these microspheres contain siloxanes networks, and perhaps the DTA peaks indicate that the microspheres underwent thermal rearrangements due to the rupture of the siloxane chain to form products of lower molecular mass.

Taking into account the properties of chitosan together with the previous findings regarding the chitosan–GPTMS–β-GP injectable hydrogels [11], it was anticipated that these microspheres follow a drug controlled release system by the conjugation of the swelling and controlled degradation mechanisms.

The phosphate release from the microspheres matrix revolved around the composition and the surface charge of the samples, due to the weak electrostatic chemical interaction between the negatively charged phosphate molecules derived from β-GP ($-PO_4^{2-}$ or $-HPO_4^{-}$) and positively charged chitosan molecules ($-NH_3^{+}$) [40]. The amino groups of ChG15 were further crosslinked with GPTMS than ChG10, inhibiting the interaction between the amino groups with the phosphate groups. As a result, when deprived of interaction with amino groups, the remaining β-GP was readily released. Concerning the silicon, the released quantity depends on the amount crosslinked with the amino groups. The elements present on the samples surface

quantified by EDS correlate to the decrease of the amounts of Si and P on all pH series after 14 days of degradation obtained from ICP analysis. The pH 1.7 displayed the highest release rate of Si from the matrix, therefore the Si release is influenced at low pH. In case of P, a release rate trend by pH influence was not identified, due to the nature of the weak electrostatic bond between phosphate and amino group from chitosan.

In general, chitosan is able to dissolve adequately in a weak acid of pH near 4.5–6.4. Nonetheless, the chitosan-GPTMS hybrid spheres progressively degraded but remained even after 14 days at pH 5.4. The obtained weight loss pattern might be advantageous for drug delivery purposes (for instance, to transport insoluble drugs, proteins or peptides), since the nutrient absorption significantly occurs in the duodenum continuing all the way through the small intestines [41]. For these microspheres to be applied as drug carriers for the gastrointestinal track, it is essential to consider the effects related to the amount the chitosan, phosphorus, and silicon released and the limit tolerated by the body without causing side effects. Taking into account that chitosan has been previously permitted as a food additive by regulatory entities, like the FDA, it is expected that the uptake of the degradation byproducts from chitosan are considered safe for the human body. It's worth to mention that the digestive tract is a complex system in which not only pH variations occur but also the presence of bacterial communities and its enzymes, such as chitinase and chitosanase, also can play a role in the degradation of the chitosan matrix [42, 43].

Regarding phosphorus, this element plays an important biological role in bone health, and its concentration in serum fluids diverges with age, i.e. in infants, the standard range is 1.50–2.65 mM, while in adults, the average range is 0.8–1.5 mM [36]. Van Dyck et al. [37] reported that the regular concentration of silicon in sera of healthy Belgians (counting also pregnant women) was around 4.24 mM. Consequently, the maximum released amount from the hybrid

microspheres of both elements were very low in comparison, suggesting no harmful consequences to the human body.

Pelargonidin was used as a drug model for the *in vitro* incorporation and release profiling using the ChG10 and ChG15 hybrid microspheres in different pHs and incubation periods, mimicking the ones from the digestive system. Besides the initial burst behavior observed for both P1 and P3 series of concentrations, ChG15P1, ChG10P3 and ChG15P3 samples continued releasing pelargonidin in a slower and sustained way than ChG10P1. The higher amounts of pelargonidin released could be related to the loosening of the chitosan-siloxane network upon the entering of water molecules, forcing the incorporated pelargonidin to leave the matrix. This was specially observed on ChG10P1 microspheres. Due to a lower GPTMS molar ratio the ChG10 samples were more susceptible to the matrix loosening, especially when containing pelargonidin, leading to an increase in the size after 57 h of incubation. Visually, ChG10P1 and ChG10P3 microspheres were swollen, more transparent like and less sturdy than the ChG10 control. On ChG15P1 microspheres, very similar observations were made, with the difference that, these were still slightly more colored even after 57 h of incubation, than ChG10P1. Suggesting that the pelargonidin is not bound to the matrix, and the release mechanism occurs by water diffusion and due to pH influence, as depicted in figure 2-24. The pH-responsive release profile by swelling in acidic environment of the gastric fluid [44] is another type of release of the incorporated drug into the chitosan microspheres.

When applying these materials as drug carries, the quantification of the reactive sites on the hybrid microspheres is an important parameter to determine, since it's relevant to expect the amount of drug that can bond on the microspheres. From the ninhydrin assay data, ChG10 possesses higher availability of amino reactive sites than ChG15. Regarding the mechanism of interaction between amino groups and anthocyanins, Gao *et al*. [45] reported that the adsorption of anthocyanins was inversely (28%, 26% or 22%) related with the degree of deacetylation of

chitosan (76%, 83% or 89%). Therefore, when the degree of deacetylation of chitosan is higher than 70%, majority of the amine groups of chitosan can be protonated at around pH 3.9 and, consequently attracting negatively charged groups. At a pH ranging from 3 to 4, a significant molar fraction of anthocyanins with multiple acyl groups (like radish anthocyanins) changed into the flavylium cation form [46], showing repulsive electrostatic interactions with the also positively charged chitosan. This correlates to the release mechanism from the microspheres, in which the pelargonidin dispersed in the matrix was not bonded to the amino groups, but to the entrance of water molecules and the portion between loose matrix/crosslinked matrix and siloxane network.

Currently, no dietary reference intakes exist for anthocyanins, nevertheless a positive association was made between anthocyanin intake and risk reduction of certain diseases [47]. Studies reporting associations between anthocyanins (berry flavonoids) and cardiovascular health from the Kuopio Ischemic Heart Disease Risk Factor Study revealed a significant risk decrease of cardiovascular related deaths among 1,950 men with the highest berry intake (>408 g/day) contrasted with men with the lowest berry intake (<133 g/day), the participants were followed-up for 12.8 years [48]. Also, post-menopausal women ($n = 34,489$) also participated in a similar study carried out by the Iowa Women's Health Study, in which a significant drop in cardiovascular mortality was connected with strawberry intake (16 year follow-up), as well as a significant decrease in coronary heart disease mortality due to the intake of blueberries, at least once per week ingestion. It was also stated that an average intake of 0.2 mg/day of anthocyanins was linked to a significant risk reduction of cardiovascular mortality in the postmenopausal participants [49]. ChG15P1, ChG10P3 and ChG15P3 microspheres presented an adequate drug release profile with a more sustained and controlled release of pelargonidin, which can be linked to the higher amount of GPTMS for ChG15P1 and ChG15P3, providing the ability to maintain the matrix more intact for longer periods. Since the beneficial daily intake

of anthocyanins is rather high, it is less likely to achieve concentration levels that cause adverse effects even with the release profile of pelargonidin from ChG10P1. In order to evaluate the potential of a polymeric device for drug delivery, the most significant time is from the beginning up until the half-life time. Since in most systems the release slows down in the later periods to a rate which can be ineffective for therapeutic purposes. Hence, it is favorable to focus on the behavior of the initial 50 to 60% of the total drug released.

Overall, when assembling the obtained results from NMR, ninhydrin, degradation, swelling behavior and element release at different SGF conditions (pH 1.7, 5.4 and 6.7), it leads to the conclusion that the following phenomena occur: (1) at low pH conditions such as pH 1.7 or 5.4, the solvent interacts with the microspheres surface facilitating the release of the weak electrostatic bond between phosphate and chitosan from the most outer layers of the matrix, (2) slowly the matrix starts to loosen up of the chitosan skeleton and therefore steadily exposing and reaching the core of the matrix. This was corroborated with the release of P occurring mostly in the first 7 days. In addition, it was also determined by ninhydrin and by NMR that the chitosan was not fully crosslinked by GPTMS, and even though, ^{29}Si NMR shows some degree of condensation and strengthening of the matrix via the Si-O-Si network, the $Si(OCH_3)_3$ did not undergo full condensation, therefore the hybrid matrix contains regions that are easier to be attacked. It is also described that at low pH occurs the cleavage of the covalent bound established between the amino and the GPTMS. (3) As mentioned, the release of P and Si indicates a decrease in the matrix crosslinking, facilitating the exposure of the matrix to the hydrolysis of the chitosan backbone and to the entrance of water molecules causing a swelling in the microspheres. The decrease of the crystallinity of the chitosan skeleton after the degradation test was confirmed by XRD. Consequently, the pH influences the degradation and swelling of the microspheres, which is accelerated at lower pH than neutral pH conditions, as confirmed by the release rates. This degradation pattern and swelling behavior from the

microspheres influenced the release profile of pelargonidin. In pH 1.7 and 5.4, both ChG10 and ChG15 have overlapping curves and release the same amounts of pelargonidin. From the previous observations, the phosphate crosslinked in the surface is being released together with the pelargonidin for both ChG10 and ChG15 at very similar rates. Nonetheless the swelling and weight gain was greater in ChG10P1 and ChG10P3 microspheres in lower pH conditions, in addition to a different release pattern of pelargonidin when entering the pH 6.7 (from 24 to 57 h). This difference between samples was affected by the initial low pH in which the matrix of the ChG10P1 and ChG10P3 samples was more easily weakened and therefore reaching the matrix core earlier, leading to a higher diffusion rate of pelargonidin and to the facilitated entrance of water molecules when compared to ChG15P1 and ChG15P3 microspheres. Furthermore, the difference between the P1 and P3 series in terms of the release behavio could be associated to the more packed environment in the matrix due to the higher concentration of pelargonidin in the P3 series microspheres, and thus reducing the available free volume between the polymeric chains, as a result reducing the drug release.

Lastly, it is described that in acidic conditions the protonated amino groups of chitosan will interact with sialic acid (N-acetylneuraminic acid) from the gastric mucus by electrostatic interaction. Therefore, chitosan microspheres have the potential to improve the residence time of a drug in the gastrointestinal track [50]. As well as protect the therapeutic agents from the hostile conditions of the upper gastrointestinal tract. Therefore, if these spheres are taken as supplements in an empty stomach the absorption of pelargonidin can be considered higher, since is also desirable for the releasing of drug to occur throughout the intestines, since the nutrients absorption occurs mainly in the small intestines lining of the gastrointestinal track.
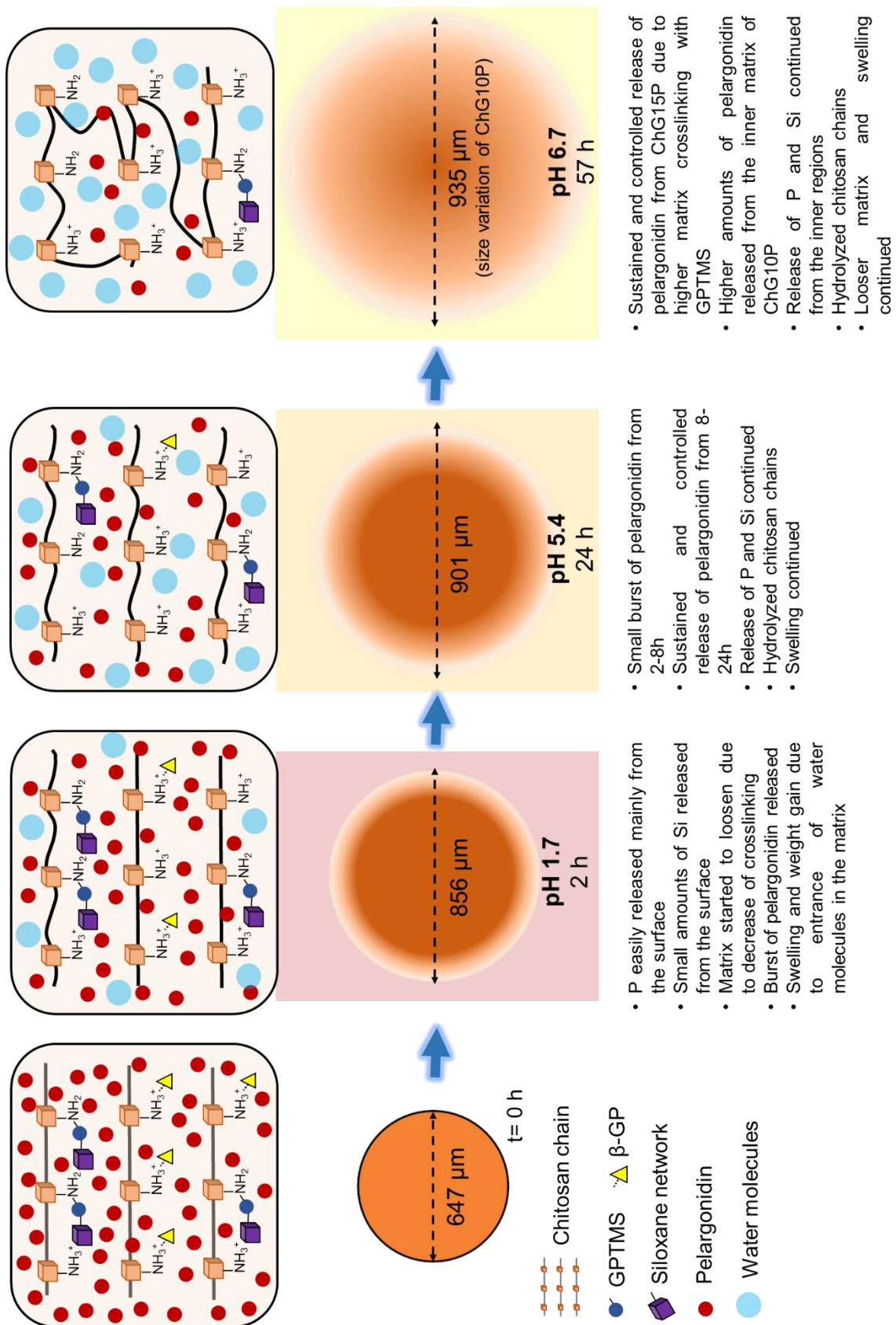
Figure 2-24 Schematic representation summing up the pelargonidin release behavior in accordance to the microspheres structure and matrix degradation performance.

2.5. Conclusions

A microfluidic approach was successfully used to synthesize chitosan-siloxane hybrids microspheres using via sol–gel process using β-GP as the neutralizing agent. The produced microspheres had spherical shapes with uniform sizes of around 650 μm. GPTMS was used as a crosslinking agent, and consequently it inhibited the degradation of chitosan even at low pH. The microspheres spherical shapes were maintained even after 14 days of the degradation at low pHs. The formation of siloxane networks occurred in the chitosan polymeric matrix and condensation was assisted by the GPTMS content. In case phosphate, the release easily occurred due to its weak electrostatic interaction with chitosan. In case of silicon, it was released together with chitosan molecules and was dependent on the initial amount of GPTMS. The hybrid microspheres endured for 14 days harsh pH conditions. This time interval is longer than the time necessary to complete a digestion cycle. The produced chitosan-siloxane hybrid microspheres incorporated pelargonidin as a drug model successfully. Under simulated gastro intestinal conditions, such as pH and digestion period, the release occurred via diffusion. On both microspheres an initial burst at pH 1.7 was observed, followed by a slower and more sustained release in pH 5.4 and 6.7 for ChG15P, whereas for ChG10P the pelargonidin was released more easily. These spheres appear to be promising for delivery of therapeutic agents for gastro intestinal applications due to its resistance to low pH and ability to retain pelargonidin for longer periods of time, since even after 57 h the spheres still present some color indicating the presence of residual pelargonidin in the matrix. Therefore, it appears to be able to protect the therapeutic agents from the hostile conditions of the upper gastrointestinal tract.

References

1.   Prajapati, V. D., Jani, G. K., and Kapadia, J. R., *Current knowledge on biodegradable microspheres in drug delivery.* Expert Opinion on Drug Delivery, 2015, **12**(8): 1283-1299.

2.   Sinha, V. R., Singla, A. K., Wadhawan, S., Kaushik, R., Kumria, R., Bansal, K., and Dhawan, S., *Chitosan microspheres as a potential carrier for drugs.* International Journal of Pharmaceutics, 2004, **274**(1): 1-33.

3.   Jalil, R. and Nixon, J. R., *Biodegradable poly(lactic acid) and poly(lactide-co-glycolide) microcapsules: problems associated with preparative techniques and release properties.* Journal of Microencapsulation, 1990, **7**(3): 297-325.

4.   Godugu, C., Patel, A. R., Doddapaneni, R., Somagoni, J., and Singh, M., *Approaches to improve the oral bioavailability and effects of novel anticancer drugs berberine and betulinic acid.* PLOS ONE, 2014, **9**(3): 1-15.

5.   Thanou, M., Verhoef, J. C., Marbach, P., and Junginger, H. E., *Intestinal absorption of octreotide: N-trimethyl chitosan chloride (TMC) ameliorates the permeability and absorption properties of the somatostatin analogue in vitro and in vivo.* Journal of Pharmaceutical Sciences, 2000, **89**(7): 951-957.

6.   Weiner, M. L., *An overview of the regulatory status and of the safety of chitin and chitosan as food and pharmaceutical ingredients*, in *Advances in chitin and chitosan*, Brine, C.J., Standford, P.A., and Zikakis, J.P., Editors. 1992, Elsevier Applied Science. 663-672.

7.   Fda. *Gras notices: Shrimp-derived chitosan*. [cited 2016 16 March]; Available from: https://www.fda.gov/downloads/Food/IngredientsPackagingLabeling/GRAS/NoticeInventory/ucm337459.pdf.

8. Coue, G. and Engbersen, J. F. J., *Cationic polymers for intracellular delivery of proteins*, in *Cationic polymers in regenerative medicine*, Samal, S. and Dubruel, P., Editors. 2014, The Royal Society of Chemistry. 365-367.

9. Chandy, T. and Sharma, C. P., *Chitosan-as a biomaterial.* Biomaterials, Artificial Cells and Artificial Organs, 1990, **18**(1): 1-24.

10. Khor, E. and Lim, L. Y., *Implantable applications of chitin and chitosan.* Biomaterials, 2003, **24**(13): 2339-2349.

11. Shirosaki, Y., Hirai, M., Hayakawa, S., Fujii, E., Lopes, M. A., Santos, J. D., and Osaka, A., *Preparation and in vitro cytocompatibility of chitosan–siloxane hybrid hydrogels.* Journal of Biomedical Materials Research Part A, 2015, **103**(1): 289-299.

12. Wan, J., *Microfluidic-based synthesis of hydrogel particles for cell microencapsulation and cell-based drug delivery.* Polymers, 2012, **4**(2): 1084-1108.

13. Cruz-Neves, S., Shirosaki, Y., Miyazaki, T., and Hayakawa, S., *Characterization and degradation study of chitosan-siloxane hybrid microspheres synthesized using a microfluidic approach.* Materials Science and Engineering: C, 2017, **81**: 571-579.

14. Carelli, V., Coltelli, S., Di Colo, G., Nannipieri, E., and Serafini, M. F., *Silicone microspheres for pH-controlled gastrointestinal drug delivery.* International Journal of Pharmaceutics, 1999, **179**(1): 73-83.

15. Khatri, S. and Awasthi, R., *Piperine containing floating microspheres: an approach for drug targeting to the upper gastrointestinal tract.* Drug delivery and translational research, 2016, **6**(3): 299-307.

16. Hale, A. and Hovey, M. J., *Fluid, electrolyte, and acid-base imbalances: content review plus practice questions*, Davis, F.A., Editor. 2013, F. A. Davis Company. 183.

17. Thomas, J. and Klingler, W., *The influence of pH and other metabolic factors on fascial properties*, in *Fascia: the tensional network of the human body: the science and clinical*

applications in manual and movement therapy, Schleip, R., Findley, T.W., Chaitow, L., and Huijing, P., Editors. 2013, Elsevier Health Sciences. 171.

18.   Herlihy, B. U., *Water, electrolyte, and acid-base balance*, in *The human body in health and illness*. 2014, Elsevier Health Sciences. 485-488.

19.   Ovesen, L., Bendtsen, F., Tage-Jensen, U., T Pedersen, N., R Gram, B., and J Rune, S., *Intraluminal pH in the stomach, duodenum, and proximal jejunum in normal subjects and patients with exocrine pancreatic insufficiency*. Gastroenterology, 1986, **90**(4): 958-962.

20.   Dressman, J. B., Berardi, R. R., Dermentzoglou, L. C., Russell, T. L., Schmaltz, S. P., Barnett, J. L., and Jarvenpaa, K. M., *Upper gastrointestinal (GI) pH in young, healthy men and women.* Pharmaceutical Research, 1990, **7**(7): 756-761.

21.   Fallingborg, J., *Intraluminal pH of the human gastrointestinal tract.* Danish Medical Bulletin, 1999, **46**(3): 183-196.

22.   Schwarz, R., Kaspar, A., Seelig, J., and Künnecke, B., *Gastrointestinal transit times in mice and humans measured with ^{27}Al and ^{19}F nuclear magnetic resonance.* Magnetic Resonance in Medicine, 2002, **48**(2): 255-261.

23.   He, B., Ge, J., Yue, P., Yue, X., Fu, R., Liang, J., and Gao, X., *Loading of anthocyanins on chitosan nanoparticles influences anthocyanin degradation in gastrointestinal fluids and stability in a beverage.* Food Chemistry, 2017, **221**: 1671-1677.

24.   Kanokpanont, S., Yamdech, R., and Aramwit, P., *Stability enhancement of mulberry-extracted anthocyanin using alginate/chitosan microencapsulation for food supplement application.* Artificial Cells, Nanomedicine, and Biotechnology, 2017: 1-10.

25.   Basu, A., Rhone, M., and Lyons, T. J., *Berries: emerging impact on cardiovascular health.* Nutrition reviews, 2010, **68**(3): 168-177.

26. Prochazkova, S., Vårum, K. M., and Østgaard, K., *Quantitative determination of chitosans by ninhydrin.* Carbohydrate Polymers, 1999, **38**(2): 115-122.

27. Cannon, J. G., *Peptic ulcer and reflux esophagitis*, in *Pharmacology for Chemists*. 2007, Oxford University Press. 288.

28. Milan, S. and Rosato, F. E., *Nutrient disposition and response*, in *Handbook of Drug-Nutrient Interactions*, Boullata, J.I. and Armenti, V.T., Editors. 2010, Humana Press. 120-125.

29. Socrates, G., *Infrared and raman characteristic group frequencies: tables and charts*. 2004: John Wiley & Sons.

30. Modrzejewska, Z., Nawrotek, K., Maniukiewicz, W., and Douglas, T., *Structural characteristics of thermosensitive chitosan glutamate hydrogels in variety of physiological environments.* Journal of Molecular Structure, 2014, **1074**(Supplement C): 629-635.

31. Shirosaki, Y., Tsuru, K., Hayakawa, S., Osaka, A., Lopes, M. A., Santos, J. D., and Fernandes, M. H., *In vitro cytocompatibility of MG63 cells on chitosan-organosiloxane hybrid membranes.* Biomaterials, 2005, **26**(5): 485-493.

32. Shirosaki, Y., Okayama, T., Tsuru, K., Hayakawa, S., and Osaka, A., *In vitro bioactivity and MG63 cytocompatibility of chitosan-silicate hybrids.* International Journal of Materials and Chemistry, 2013, **3**(3A): 1-7.

33. Pujala, R. K., *Dispersion stability, microstructure and phase transition of anisotropic nanodiscs*. 2014, School of Physical Sciences, Jawaharlal Nehru University, New Delhi, India: Springer Theses.

34. Mu, L. and Feng, S. S., *Fabrication, characterization and in vitro release of paclitaxel (Taxol®) loaded poly (lactic-co-glycolic acid) microspheres prepared by spray drying*

technique with lipid/cholesterol emulsifiers. Journal of Controlled Release, 2001, **76**(3): 239-254.

35. López, F. A., Mercê, A. L. R., Alguacil, F. J., and López-Delgado, A., *A kinetic study on the thermal behaviour of chitosan.* Journal of Thermal Analysis and Calorimetry, 2008, **91**(2): 633-639.

36. Nieto, J. M., Peniche-Covas, C., and Padro´N, G., *Characterization of chitosan by pyrolysis-mass spectrometry, thermal analysis and differential scanning calorimetry.* Thermochimica Acta, 1991, **176**: 63-68.

37. Neto, C. G. T., Giacometti, J. A., Job, A. E., Ferreira, F. C., Fonseca, J. L. C., and Pereira, M. R., *Thermal analysis of chitosan based networks.* Carbohydrate Polymers, 2005, **62**(2): 97-103.

38. Peniche-Covas, C., Jiménez, M. S., and Núñez, A., *Characterization of silver-binding chitosan by thermal analysis and electron impact mass spectrometry.* Carbohydrate Polymers, 1988, **9**(4): 249-256.

39. Murphy, C. M., Saunders, C. E., and Smith, D. C., *Thermal and oxidation stability of polymethylphenylsiloxanes.* Industrial & Engineering Chemistry, 1950, **42**(12): 2462-2468.

40. Cho, J., Heuzey, M.-C., Bégin, A., and Carreau, P. J., *Physical gelation of chitosan in the presence of β-glycerophosphate: the effect of temperature.* Biomacromolecules, 2005, **6**(6): 3267-3275.

41. Gropper, S. S., Smith, J. L., and Groff, J. L., *The digestive system: mechanism for nourishing the body*, in *Advanced Nutrition and Human Metabolism*. 2008, Cengage Learning. 33-53.

42. Gooday, G. W., *Physiology of microbial degradation of chitin and chitosan.* Biodegradation, 1990, **1**(2): 177-190.

43. Zhang, H. and Neau, S. H., *In vitro degradation of chitosan by bacterial enzymes from rat cecal and colonic contents.* Biomaterials, 2002, **23**(13): 2761-2766.

44. R. Patel, V. and Amiji, M., *Preparation and characterization of freeze-dried chitosan-poly(ethylene oxide) hydrogels for site-specific antibiotic delivery in the stomach.* Pharmaceutical Research, 1996, **13**(4): 588-593.

45. Gao, R., Jing, P., Ruan, S., Zhang, Y., Zhao, S., Cai, Z., and Qian, B., *Removal of off-flavours from radish (Raphanus sativus L.) anthocyanin-rich pigments using chitosan and its mechanism(s).* Food Chemistry, 2014, **146**(Supplement C): 423-428.

46. Dangles, O., Saito, N., and Brouillard, R., *Anthocyanin intramolecular copigment effect.* Phytochemistry, 1993, **34**(1): 119-124.

47. Wallace, T. C. and Giusti, M. M., *Anthocyanins.* Advances in Nutrition, 2015, **6**(5): 620-622.

48. Rissanen, T. H., Voutilainen, S., Virtanen, J. K., Venho, B., Vanharanta, M., Mursu, J., and Salonen, J. T., *Low intake of fruits, berries and vegetables is associated with excess mortality in men: the Kuopio Ischaemic Heart Disease risk factor (KIHD) study.* The Journal of Nutrition, 2003, **133**(1): 199-204.

49. Mink, P. J., Scrafford, C. G., Barraj, L. M., Harnack, L., Hong, C.-P., Nettleton, J. A., and Jacobs, D. R., *Flavonoid intake and cardiovascular disease mortality: a prospective study in postmenopausal women.* The American Journal of Clinical Nutrition, 2007, **85**(3): 895-909.

50. Lehr, C.-M., Bouwstra, J., Schacht, E., and E. Junginger, H., *In vitro evaluation of mucoadhesive properties of chitosan and some other natural polymers.* International Journal of Pharmaceutics, 1992, **78**(1-3): 43-48.

Chapter 3.

BACTERIAL BEHAVIOR ON CHITOSAN-SILOXANE HYBRID MICROSPHERES AND HYDROGELS CONTAINING CERIUM

3.1. Introduction

The growing resistance towards antibiotics in bacteria is a serious problem that requires the researchers to come up with new strategies to overcome this situation. The use of biomaterials with antibacterial agents is one of the strategies adopted.

Biomaterials hold functional groups like –OH, –COOH and –NH$_2$, therefore having the potential to stabilize and/or capture ions, such as metal ions [1]. Cerium (Ce) is rare earth element of the lanthanide group (or rare earth metals) and received the researcher's attention due to its antimicrobial activity (towards fungi and bacteria). Systematic investigations confirmed the bacteriostatic and bactericidal activity of cerium compounds in a wide variety of bacteria [2-4]. The biological role of cerium is not yet clearly understood, but it has been noticed that cerium salts can have a role in the stimulation of the metabolism [5]. But in the case of bacteria, the action mechanism is based on the uptake of cerium ions into the cytoplasm of the bacterium cell and cause the following events: inhibit cellular respiration, oxygen uptake, glucose metabolism, and also disrupt the cell membrane [6, 7]. Some researchers investigated the use of cerium oxide [8] or nitrate (Ce(NO$_3$)$_3$) [9], but very few studies are available using cerium (III) chloride (CeCl$_3$) as an antibacterial agent, in drug delivery systems. Chlorides are widely present in nature as salts. Chloride in food occurs naturally at levels generally less than 0.36 mg/g, and during the food processing the mean dietary intake can range 6-12g/day [10]. The toxicity of nitrate ion itself is debatable [11], but the anaerobic bacteria present in the

gastrointestinal tract and oral cavity converts it to a more toxic nitrite leading to increased risk of methaemoglobinaemia and gastrointestinal cancer [12].

In the previous chapter the chitosan-siloxane hybrid microspheres were characterized [13] and tested as drug carrier, using pelargonidin as a drug model. It was indicated that the microspheres have good uniformity of size, stability and resistance towards harsh pH environments, and that the spheres hold free amino reactive sites available to interact with therapeutic molecules. Taking these microspheres features into account and the advantages referred by cerium as an antibacterial agent, the incorporation of cerium in this biomaterial formulation was used as a strategy to inhibit bacterial growth (figure 3-1). In this study, two different approaches were tested to include cerium. The incorporation and adsorption ability of cerium ions on the chitosan–GPTMS–β-GP hybrid microspheres were tested, in addition to the incorporation of cerium into the chitosan–GPTMS–β-GP hydrogels. The bacterial behavior of both materials was observed with pathogenic gram-negative strain (*E. coli*) and gram-positive strain (*S. aureus*).
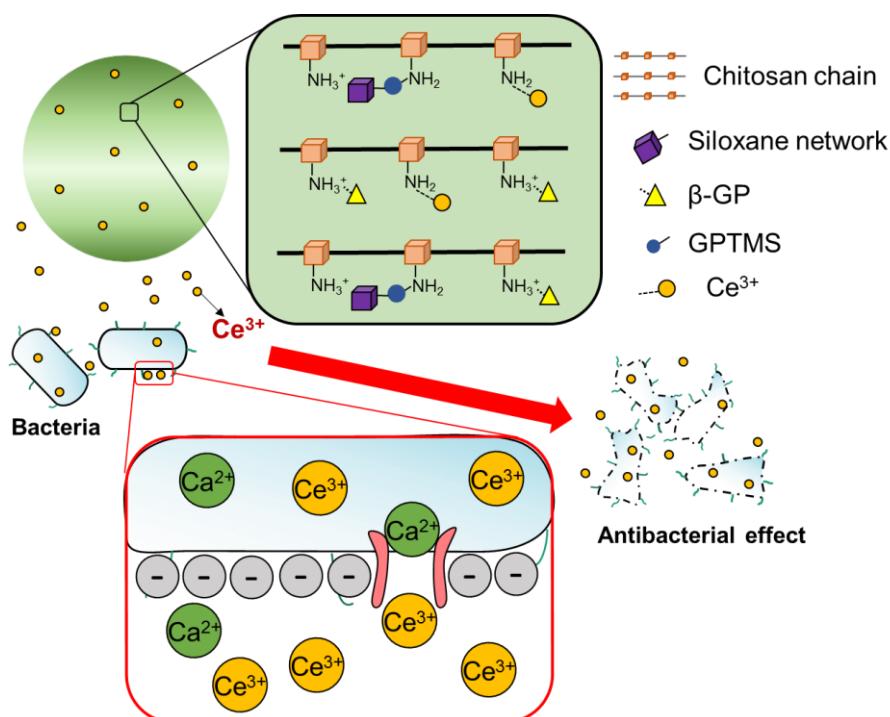
Figure 3-1 Schematic representation of the material design and antibacterial action mechanism of cerium.

3.2. Materials and methods

3.2.1. MIC of cerium

S. aureus 209P (ATCC 6538P) and *E. coli* NIHJ were streak directly from the stock to fresh Luria-Bertani Broth (Liofilchem, Roseto degli Abruzzi, Italy) agar plates and incubated at 37°C for 18 h. To perform the inoculum, a single colony from a bacteria strain was removed from the plate and inoculated in a glass test tube with 5 mL fresh LB medium and incubated at 37°C and 120 rpm for 18 h. From the prepared inoculum, 1 mL was removed and transferred to an Eppendorf tube and centrifuged at 10,000 rpm for 1 min. The supernatant was discarded and the pellet resuspended in 1 mL PBS. This washing with PBS step was repeated twice. The same steps were applied to the other bacterial strain. For each bacterial strain dilutions with LB to achieve a bacterial concentration of 1×8^3 CFU/mL were prepared for the experiments.

For the MIC determination experiment, an appropriate amount of $CeCl_3$ was dissolved in 0.1 M HCl. The solution was sterilized by filtration. The dilutions were prepared using fresh LB and the bacterial inoculum to make the following final concentrations of 1.5, 3, 4.5, 6 and 7 mM of cerium. The pH of the solutions remained neutral (pH 7.0). The Eppendorf tubes were taken to the incubator at 37°C and 300 rpm. After 4 h of incubation, 100 μL of 5 mg/mL of 3-(4,5-dimethylthiazol-2-yl)-2,5-diphenyl tetrazolium bromide (MTT) was added and taken again to the incubator at 37°C for 4 h without shaking. MTT is reduced to a purple formazan reaction product by living cells and bacteria [14]. After 4 h, the samples were centrifuged at 10,000 rpm for 1 min and the supernatant was removed. Afterwards, 500 μL of dimethyl sulfoxide (DMSO, Wako, Osaka, Japan) were added and kept at room temperature for 30 min. The supernatant was transferred to a 96 well plate and read at λ=600 nm in a spectrophotometer.

3.2.2. Preparation of chitosan-siloxane microspheres with cerium

To include cerium [cerium (III) chloride heptahydrate ($CeCl_3 \bullet 7H_2O$), Nacalai tesque, Kyoto, Japan] in the samples, an incorporation method and immersion method were tested. An appropriate amount of cerium was dissolved in 0.1 M HCl. Briefly, chitosan as dissolved in 0.1 M HCl to achieve a 2% (w/v) concentration. The chitosan solution was mixed in a planetary centrifugal mixer at room temperature, followed by autoclaving at 121°C for 20 min and filtering to obtain a homogeneous solution. A determined amount of GPTMS was added to the chitosan solution, and the mixture was stirred at room temperature for 2 h. For the incorporation method, $CeCl_3$ was added into the chitosan-GPTMS precursor sol in a molar ration of 1:1 for chitosan:cerium. The mixture was stirred for 30 min at room temperature. And then, 0.68 mL of 2.5 M β-GP were added at 0°C stirring for 10 min. The final pH of the hybrid solution including cerium was 7.0. The solution including cerium was applied in the microfluidic system following the parameters described in chapter 2, section 2.2.1, and table 2-1 for ChG10 microspheres. In order to decrease the release of cerium, the washing steps were reduced to ethanol 100 (3x), 70% (3x) and in PBS (2x). The n=200 spheres/flask in ultrapure water were sterilized by autoclaving at 121°C for 20 min.

The immersion method was performed after the microspheres were produced and washed as explained in chapter 2, section 2.2.1. Therefore, ChG10 spheres n=200 spheres/flask were immersed in 1 mL of 10, 15 and 20 mM cerium solutions overnight at room temperature and 130 rpm. After autoclaving, the samples were washed twice with PBS.

The samples from both methods were dried at 50°C and their surface morphology and atomic composition were analyzed by SEM-EDS. The samples were coated with a 15 nm layer of Pt/Pd using a magnetron-sputter coater.

3.2.3. Preparation of chitosan-siloxane hybrid hydrogels with cerium

The incorporation of cerium in the chitosan-siloxane hybrid hydrogels followed similarly the initial steps, with the exception of the synthesis of the hydrogels always under sterile conditions. Briefly, a 2% (w/v) chitosan solution was prepared, autoclaved and filtered. Next, GPTMS in the chitosan:GPTMS molar ratio 1:1 proportion. Afterwards, a freshly prepared cerium solution dissolved in 0.1 M HCL was added into the chitosan-GPTMS precursor sol achieving the final concentrations of 4.5 and 13.5 mM of cerium. At last, β-GP was added for neutralization. For the direct method, 200 µL of the solution were inserted into Eppendorf tubes, while for the indirect method, the same volume was poured into special cell culture inserts (8.0 µm pores size, Falcon, New York, USA) for 24 well plates (with low evaporation lid, Falcon, New York, USA). The samples were inserted in a humidified chamber at 37°C and 5% CO_2 atmosphere overnight.

3.2.4. *E. coli* and *S. aureus* culture on microspheres and hydrogels containing cerium

For the culture experiment using the microspheres, a 96 well plate was used for the bacterial culture. Microspheres n=200/replicate were incubated with 200 µL of 1×8^3 CFU/mL of bacterial suspensions prepared from both *E. coli* and *S. aureus* strains. The plate was taken to the incubator at 37°C and 300 rpm. After 4 h of incubation, 20 µL of MTT solution were added to each well and taken again to the incubator at 37°C for 4 h. After 4 h, the solutions and spheres were transferred to Eppendorf tubes and centrifuged at 10,000 rpm for 2 min and the supernatant was removed. The deposited formazan salts were dissolved with 100 µL of DMSO and incubated at room temperature for 30 min. The supernatant was transferred to a new plate and read at λ=600 nm. Whereas, for the hydrogels, the culture was performed using cell culture inserts with 200 µL of the chitosan–GPTMS–Ce-β-GP hydrogels in a 24 well plate for the

indirect mode. The same bacterial concentration of 1.8×10^3 CFU/mL was used in 1 mL of bacterial inoculum for each well. The same conditions were applied concerning the incubation times and for the MTT test (with the exception of using 100 µL of MTT solution instead). Figure 3-2 represents the direct and indirect methods used for the culture of bacteria in the chitosan-GPTMS-Ce-β-GP hydrogels.
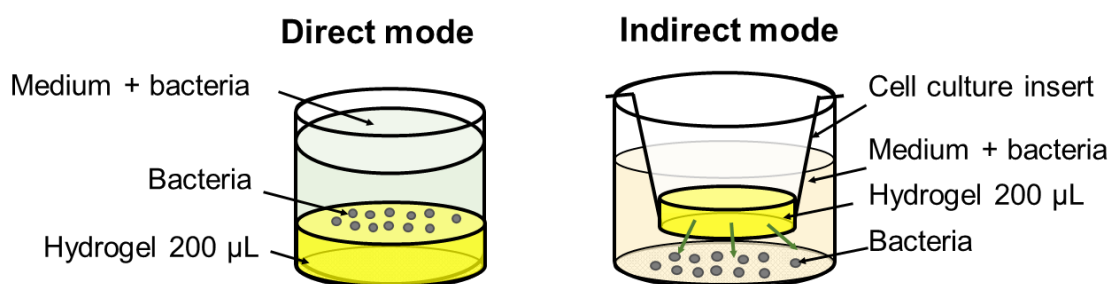
Figure 3-2 Representation of the direct and indirect methods used for the culture of bacteria in the chitosan–GPTMS–Ce–β-GP hydrogels.

To observe *E. coli* and *S. aureus* strains behavior when in contact with the chitosan–GPTMS–Ce-β-GP hydrogels, a direct culture of the bacteria in Eppendorf tubes containing 200 µL of the hydrogels containing 4.5 and 13.5 mM of cerium was performed. After 24 h of culture at 37°C these samples were prepared for SEM observations. The hydrogels were fixed in a 1.5% glutaraldehyde (Wako, Osaka, Japan) in 0.14 M sodium cacodylate trihydrate buffer (Sigma-Aldrich®, St. Louis, USA) at room temperature for 15 min. Samples were gently washed with distilled water. Afterwards, the dehydration was performed using a series of graded ethanol solutions, specifically 50, 70, 80, 90 and 100%, for 10 min in each. The samples were dried overnight at room temperature. At last, the samples were coated with a 15 nm layer of Pt/Pd gold film and observed using SEM.

3.2.5. Evaluation of the *E. coli* and *S. aureus* viability cultured with cerium phosphate

To understand if the phosphate from β-GP nullifies the antibacterial activity of cerium, sterile solutions of cerium and β-GP (containing final concentration of 13.5 mM cerium with 625 mM β-GP and 6.75 mM cerium with 312.5 mM β-GP), cerium (13.5 and 6.75 mM) and β-β-GP (625 and 312.5 mM) were prepared. For each condition 0.2 mL of solution were inserted in Eppendorf tubes together with the *E. coli* and *S. aureus* bacterial suspensions to make a final concentration of 1×10^2 CFU/mL. The solutions were incubated at 37°C for 24 h at 300 rpm. The bacterial viability was measured on both strains using the MTT assay, in which 0.1 mL of MTT were added to each tube and taken again to the incubator at 37°C for 4 h. After 4 h, the Eppendorf tubes were centrifuged at 10,000 rpm for 5 min and the supernatant was removed. The formazan salts were dissolved with 1 mL of DMSO and incubated at room temperature for 30 min. The supernatant was transferred to a 96 well plate and read at λ=600 nm.

3.2.6. Statistical analysis

The statistical analysis was performed using one-way analysis of variance ANOVA followed by Tukey's test and the significance level of $p < 0.05$. GraphPad Prism (GraphPad Prism Software version 6, CA, United States) was used to run the statistical analysis.

3.3. Results

3.3.1. Viability of *E. coli* and *S. aureus* on chitosan-siloxane microspheres with cerium

The minimum inhibitory concentration (MIC) is as important parameter to determine on microorganisms like bacteria. Figure 3-3 shows the MIC of $CeCl_3$ values for both *Escherichia coli* and *Staphylococcus aureus*. Bacterial inhibition was observed when using a concentration

of 3 mM of $CeCl_3$, almost complete eradication was observed in this condition, therefore higher concentration that 3 mM is advised to have a complete antibacterial effect.

Table 3-1 shows the comparison of the atomic ratio of Ce/C via EDS, on the ChG10 surfaces using the immersion and incorporation method. The immersion method retained the cerium on ChG10 microspheres, whereas the incorporation method was not effective to maintain the cerium incorporated on the hybrid microspheres. From the SEM images on figure 3-4, it was possible to observe a clear difference between the microspheres surface. A film like matter was covering, partially or completely, the surface of the ChG10Ce microspheres. Despite using fewer washing steps, when washing the samples with ethanol to remove the oil, the cerium was removed from the microspheres and possibly some of the oil lingered on the microspheres surface. In the immersion method the surface of the samples was identical to the original ChG10 and cerium was also detected, therefore the immersion method was chosen for the bacterial tests.

Figure 3-5 displays the bacterial viability when with ChG10 with cerium from the immersion method. Upon contact with both *E. coli* and *S. aureus* suspensions, no antibacterial effect was observed. Possibly due to not enough cerium on the ChG10 spheres, even at 20 mM.
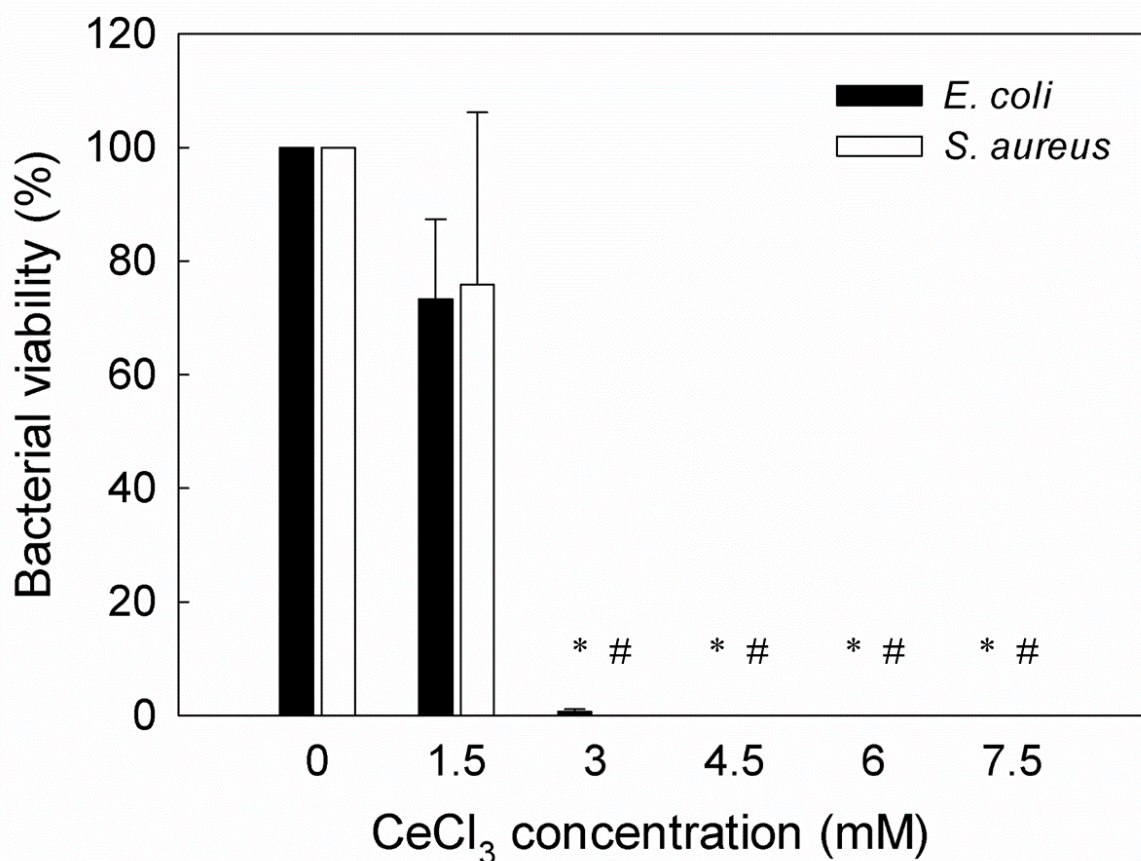
Figure 3-3 MIC of CeCl₃ in *E. coli* and *S. aureus*. The viability is presented in ratio towards the control (only bacteria). A statistically significant difference (p<0.05) was observed when comparing to *E. coli* (*) control and *S. aureus* (#) control (no sample).

Table 3-1 Comparison of the atomic ratio of Ce/C still present on the ChG10 microspheres surfaces via EDS analysis, when using the immersion method (25 mM cerium) and incorporation method (25 mM cerium).

Sample	Method	Ce/C (atomic %)
ChG10-Ce	Immersion	0.115 ± 0.042
ChG10Ce	Incorporation	0.000 ± 0.000
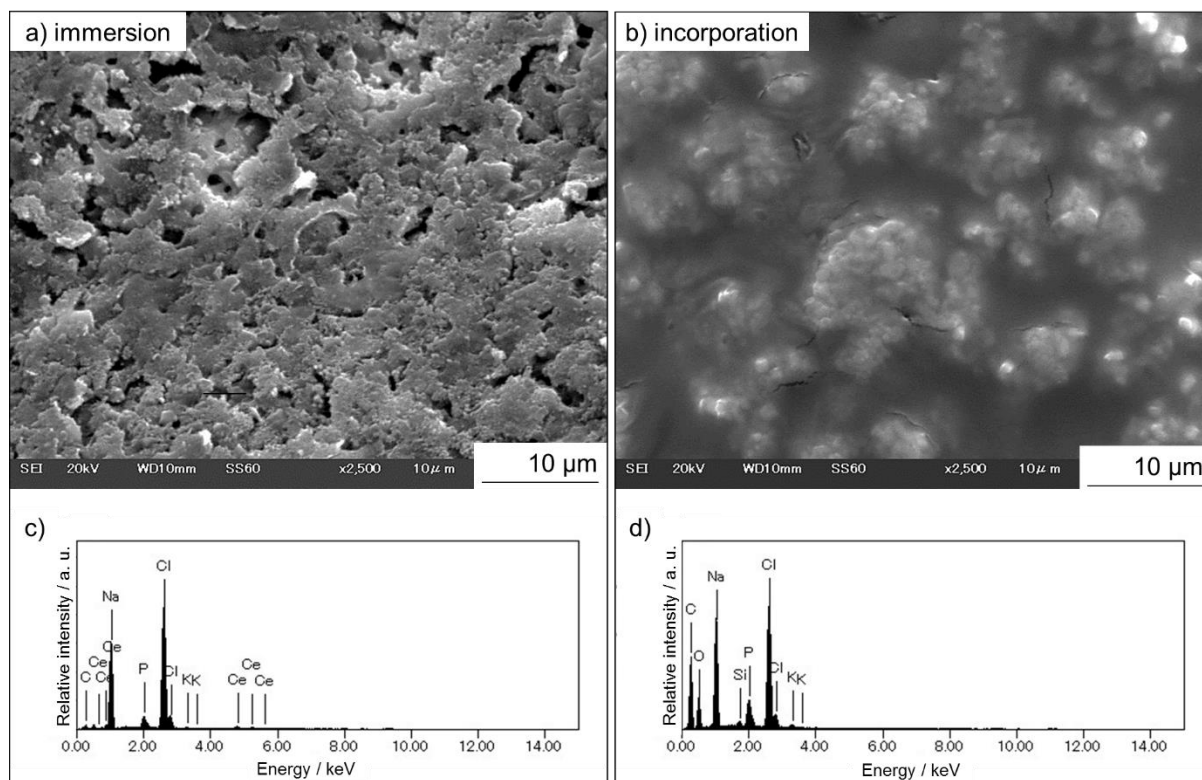
Figure 3-4 SEM images of dried ChG10 samples with cerium using a) immersion method, in which the samples were immersed in a cerium solution, and c) respective EDS. b) incorporation method, where cerium was incorporated in the hybrid solution (chitosan–GPTMS–Ce–β-GP), and d) respective EDS.
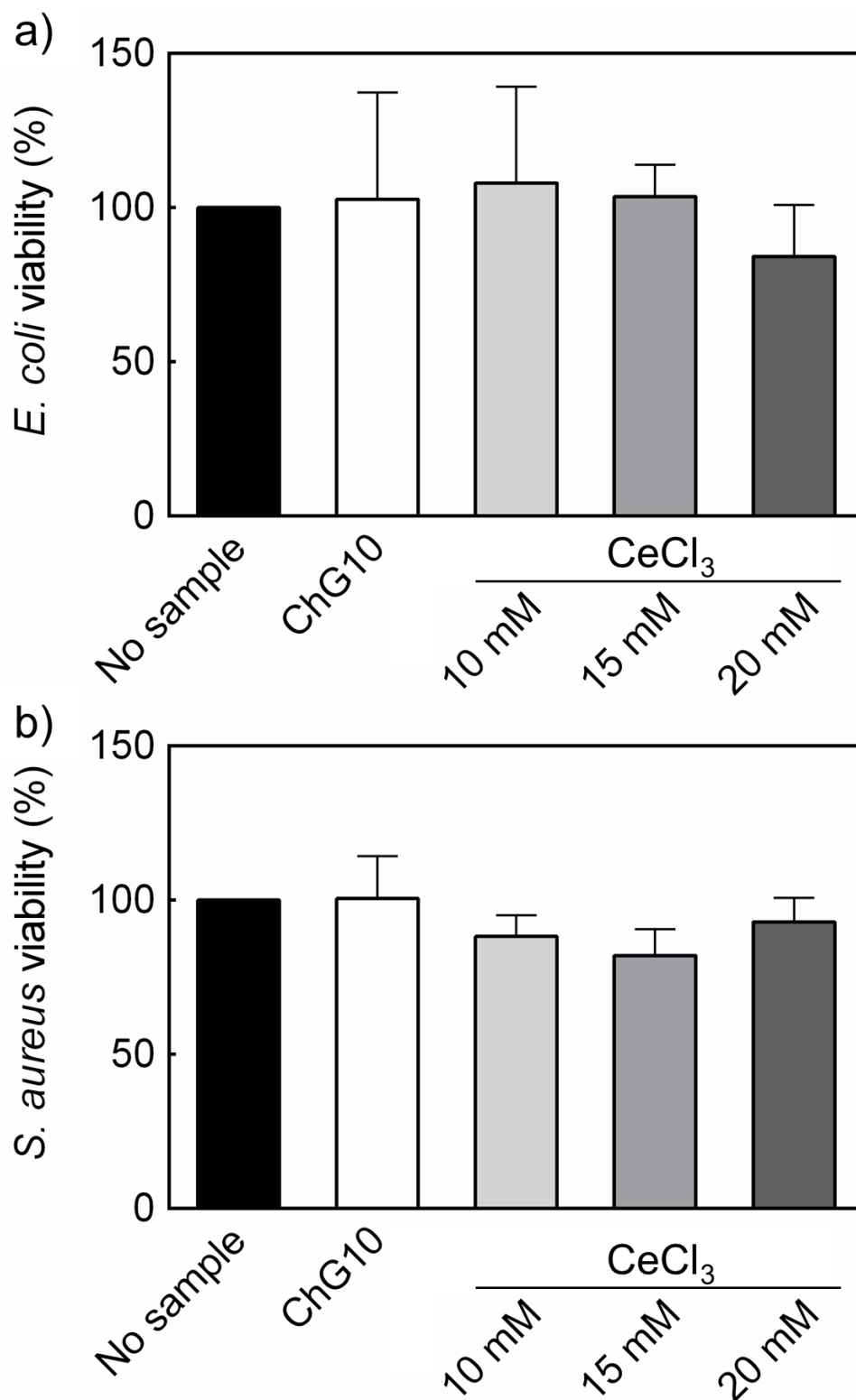
Figure 3-5 Bacterial viability of a) *E. coli* and b) *S. aureus* (using MTT assay) cultured on ChG10 microspheres previously immersed in CeCl$_3$ solutions. The viability is presented in ratio towards the positive control (only bacteria).

3.3.2. Viability of *E. coli* and *S. aureus* on chitosan-siloxane hydrogels with cerium

The SEM micrographs exhibited in figure 3-6, are from the culture of *E. coli* and *S. aureus* when in direct contact with the hydrogels with and without cerium. The higher the loading of cerium in the hydrogel, apparently the more the bacteria was able colonize when compared to lower amounts of cerium in the hydrogel. The hydrogel surface of ChG10Ce13.5 was completely covered with *E.coli* and *S. aureus* cells. In terms of cell morphology, the typical rod shape of *E.coli* was observed with a size around 1 x 3μm [15, 16]. As well as, the spherical organisms in grape-like clusters with diameter around 1 μm for *S. aureus*. Both cycles of apoptosis and division [17] were observed in the hydrogel samples with and without cerium.

To increase the loading amount, cerium was incorporated on chitosan-GPTMS-β-GP hydrogels instead of the microspheres. During the preparation of the chitosan-GPTMS-β-GP hydrogels with cerium, immediately after adding the β-GP it was visually noticeable a change in the color of the precursor sol, from a transparent to a more whitish opaque appearance. The higher the amount of cerium added, the more whitish opaque it would become. Figure 3-7 shows this visible change.

Figure 3-8 displays no antibacterial effect at the highest concentration of cerium on the ChG10Ce13.5 hydrogel. On the contrary, the viability of *S. aureus* increased on ChG10, around 0.3 fold, and also nearly 0.3 fold on ChG10Ce13.5 hydrogels.

Cerium phosphate solutions were prepared using the same concentration as the cerium and β-GP components as present in the hydrogel from figure 3-8, as well as half of its concentration. Figure 3-9 shows these solutions cultured with *E.coli* and *S. aureus*. Cerium phosphate showed no antibacterial effect since the two concentrations of cerium phosphate were equal or higher than the positive control. A similar trend was observed with only β-GP, whereas only with cerium an antibacterial activity was observed.
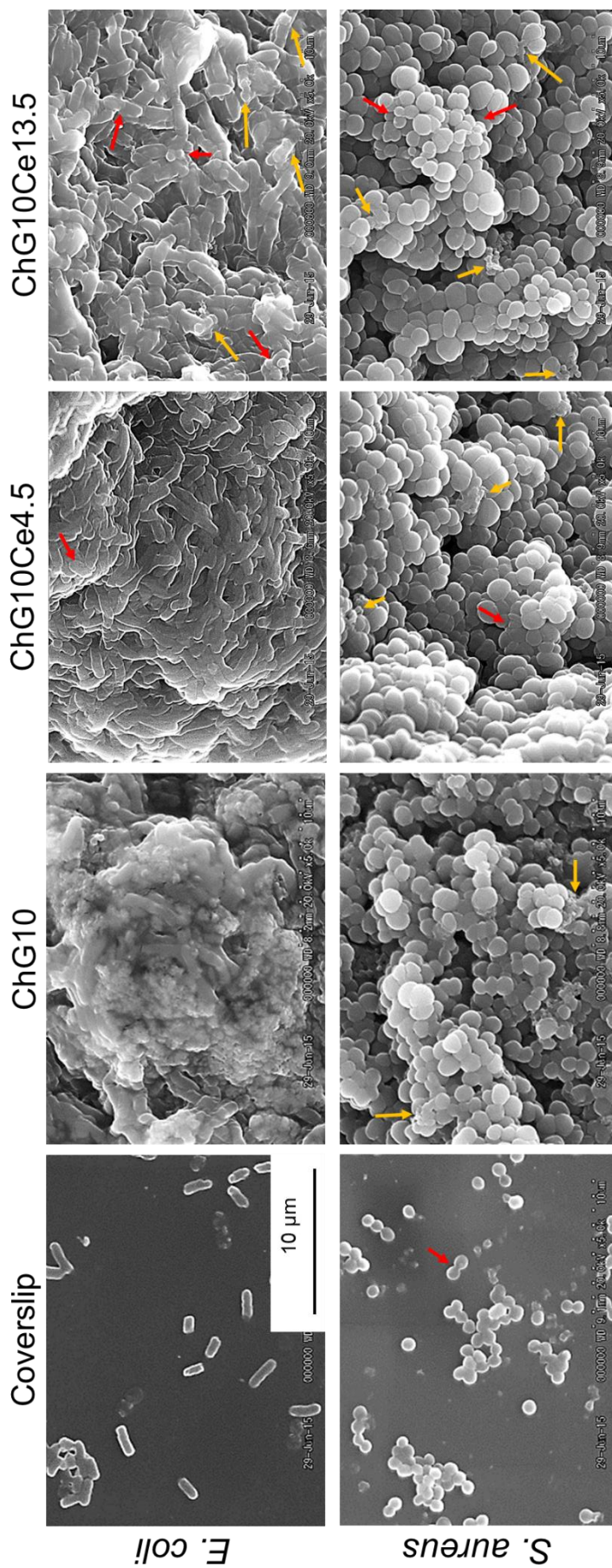
Figure 3-6 SEM micrographs of *E. coli* and *S. aureus* cultured on the ChG10 and ChG10Ce hydrogels after 24 h. The control (only bacteria) was cultured in a coverslip. Red arrows identify cells in division, whereas orange arrows indicate cells in apoptosis.
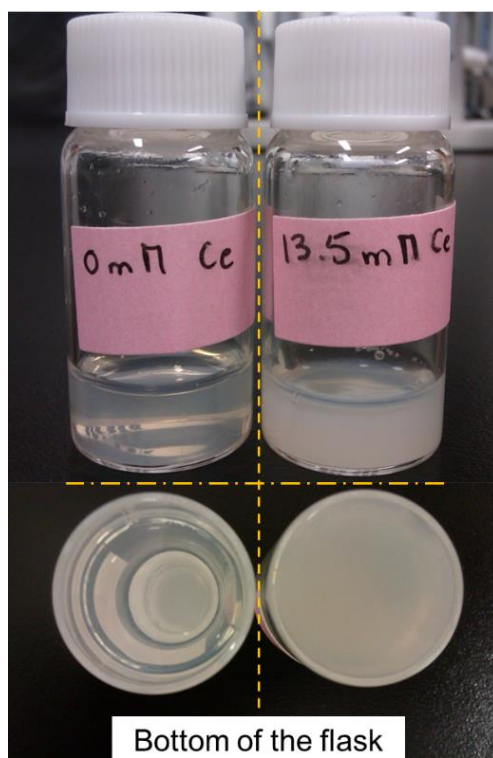
Figure 3-7 Visual appearance of the chitosan–GPTMS–β-GP hydrogels (after gelation) without cerium (0 mM Ce) and chitosan–GPTMS–Ce–β-GP containing cerium (13.5 mM Ce).
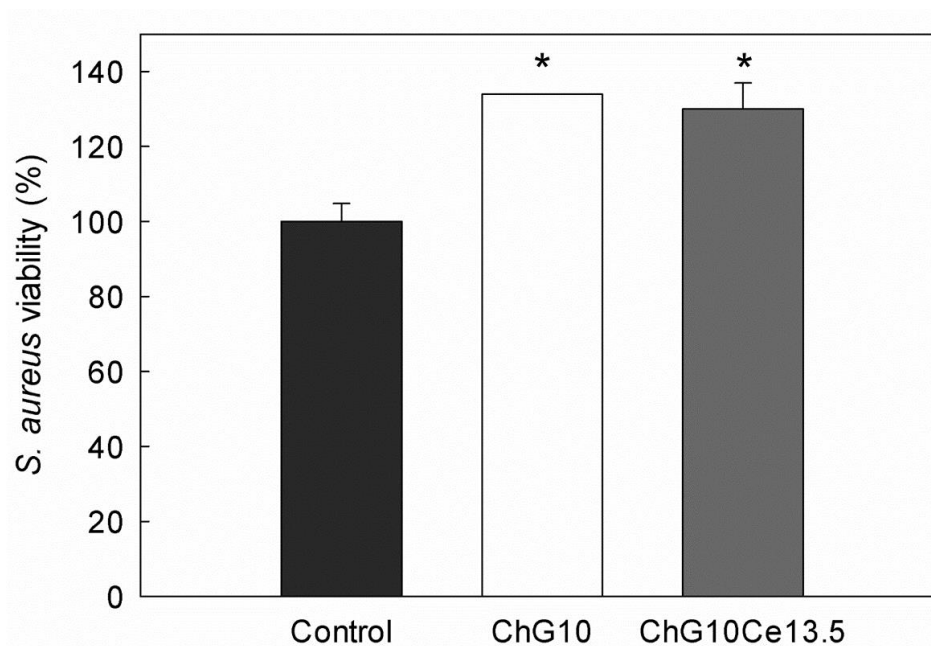
Figure 3-8 *S. aureus* viability on hydrogels using MTT assay after 24 h of culture (indirect method). A statistically significant difference ($p<0.05$) was observed when comparing to *S. aureus* (#) control (no sample).
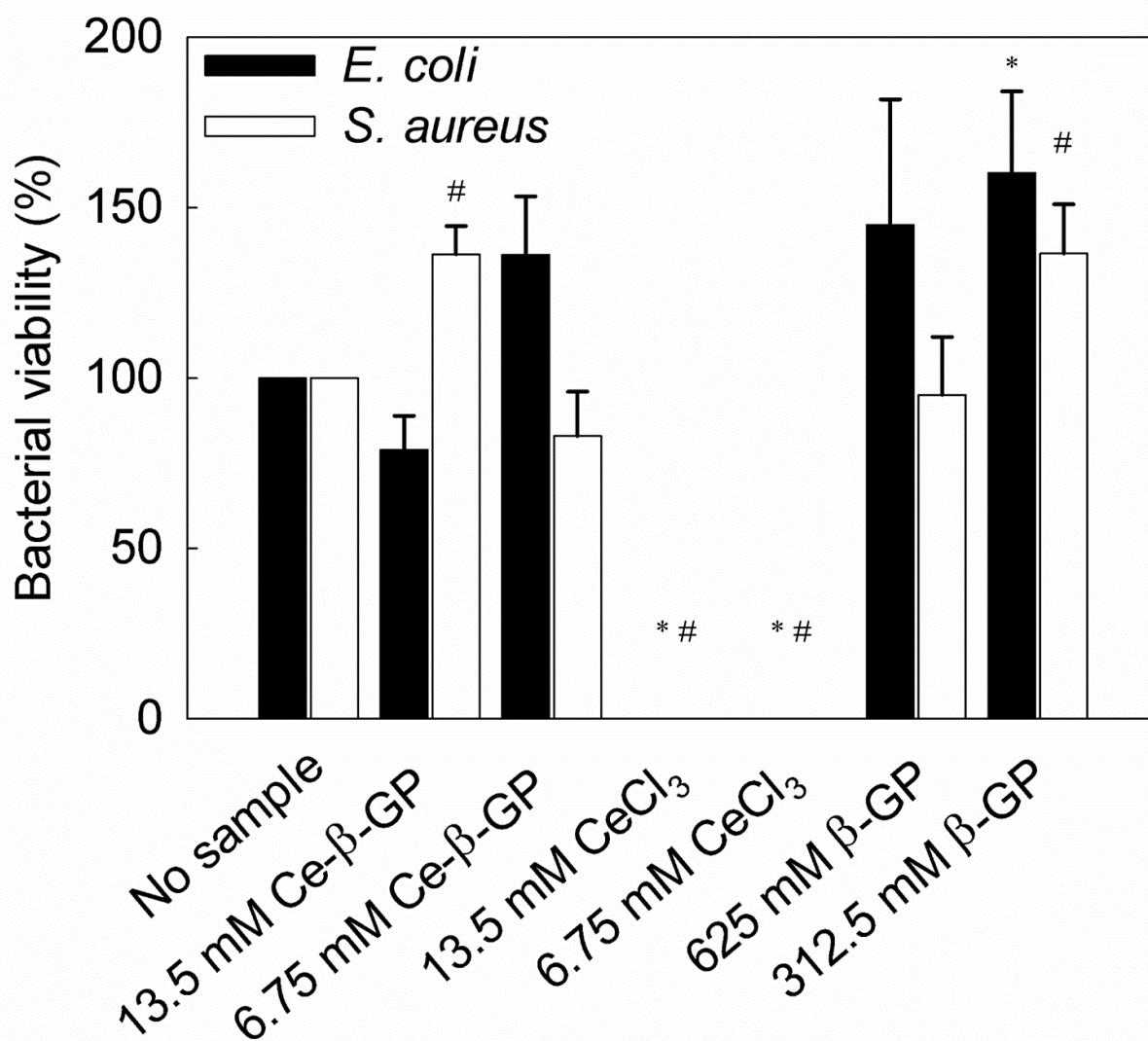
Figure 3-9 *E. coli* and *S. aureus* viability upon contact with Ce–β-GP colloid and $CeCl_3$ (both containing 13.5 and 6.75 mM of cerium) and β-GP (625 and 312.5 mM) using MTT assay after 24 h of culture. A statistically significant difference ($p<0.05$) was observed when comparing to *E. coli* (*) and *S. aureus* (#) control (no sample).

3.4.   Discussion

Very few studies are available with cerium chloride in biomaterials. The MIC is as important factor to take into account, especially when the working target is pathogenic bacteria. This feature is dependable on the concentration and action mechanism of the antibacterial agent, as well as the bacterial strain. Bacterial inhibition caused by cerium was observed, and above 3 mM (1118 µg/mL) an antibacterial effect was already detected. An *in vitro* activity study was performed in oxacillin- and mupirocin-resistant *S. aureus* strains found in hospitals to determine the MIC of cerium nitrate, and the MIC for all isolates was 2,048 µg/mL [18]. Whereas, the MIC for cerium oxide nanoparticles was around 50 µg/mL [19] for *E. coli*, even though the MIC of cerium oxide nanoparticles is lower than cerium chloride, CeO_2 nanoparticles internalization has been found to be a problem in human cell lines [20, 21]. A similar behavior was observed with silver ions (Ag^+) against *S. aureus* and *E. coli*, in which the MIC for both was 10^{-7} M, however with the L929 cell proliferation rate in the presence of Ag^+ decreased with the increase of Ag^+ concentrations. In case of zinc ions (Zn^{2+}) the MIC was 10^{-7} M, but only if below 10^{-4} M of Zn^{2+} the cell proliferation rate was over 80%. Likewise, the MIC range for copper ions (Cu^{2+}) ions were around 10^{-4}–10^{-5} M [22]. Although these metal ions are well known as antibacterial agents, questions regarding clinical effectiveness and mammalian cells and tissue damage are still a subject of controversy [23-25]. Therefore, the need to explore other sources of ions with antibacterial effect. The antibacterial mechanism of cerium is based on the uptake of cerium ions into the cell cytoplasm, leading to a number of biological reactions, such as inhibition of cellular respiration, glucose metabolism, oxygen uptake and disruption of the cell membrane [6, 7].

The ChG10 microspheres immersed in 10, 15 and 20 mM did not show bacterial inhibition upon contact with both *E. coli* and *S. aureus* suspensions. Possibly due to not enough

cerium absorbed on the ChG10 spheres, even at 20 mM. Even the amount of free amino groups of ChG10, reported on chapter 2, were not enough to show an antibacterial effect on both strains, due to the previous covalent bond establish between amino and GPTMS, as well as electrostatic interaction between amino groups and β-GP.

In case of the hydrogels containing cerium, the surface of ChG10Ce13.5 was extensively covered with *E. coli* and *S. aureus* cells as observed via SEM. The immediate color change imply that Ce^{3+} and the PO_4^{3-} (from β-GP) have immediate and high affinity for interaction. The similar behavior between trivalent cerium and bivalent calcium, since calcium ions form complexes, not just with the amino groups of chitosan, but also can absorb a negatively charged PO_4^{3-} ion [26]. The quick reaction and ionic bonding between the $CeCl_3$ and β-GP, makes it challenging for the cerium to form complexes with the amino groups of chitosan, similarly to calcium in terms of bonding preference [26], and also challenging for cerium to interact afterwards with the bacteria. This was observed in figure 3-8, in which at the highest concentration of cerium on the ChG10Ce13.5 hydrogel had no antibacterial effect on *S. aureus*. On the contrary, the viability of gram-positive *S. aureus* strain increased on ChG10 and also on ChG10Ce13.5. This neutralization of cerium when β-GP was included in the system was clearly confirmed in figure 3-9, in which on both concentrations of cerium phosphate the bacterial viability was equal or higher than the positive control without sample. This interaction between cerium and β-GP also observed in the hydrogel, makes cerium inaccessible to the bacteria consequently losing its antibacterial properties. In addition, the β-GP control also displayed equal or higher bacterial activity than the positive control. Regarding the effect of phosphorus, Miettinen *et al.* stated that the addition of same amounts of phosphorus to the tested drinking water samples greatly increased the growth of heterotrophic bacteria [27].

These hydrogels appear to stimulate the bacteria viability, therefore they can be useful for more suitable applications in which the bacterial growth stimulation is desirable, for instance the stimulation of probiotic bacteria (nonpathogenic strains).

3.5.   Conclusions

The bacterial behavior towards *Escherichia coli* and *Staphylococcus aureus* was observed with the chitosan-GPTMS-β-GP spheres and hydrogels containing cerium chloride (CeCl$_3$), and no antibacterial effect was observed due to the immediate interaction between β-GP and cerium, making it inaccessible to the bacteria. Moreover, the viability increased for both strains on ChG10 and on ChG10Ce13.5 hydrogels. Therefore, these hybrid hydrogels appear to stimulate the bacteria viability, therefore they can be useful for more suitable applications in which the bacterial growth stimulation is desirable, for instance the stimulation of probiotic bacteria (nonpathogenic strains).

References

1. Charbgoo, F., Ahmad, M. B., and Darroudi, M., *Cerium oxide nanoparticles: green synthesis and biological applications.* International Journal of Nanomedicine, 2017, **12**: 1401-1413.

2. Jakupec, M. A., Unfried, P., and Keppler, B. K., *Pharmacological properties of cerium compunds.* Reviews of Physiology, Biochemistry and Pharmacology, 2005, **153**: 101-111.

3. Burkes, S. and Mccleskey, C. S., *The bacteriostatic activity of cerium, lanthanum, and thallium.* Journal of Bacteriology, 1947, **54**(4): 417-424.

4. Muroma, A., *Studies in the bactericidal action of salts of certain rare earth metals.* Annales Medicinae Experimentalis Et Biologiae Fenniae, 1958, **36**(Suppl. 6): 1-54.

5. Emsley, J., *Cerium*, in *Nature's building blocks: an A-Z guide to the elements*. 2011, Oxford University Press Inc. 120-125.

6. Cobrado, L., Azevedo, M. M., Silva-Dias, A., Ramos, J. P., Pina-Vaz, C., and Rodrigues, A. G., *Cerium, chitosan and hamamelitannin as novel biofilm inhibitors?* Journal of Antimicrobial Chemotherapy, 2012, **67**(5): 1159-1162.

7. Garner, J. P. and Heppell, P. S. J., *Cerium nitrate in the management of burns.* Burns, 2005, **31**(5): 539-547.

8. Shah, V., Shah, S., Shah, H., Rispoli, F. J., Mcdonnell, K. T., Workeneh, S., Karakoti, A., Kumar, A., and Seal, S., *Antibacterial Activity of Polymer Coated Cerium Oxide Nanoparticles.* PLOS ONE, 2012, **7**(10): 1-13.

9. Morais, D. S., Rodrigues, M. A., Lopes, M. A., Coelho, M. J., Maurício, A. C., Gomes, R., Amorim, I., Ferraz, M. P., Santos, J. D., and Botelho, C. M., *Biological evaluation of alginate-based hydrogels, with antimicrobial features by Ce(III) incorporation, as*

vehicles for a bone substitute. Journal of Materials Science: Materials in Medicine, 2013, **24**(9): 2145-2155.

10.   *Guidelines for Canadian drinking water quality*. 1996 [cited 2017 5 November]; Available from: http://publications.gc.ca/Collection/H48-10-1-46-1997E.pdf.

11.   Gangolli, S. D., Van Den Brandt, P. A., Feron, V. J., Janzowsky, C., Koeman, J. H., Speijers, G. J. A., Spiegelhalder, B., Walker, R., and Wishnok, J. S., *Nitrate, nitrite and N-nitroso compounds.* European Journal of Pharmacology: Environmental Toxicology and Pharmacology, 1994, **292**(1): 1-38.

12.   Spiegelhalder, B., Eisenbrand, G., and Preussmann, R., *Influence of dietary nitrate on nitrite content of human saliva: Possible relevance to in vivo formation of N-nitroso compounds.* Food and Cosmetics Toxicology, 1976, **14**(6): 545-548.

13.   Cruz-Neves, S., Shirosaki, Y., Miyazaki, T., and Hayakawa, S., *Characterization and degradation study of chitosan-siloxane hybrid microspheres synthesized using a microfluidic approach.* Materials Science and Engineering: C, 2017, **81**: 571-579.

14.   Mshana, R. N., Tadesse, G., Abate, G., and Miörner, H., *Use of 3-(4,5-dimethylthiazol-2-yl)-2,5-diphenyl tetrazolium bromide for rapid detection of rifampin-resistant Mycobacterium tuberculosis.* Journal of Clinical Microbiology, 1998, **36**(5): 1214-1219.

15.   Reshes, G., Vanounou, S., Fishov, I., and Feingold, M., *Cell shape dynamics in Escherichia coli.* Biophysical Journal, 2008, **94**(1): 251-264.

16.   Huang, K. C., Mukhopadhyay, R., Wen, B., Gitai, Z., and Wingreen, N. S., *Cell shape and cell-wall organization in Gram-negative bacteria.* Proceedings of the National Academy of Sciences, 2008, **105**(49): 19282-19287.

17.   Monteiro, J. M., Fernandes, P. B., Vaz, F., Pereira, A. R., Tavares, A. C., Ferreira, M. T., Pereira, P. M., Veiga, H., Kuru, E., Vannieuwenhze, M., Brun, Y. V., Filipe, S. R.,

and Pinho, M. G., *Cell shape dynamics during the staphylococcal cell cycle.* Nature communications, 2015, **6**: 8055-8055.

18.   Schuenck, R. P., Dadalti, P., Silva, M. G., Fonseca, L. S., and Santos, K. R. N., *Oxacillin- and mupirocin-resistant Staphylococcus aureus: in vitro activity of silver sulphadiazine and cerium nitrate in hospital strains.* Journal of Chemotherapy, 2004, **16**(5): 453-458.

19.   Masadeh, M. M., Karasneh, G. A., Al-Akhras, M. A., Albiss, B. A., Aljarah, K. M., Al-Azzam, S. I., and Alzoubi, K. H., *Cerium oxide and iron oxide nanoparticles abolish the antibacterial activity of ciprofloxacin against gram positive and gram negative biofilm bacteria.* Cytotechnology, 2015, **67**(3): 427-435.

20.   Asati, A., Santra, S., Kaittanis, C., and Perez, J. M., *Surface-charge-dependent cell localization and cytotoxicity of cerium oxide nanoparticles.* ACS nano, 2010, **4**(9): 5321-5331.

21.   Pulido-Reyes, G., Rodea-Palomares, I., Das, S., Sakthivel, T. S., Leganes, F., Rosal, R., Seal, S., and Fernández-Piñas, F., *Untangling the biological effects of cerium oxide nanoparticles: the role of surface valence states.* Scientific Reports, 2015, **5**: 15613-15627.

22.   Ning, C., Wang, X., Li, L., Zhu, Y., Li, M., Yu, P., Zhou, L., Zhou, Z., Chen, J., Tan, G., Zhang, Y., Wang, Y., and Mao, C., *Concentration ranges of antibacterial cations for showing the highest antibacterial efficacy but the least cytotoxicity against mammalian cells: implications for a new antibacterial mechanism.* Chemical research in toxicology, 2015, **28**(9): 1815-1822.

23.   Gosheger, G., Hardes, J., Ahrens, H., Streitburger, A., Buerger, H., Erren, M., Gunsel, A., Kemper, F. H., Winkelmann, W., and Von Eiff, C., *Silver-coated*

megaendoprostheses in a rabbit model—an analysis of the infection rate and toxicological side effects. Biomaterials, 2004, **25**(24): 5547-5556.

24.   Giovanni, M., Yue, J., Zhang, L., Xie, J., Ong, C. N., and Leong, D. T., *Pro-inflammatory responses of RAW264.7 macrophages when treated with ultralow concentrations of silver, titanium dioxide, and zinc oxide nanoparticles.* Journal of Hazardous Materials, 2015, **297**: 146-152.

25.   Hardes, J., Ahrens, H., Gebert, C., Streitbuerger, A., Buerger, H., Erren, M., Gunsel, A., Wedemeyer, C., Saxler, G., Winkelmann, W., and Gosheger, G., *Lack of toxicological side-effects in silver-coated megaprostheses in humans.* Biomaterials, 2007, **28**(18): 2869-2875.

26.   Yamaguchi, I., Tokuchi, K., Fukuzaki, H., Koyama, Y., Takakuda, K., Monma, H., and Tanaka, J., *Preparation and microstructure analysis of chitosan/hydroxyapatite nanocomposites.* Journal of Biomedical Materials Research Part A, 2001, **55**(1): 20-27.

27.   Miettinen, I. T., Vartiainen, T., and Martikainen, P. J., *Phosphorus and bacterial growth in drinking water.* Applied and Environmental Microbiology, 1997, **63**(8): 3242-3245.

Chapter 4.

BACTERIAL BEHAVIOR WITH CHITOSAN-SILOXANE HYBRID SPHERICAL BEADS CONTAINING CERIUM

4.1. Introduction

Microporous beads have advantages in a range of applications, e.g., can be injected into bone defects through minimally invasive procedures, therefore avoiding unnecessary surgical trauma [1]; the size of the spheres allow them to fill different defect shapes with close packing [2]; serve as vehicles for transplantation of cultured cells and materials for filling defect in human tissues [3, 4]; and can also be used to carry drugs, proteins and genes, which further enhances their bioactivity.

In the previous chapter the antibacterial efficiency of cerium could not be achieved using the chitosan–GPTMS–β-GP hybrid formulation either in the microsphere form, by adsorption or incorporation methods, or when incorporating cerium chloride into the hydrogels to increase the cerium loading. The neutralization of cerium when β-GP was included in the system was confirmed, consequently this interaction made cerium inaccessible to the bacteria losing its antibacterial properties. In fact, an increase in the bacterial viability of both strains was observed in the presence of cerium–β-GP colloid and β-GP. Therefore, β-GP was removed from the hybrid structural formulation and the method for the synthesis of the samples was reconsidered, since chitosan–GPTMS hybrids without β-GP could not be synthetized in the microfluidic systems using the previous tested conditions. As a result, in this chapter, microporous chitosan-GPTMS hybrid beads were synthetized by using a syringe pump to drop chitosan-GPTMS sols droplets into liquid nitrogen and then freeze dry the beads. Cerium chloride was incorporated

into the hybrid beads, the surface and porosity was evaluated, as well as the free amino groups available. In addition, the antibacterial potential of these beads carrying cerium were investigated against *E. coli* and *S. aureus*.

4.2. Materials and methods

1.3.1. 4.2.1. Preparation of chitosan-siloxane hybrid beads without/with cerium

A 2 w/v% chitosan solution was prepared by dissolving high molecular weight chitosan powder (310,000-375,000 Da, DA > 75%; Sigma-Aldrich®, St. Louis, USA) in 0.25 M aqueous acetic acid using a planetary centrifugal mixer (ARE-310, Thinky, Tokyo, Japan). The desired amount of GPTMS (97%, Alfa Aesar, Heysham, UK) was hydrolyzed for 1 h in 0.25 M aqueous acetic acid at room temperature. Then, the hydrolyzed GPTMS was added to the chitosan solution and the solution was stirred for 1 h at room temperature. The proper amount of cerium chloride was also dissolved in the same concentration of 0.25 M aqueous acetic acid and the solution was added to the previously prepared chitosan-GPTMS precursor sol. This mixture was stirred at room temperature for 1 h. The prepared compositions and respective sample codes are given in table 4-1. Each solution with the specific composition was placed in a syringe with a needle gauge size of 27G (with a sharp 10-12° beveled needle point style), and dropped into liquid nitrogen using a syringe pump at a rate of 0.04 mL/min. When finished, the formed ice droplets were maintained in liquid nitrogen (-196°C), then transferred directly to the freeze dryer (FDU-1200, EYELA, Tokyo, Japan). The beads were lyophilized by freeze drying until completely dried. Then, the porous beads were soaked in 0.1 M NaOH aqueous solution to neutralize the acetic acid, followed by a washing step with distilled water, and finally, lyophilized again in the freeze dryer.

Table 4-1 Starting composition of the chitosan-siloxane hybrid beads.

Sample	Molar ratio		
	Chitosan	GPTMS	$CeCl_3$
Ch	1.0	0	0
ChG10	1.0	1.0	0
ChG10Ce01	1.0	1.0	0.1
ChG10Ce025	1.0	1.0	0.25
ChG10Ce05	1.0	1.0	0.5

1.3.2. 4.2.2. Characterization of chitosan-siloxane hybrid beads

The surface morphology was examined using SEM equipped with EDS. Before the observations, the preparation of the beads involved the use of a carbon paint (XC-12, JEOL, Tokyo, Japan) to make a conductive "bridge" to reduce the charge effect. Then, the beads were coated with a Pt/Pd layer of thickness around 20 nm. The mean pore diameter was obtained from the SEM images using ImageJ v1.48 software. Around 20 pores were measured from three different areas of the same sample.

The crosslinking degree was evaluated using the ninhydrin assay, to define the percentage of free amino groups in the beads [5]. A single bead was suspended in 0.9 mL of ninhydrin buffer solution. Then, 0.3 mL of ninhydrin reagent was added and the Eppendorf tubes containing the mixture was kept at 80°C for 20 min. The optical absorbance of the supernatant solution was recorded at $\lambda=570$ nm using a spectrophotometer. The relative percentages of free amino groups in the chitosan-GPTMS-cerium beads were calculated using as a reference the beads composed only of chitosan.

1.3.3.   4.2.3. *E. coli* and *S. aureus* culture on beads containing cerium

The beads were sterilized using ethylene oxide gas and kept for 1 week at room temperature to clear the remaining gas. *E. coli* NIHJ and *S. aureus* 209P were suspended in LB medium. The optical density of the bacterial suspension was adjusted to 1.0 (1×10^2 CFU/mL). For each condition, 5 sterilized beads were placed in a sterile 96 well plate and 200 μL of the bacterial suspension was added. The bacterial viability that was in contact with the beads was determined using the MTT assay. After 24 h of incubation at 37°C, 20 μL of MTT reagent was added. The beads were incubated for 4 h at 37°C, and then transferred to a new 96 well plate. The formazan salts were dissolved with 200 μL of DMSO and the absorbance was measured at λ=600 nm to evaluate the bacterial viability. The beads were inserted in PBS to monitor pH changes.

4.3.   Results

1.3.4.   4.3.1. Beads characterization

Figure 4-1 displays the beads in which shows the beads spherical shape and the diameter was determined to be around 2 mm. The beads presented interconnected porous in all compositions as observed in figure 4-2. Additionally, the porous structure looks smooth and similar on all compositions indicating that the cerium was well dissolved and homogenized with the hybrid solution.
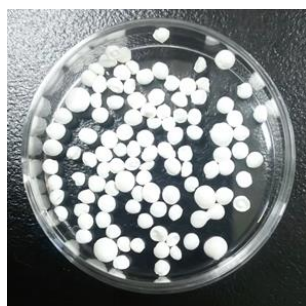
Figure 4-1 Digital image of ChG10Ce05 beads.

In table 4-2, the results from the ninhydrin assay show the amount of free amino groups from each composition. Chitosan was used as the reference since all amino groups are protonated. In case of ChG10, approximately 25% of amino groups are still free, similarly to ChG10Ce01 beads. With the addition of increasing amounts of cerium in the beads, the quantity of free amino groups also increases, specifically 38% on ChG10Ce025 and the highest amount of 96% of free amino groups on ChG10Ce05.

Table 4-2 Degree of free amino groups of chitosan-siloxane hybrid beads.

Sample	Free amino groups (%)
Ch	100
ChG10	24.6 ± 2.9
ChG10Ce01	25.5 ± 9.1
ChG10Ce025	37.8 ± 4.0
ChG10Ce05	95.8 ± 12.8

The EDS data in table 4-3 shows that the cerium present on the surface of the beads increased with the increasing molar ratio of cerium chloride added to be incorporated in the beads, leading to a higher Ce/C atomic ratio as expected. Additionally, regardless of the composition and molar ratio of cerium used, the pore size observed in the beads was very similar between the samples.
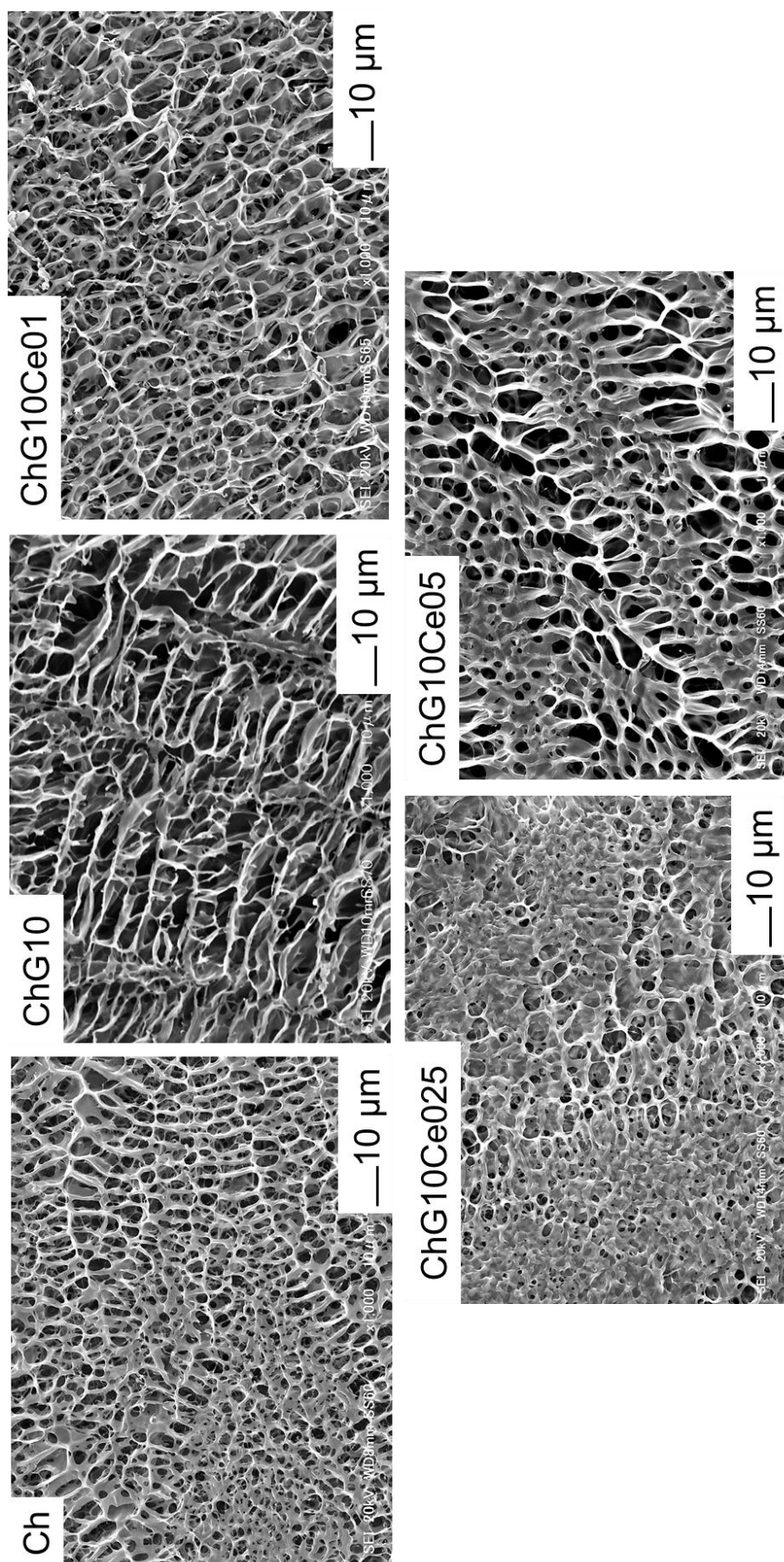
Figure 4-2 SEM images of Ch and ChG10 chitosan-siloxane hybrid beads surfaces without and with different amounts of cerium chloride incorporated.

Table 4-3 Pore size determined from SEM images and atomic ratio of Ce/C on the beads surfaces from EDS analysis.

Sample	Pore size (µm)	Ce/C (atomic %)
Ch	5.6 ± 13.6	0
ChG10	5.9 ± 5.2	0
ChG10Ce01	6.2 ± 5.1	0.007
ChG10Ce025	5.6 ± 2.2	0.019
ChG10Ce05	6.6 ± 3.7	0.032

1.3.5. 4.3.2. Antibacterial properties of the beads with cerium

The pH values after soaking the beads on PBS are listed in table 4-4 below. Regardless of the composition, the pH of the supernatant of all beads slightly increases from 2 h to 24 h of incubation on PBS buffer. In terms of changes on the appearance of the beads it was observed that the Ch and ChG10Ce05 beads were the samples which presented visible physical modifications such as color change, from white to transparent with loss of spherical shape and a swelling behavior, respectively.

Table 4-4 pH changes after the beads were soaked on PBS and their macroscopical appearances.

Sample	2 h	24 h	Appearance after 24 h
Ch	6.6	6.8	Transparent
ChG10	6.5	6.6	No change
ChG10Ce01	5.9	6.1	No change
ChG10Ce025	5.7	5.8	No change
ChG10Ce05	5.3	5.9	Swelling

Figure 4-3 shows the viabilities of both *E. coli* and *S. aureus* cultured with the beads for 24 h. In general, the bacterial viabilities with the beads was lower than the positive control without beads. Non-crosslinked chitosan (Ch) beads had an antibacterial effect on both strains, but more effective towards *E. coli*. The ChG10 and ChG10Ce01 beads had a very similar bacterial viability displaying the highest values on both strains among the beads. Meanwhile, ChG10Ce025 and ChG10Ce05 beads presented a bacterial viability close to zero, indicating to be the most effective compositions of all tested beads for bacterial inhibition on both *E. coli* and *S. aureus* strains.

Figure 4-3 Viability of *E. coli* and *S. aureus* cultured after 24h with the hybrid beads containing several molar ratios of cerium chloride. A statistically significant difference (p<0.05) was observed when comparing to chitosan beads, * for *E. coli* and # for *S. aureus* strain.

4.4. Discussion

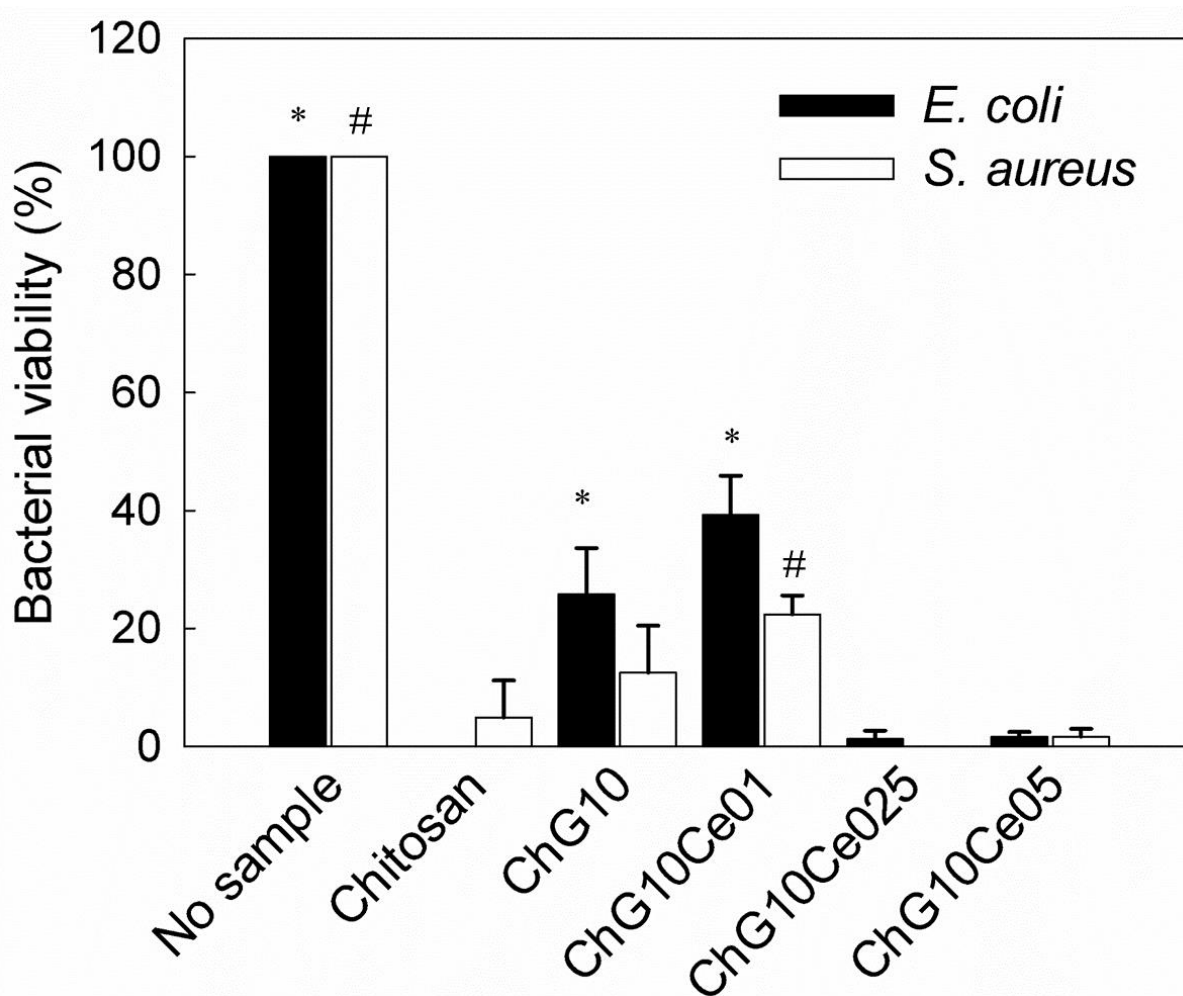Regardless of the composition and molar ratio of cerium used, the pore size observed in the beads was very similar between the samples. When using the freeze drying method, the pore size is determined by the size of the ice crystals formed along the samples [6].

The ninhydrin assay data, was useful to determine quantitatively the amount of free amino groups on each beads composition. Ch beads had 100% of free amino groups, whereas on ChG10 the GPTMS crosslinked with 75% of the chitosan amino groups, leaving only 25% of reactive amino groups. A similar percentage was observed for ChG10Ce01 since the amount of cerium present was very low to cause an impact. While, the amount of free amino groups increased significantly on ChG10Ce05 beads. This apparently divergent behavior can be explained by the physicochemical properties of cerium. Trivalent cerium of ionic radius: 1.01 Å, is similar to bivalent calcium of ionic radius: 1.00 Å in terms of size, bonding, and preferences for donor atoms [7]. Consequently, the chemical behavior of trivalent cerium is identical to bivalent calcium. It is known that, the amino groups from chitosan form complexes with calcium ions [8]. In this case, cerium formed complexes with the reactive amino groups and inhibited the crosslinking reaction between the amino groups and the epoxide groups of GPTMS.

The viabilities of *E. coli* and *S. aureus* upon contact with the beads was lower than without the samples. Non-crosslinked chitosan beads had an antibacterial effect, similarly to previous research statements [9-12]. When protonated, the amino groups are positively charged (below pH 6) and interact with the negatively charged bacterial cell membranes, inducing the leakage of proteins [9, 10, 13] via hydrolysis of peptidoglycans present in the bacterial cell walls and causing alterations in the properties of the cell membrane permeability of the bacteria.

The pH of the medium was close to neutral after 24 h at pH 6.8, however the free amino groups of Ch were sufficiently protonated to induce bacterial death. However, crosslinking with GPTMS lowered the antibacterial effect of chitosan caused by the drop on the amount of free amino groups. The quantity of free amino groups on the ChG10Ce01 surfaces was identical as on ChG10. This indicates that a small amount of cerium, such as the one used on ChG10Ce01, cannot inhibit crosslinking between amino groups and epoxide groups, in addition to being insufficient to inhibit bacterial growth. Whereas, the cerium added on ChG10Ce025 and ChG10Ce05 beads greatly reduced the bacterial viability. On ChG10Ce05 beads, the percentage of free amino groups was around 96% due to the inhibition of the GPTMS crosslinking towards the amino groups by the cerium ions, thereby causing the inhibition of both bacterial growth. On the other hand, ChG10Ce025 had only 38% free amino groups but then showed the best antibacterial properties because of the synergies acquired by the cerium ion, or released from the beads surface. The obtained results suggested that the 0.25-0.5 molar ratio of cerium is the most favorable amount for these antibacterial beads. The MIC of cerium chloride for both bacteria was 3 mM (data shown in chapter 3 section 3.3.1). On ChG10Ce025 samples, the concentration of cerium chloride in the cell suspension was 1.7 mM, if all the cerium chloride is released from the beads. This concentration is below the MIC. Indicating that the antibacterial properties of the chitosan-siloxane beads depended on the coaction of both cerium and free amino groups derived from chitosan. Cerium is not a foreigner compound in the human body. In the literature it was described that cerium can perform a similar role in physiological functions of the organisms, therefore cerium can accumulate in small portions in the bones [14, 15]. Concerning the amount of cerium present in the human body, it was reported that the blood comprises around 0.001 ppm, the tissues about 0.3 ppm, and in the bones nearly 3 ppm of cerium. Therefore, in an average 70 kg human, a total of 40 mg of cerium is comprised in the body. Very few cerium is stored in the food chain, and so humans usually intake less than

1 mg/per day [15, 16]. This value corresponds to 20 mM if using the tested experimental settings (for the 0.2 mL of the bacterial suspension), therefore the use of cerium can be considered fairly safe since a good MIC of 1.7 mM was observed when using ChG10Ce025.

This cationic polymer normally shows a stronger activity against gram-positive bacteria, such as *S. aureus*, than against gram-negative bacteria, like *E. coli*, because of their hydrophilicities [10, 11, 13]. The outer membrane that surrounds the cell wall of gram-negative bacteria, restricts drugs from interacting with the peptidoglycans that constitute the cell wall [17]. Nonetheless, gram-positive bacteria do not have this outer membrane and their cell walls are more vulnerable. Although the chitosan-siloxane beads had greater antibacterial activity against *S. aureus* than against *E. coli*, they showed antibacterial activity even against *E. coli*. The biological role of cerium is not yet clearly understood, but it has been noticed that cerium salts can have a role in the stimulation of the metabolism [18]. In this case, the lipopolysaccharides (LPS) present in the outer membrane are linked electrostatically via divalent cations, in particular Mg^{2+} and Ca^{2+}, and these cations contribute to resistance against hydrophobic antimicrobial agents [19]. Therefore, leading to assume that the LPS mixed up Ce^{3+} with Ca^{2+} and transported Ce^{3+} into the outer membrane, resulting in antibacterial effects from the free amino groups of chitosan or by uptaking it into the cytoplasm to inhibit the cellular respiration, glucose metabolism and triggering membrane disruption of the bacterial cells [20].

4.5.   Conclusions

Hybrid microporous beads of chitosan-GPTMS were prepared using liquid nitrogen and freeze-drying method. Incorporation of an antibacterial agent such as cerium chloride was successfully achieved, in which the beads with cerium showed antibacterial effects against both *E. coli* and *S. aureus*, a gram-negative and gram-positive strain, respectively. The antibacterial properties were instigated by the (1) positively charged free amino groups on chitosan and (2)

the adsorption and uptake of cerium ions instead of calcium ions by the bacteria. These chitosan-siloxane hybrid beads containing cerium have promising applications as tissue engineering scaffolds and as antibacterial materials.

References

1.   Shen, H., Hu, X., Yang, F., Bei, J., and Wang, S., *An injectable scaffold: rhBMP-2-loaded poly(lactide-co-glycolide)/hydroxyapatite composite microspheres.* Acta Biomaterialia, 2010, **6**(2): 455-465.

2.   Lee, J.-Y., Kim, K.-H., Shin, S.-Y., Rhyu, I.-C., Lee, Y.-M., Park, Y.-J., Chung, C.-P., and Lee, S.-J., *Enhanced bone formation by transforming growth factor-β1-releasing collagen/chitosan microgranules.* Journal of Biomedical Materials Research Part A, 2006, **76A**(3): 530-539.

3.   Keshaw, H., Georgiou, G., Blaker, J. J., Forbes, A., Knowles, J. C., and Day, R. M., *Assessment of polymer/bioactive glass-composite microporous spheres for tissue regeneration applications.* Tissue Engineering Part A, 2008, **15**(7): 1451-1461.

4.   Keshaw, H., Thapar, N., Burns, A. J., Mordan, N., Knowles, J. C., Forbes, A., and Day, R. M., *Microporous collagen spheres produced via thermally induced phase separation for tissue regeneration.* Acta Biomaterialia, 2010, **6**(3): 1158-1166.

5.   Prochazkova, S., Vårum, K. M., and Østgaard, K., *Quantitative determination of chitosans by ninhydrin.* Carbohydrate Polymers, 1999, **38**(2): 115-122.

6.   Kang, H.-W., Tabata, Y., and Ikada, Y., *Fabrication of porous gelatin scaffolds for tissue engineering.* Biomaterials, 1999, **20**(14): 1339-1344.

7.   Jakupec, M. A., Unfried, P., and Keppler, B. K., *Pharmacological properties of cerium compunds.* Reviews of Physiology, Biochemistry and Pharmacology, 2005, **153**: 101-111.

8.   Yamaguchi, I., Tokuchi, K., Fukuzaki, H., Koyama, Y., Takakuda, K., Monma, H., and Tanaka, J., *Preparation and microstructure analysis of chitosan/hydroxyapatite nanocomposites.* Journal of Biomedical Materials Research Part A, 2001, **55**(1): 20-27.

9.   Kong, M., Chen, X. G., Xing, K., and Park, H. J., *Antimicrobial properties of chitosan and mode of action: a state of the art review.* International Journal of Food Microbiology, 2010, **144**(1): 51-63.

10.   Dutta, P. K., Tripathi, S., Mehrotra, G. K., and Dutta, J., *Perspectives for chitosan based antimicrobial films in food applications.* Food Chemistry, 2009, **114**(4): 1173-1182.

11.   Shahidi, F., Arachchi, J. K. V., and Jeon, Y.-J., *Food applications of chitin and chitosans.* Trends in Food Science & Technology, 1999, **10**(2): 37-51.

12.   Coma, V., Deschamps, A., and Martial-Gros, A., *Bioactive packaging materials from edible chitosan polymer—antimicrobial activity assessment on dairy-related contaminants.* Journal of Food Science, 2003, **68**(9): 2788-2792.

13.   No, H. K., Young Park, N., Ho Lee, S., and Meyers, S. P., *Antibacterial activity of chitosans and chitosan oligomers with different molecular weights.* International Journal of Food Microbiology, 2002, **74**(1): 65-72.

14.   Gehlhaus, M., Osie, M., Llados, F., Plewak, D., Lumpkin, M., Odin, M., and Rooney, A., *Toxicological review of cerium oxide and cerium compounds*. 2009, EPA - U.S. Environmental Protection Agency. 1-118.

15.   Pol, A., Barends, T. R. M., Dietl, A., Khadem, A. F., Eygensteyn, J., Jetten, M. S. M., and Op Den Camp, H. J. M., *Rare earth metals are essential for methanotrophic life in volcanic mudpots.* Environmental Microbiology, 2014, **16**(1): 255-264.

16.   Kaya, M. O., Kaya, Y., Çelik, G., Kurtuluş, F., Arslan, O., and Güler, Ö. Ö., *Differential in vitro inhibition studies of some cerium vanadate derivatives on xanthine oxidase.* Journal of Enzyme Inhibition and Medicinal Chemistry, 2015, **30**(2): 286-289.

17.   Salton, M. R. J. and Kim, K. S., *Structure*, in *Medical Microbiology*, Baron, S., Editor. 1996, University of Texas Medical Branch at Galveston.

18. Emsley, J., *Cerium*, in *Nature's building blocks: an A-Z guide to the elements*. 2011, Oxford University Press Inc. 120-125.

19. Schneck, E., Schubert, T., Konovalov, O. V., Quinn, B. E., Gutsmann, T., Brandenburg, K., Oliveira, R. G., Pink, D. A., and Tanaka, M., *Quantitative determination of ion distributions in bacterial lipopolysaccharide membranes by grazing-incidence X-ray fluorescence*. Proceedings of the National Academy of Sciences of the United States of America, 2010, **107**(20): 9147-9151.

20. Cobrado, L., Azevedo, M. M., Silva-Dias, A., Ramos, J. P., Pina-Vaz, C., and Rodrigues, A. G., *Cerium, chitosan and hamamelitannin as novel biofilm inhibitors?* Journal of Antimicrobial Chemotherapy, 2012, **67**(5): 1159-1162.

SUMMARY

The main results of each chapters were summarized as follows:

Chapter 2: Hybrids microspheres containing chitosan–GPTMS–β-GP were successfully produced using a microfluidic system via sol–gel process. The synthetized microspheres had sizes of approximately 650 μm with uniform spherical shapes. When the microspheres were submitted to pH 1.7 and 5.4, simulating the fluids of gastric conditions, the GPTMS crosslinking inhibited the chitosan degradation even at the lowest pH. In addition, the formation of siloxane networks occurred in the chitosan polymeric matrix and condensation was promoted by the GPTMS content. The release of phosphate was facilitated because of its weak electrostatic interaction with chitosan. Concerning silicon, it was released together with chitosan degradation and it was dependent on the composition of GPTMS present. The hybrid micro sized spheres endured harsh pH conditions for 14 days. The drug delivery ability of the produced chitosan-siloxane hybrid microspheres was tested. The incorporation of antioxidant pelargonidin was successful. Under simulated gastro intestinal conditions, such as pH and digestion period, an initial burst at pH 1.7 was observed, followed by a slower and more sustained release in pH 5.4 and 6.7. The release of pelargonidin from the spheres matrix occurred via diffusion. These spheres appear to be promising for delivery of therapeutic agents for gastro intestinal applications due to its resistance to low pH and ability to retain pelargonidin for longer periods of time, since even after 57 h the presence of residual pelargonidin in the matrix was seen. Therefore, it appears to be able to protect the therapeutic agents from the hostile conditions of the upper gastrointestinal tract. Therefore, these results propose that the synthesized hybrid microspheres are a good candidate to be used as drug carriers for the gastrointestinal track via oral administration.

Chapter 3: The bacterial behavior towards *Escherichia coli* (gram-negative) and *Staphylococcus aureus* (gram-positive) was observed with the chitosan-GPTMS-β-GP spheres and hydrogels containing cerium chloride, an antibacterial agent. No antibacterial effect was observed due to the immediate interaction between β-GP and cerium, making cerium inaccessible to the bacteria. Interestingly, the viability increased for both strains on ChG10 and also on ChG10Ce13.5. Therefore, these hydrogels appear to stimulate the bacteria viability, consequently they can be useful for more suitable applications in which the bacterial growth stimulation is desirable, for instance the stimulation of probiotic bacteria (nonpathogenic strains).

Chapter 4: Microporous chitosan-GPTMS hybrid spheres were successfully prepared using liquid nitrogen and a freeze-drying system. The spheres with higher amounts of cerium chloride showed antibacterial effects against both *E. coli* and *S. aureus*. The antibacterial properties were caused by the free amino groups on chitosan and the adsorption and uptake of cerium ions instead of calcium ions into the bacteria. Due to its 3D structure these microporous spheres have the potential to be used as scaffolds to fill soft tissue defects with antibacterial properties.

In conclusion, this study explores the potential of chitosan-siloxane hybrids for (1) increasing the uptake of drugs in the gastrointestinal using track using microspheres as carriers, via oral administration; and (2) develop strategy to fight bacterial resistance to common antibiotics using chitosan-siloxane spheres for the targeted delivery of antibacterial agents.

Hopefully, these findings will help in the improvement of medical approaches to treat individuals.

ACKNOWLEDGMENTS

My words will never be enough to show how grateful I am to the people who supported and encouraged me throughout this journey and made this thesis possible.

I am very grateful to my supervisors Associate Professor Yuki Shirosaki and Professor Toshiki Miyazaki, for kindly receiving me and helping me in the adaptation process, for sharing their scientific knowledge, for the prompt availability to discuss with me, for all the contributions and opportunities provided, along with the constructive comments and guidance. I also want to express my great gratitude to Professor Toshinari Maeda for kindly welcoming me to his laboratory to collaborate. His support and guidance was also a great and irreplaceable contribution for this work. I felt like I was also part of his laboratory members.

I want to express my sincere gratitude to my laboratory colleagues for receiving me with kindness and for their help and availability whenever needed. I wish to express a special appreciation to Saki Yasutomi, Ryo Hamai and Okada Takuma for all the experimental support provided and knowledge shared. The same feelings extend to the students from Prof. Toshinari Maeda laboratory, which kindly took their time to teach me and guide me whenever I needed help, especially Nurul Asyifah Mustapha. I'm very grateful.

I also wish to thank Professor Satoshi Hayakawa from Graduate School of Natural Science and Engineering from Okayama University for the collaboration and NMR analysis performed.

I also wish to express my gratitude to all staff from Wakamatsu campus, especially from the student's office, for all kinds of support.

I am very thankful for the support of my precious friends, for their companionship, their unique ability to make me laugh, especially in the toughest times, for encouraging and believing in me.

Last but not least, I wish to convey my unmeasurable gratitude to my family for all the support and encouragement during this journey.

A sincere and grateful thank you to all of the people who were directly and indirectly involved. This opportunity led me to meet remarkable people and irreplaceable friends.

LIST OF PUBLICATIONS AND CONFERENCES

International journal publications

1. **Susana Cruz-Neves**, Yuki Shirosaki, Toshiki Miyazaki, Satoshi Hayakawa. Characterization and degradation study of chitosan-siloxane hybrid microspheres synthesized using a microfluidic approach. Materials Science & Engineering C, 2017, **81**:571–579. *Accepted.*

2. Yuki Shirosaki, Manato Nakatsukasa, Saki Yasutomi, **Susana Cruz-Neves**, Satoshi Hayakawa, Akiyoshi Osaka, Toshinari Maeda, Toshiki Miyazaki. Cytocompatible and antibacterial properties of chitosan−siloxane hybrid spheres. RSC Advances. *Submitted.*

Other related publications

3. **Susana Cruz-Neves**, Nilza Ribeiro, Inês Graça, Carmen Jerónimo, Susana R. Sousa, Fernando J. Monteiro. Behavior of prostate cancer cells in a nanohydroxyapatite/collagen bone scaffold. Journal of Biomedical Materials Research Part A, 2017, **105**(7):2035–2046. *Accepted.*

Grant

1. 2015 / 4 〜 2016 / 2: **Susana Neves**, Sasakawa Research Grant for 2015 from the Japan Science Society, "Preparation of antibacterial chitosan-siloxane microspheres using a microfluidic system approach".

Conferences, symposiums attended and awards

Oral presentations

1. **Susana Neves**, Yuki Shirosaki, Toshinari Maeda, Toshiki Miyazaki, "Bacterial behavior on chitosan-siloxane hybrid hydrogels", 54th Symposium on Basic Science of Ceramics, Poster No: 1E02, Lecture proceedings page 82, 2016.1.7-8, Saga, Japan. **Award for "Good Presentation".**

2. **Susana Neves**, Yuki Shirosaki, Toshiki Miyazaki, "Characterization of chitosan-siloxane hybrid microspheres prepared via sol-gel method", 28th Fall Symposium of the Ceramic Society of Japan, Lecture No: 1O24, 2015.9.16-18, Toyama, Japan.

Poster presentations

1. **Susana Cruz-Neves**, Yuki Shirosaki, Toshiki Miyazaki, "Preparation of chitosan-siloxane hybrid microspheres for drug delivery system"; The First Asian Symposium on Chemistry-based Biotechnology in Kitakyushu (1st ASCBC) as joint bid with the Eighth Japan-Korea Joint Symposium on Bio-microsensing Technology (8th JKBT), Poster No: 12, 2015.06.11-12, Kitakyushu, Japan. **Award for "Outstanding Poster Presentation".**

2. **Susana Cruz-Neves**, Yuki Shirosaki, Toshiki Miyazaki, "Fabrication of biodegradable microspheres derived from chitosan-siloxane hybrid using a microfluidic system"; 7th World Congress on Preventive & Regenerative Medicine (WCPRM2014), Poster Exhibition, P066, 2014.11.04-07, Taipei, Taiwan.